



Physical and Electrochemical properties of aqueous electrolytic solutions based on sodium salt eutectic mixtures for EDLC supercapacitor application

Inês Gomes da Silva

Thesis to obtain the Master of Science Degree in

Chemical Engineering

Supervisors:

Prof. Dr. Isabel Marrucho

Prof. Dr. Mérièm Anouti

Examination Committee

Chairperson: Prof. Dr. José Nuno Lopes

Supervisor: Prof. Dr. Isabel Marrucho

Members of the Committee: Prof. Dr. Fátima Montemor

October 2022

Acknowledgments

The development of this work would have not been possible without the direct and indirect contribution and support of several people. To them I would like to express my immense gratitude.

Firstly, I would like to express my gratitude to my supervisor Isabel Marrucho for all the guidance and help through the development of this project and all the support through my academic path. I am grateful for the opportunity to work with Professor Isabel, as she is a major inspiration and showed me the role of science as a powerful tool to mitigate environmental problems.

I would also like to extend my deepest gratitude to professor Mérièm Anouti for making my stay in Tours a pleasing experience, for all her guidance, availability, and advice through this process.

I want to thank Bruna F. Soares, who followed all my first steps in research, I am grateful for all the support, advice, and friendship. I am also grateful to João Afonso, who is always available to help me and also to exchange laughs. To Bárbara Jesus and José Maria Pires, great lab partners and above all, great friends. I could not have asked for better team!

Regarding my stay in Tours, I would like to thank the PCM2E lab members for all the help during my stay.

I am grateful for all the support, effort and trust given by my family. Special thanks to my mum and dad for all the love and support. To Chica, that since I can remember is always available for a hug and advice.

I would also like to thank my partner Henrique Linhales Rangel, an amazing artist, and a major inspiration, firstly for all the love and emotional support, and for the help with the illustrations present in this document.

Additionally, I would like to thank to friends I made during this five year journey: Maria Cocco, Mariana Canhoto, Inês Cabral, Inês Sendin, João Rodrigues, Filipe Duthoit, Bernardo Canudo, Hugo Guerreiro, Guilherme Damião, Alexandrina Martins, Diogo Gaspar, Vasco Cruz, Cristiana Ferreira, Carolina Mira, and Mafalda Estevão without all of you, this achievement would have been even more difficult.

Finally, I have to thank my stage partners, member of GTIST, for all the inspiration and friendship: Adriano Mendes, Anabela Caetano, Emanuel Frazão, Sérgio Marcelino, Sofia Sequeira, José Pedro Fernandes, João Albano I look forward to keeping up this creative journey.

Resumo

O eletrólito é um elemento central dos supercondensadores tendo um grande impacto na performance destes. Sistemas eutéticos, nomeadamente aqueles nos quais os componentes apresentam boa compatibilidade ambiental, têm sido alvo de uma crescente atenção nos últimos anos. No presente estudo, misturas de água com sistemas eutéticos de hexanoato de sódio com ácidos carboxílicos (ácido hexanóico, octanóico, nonanóico e decanóico) são estudados como possíveis eletrólitos para Supercondensadores Eletroquímicos de Dupla Camada.

Na primeira parte deste estudo, é efetuada a caracterização físico-química destas misturas a partir de várias propriedades como condutividade, viscosidade, densidade, tensão superficial e pH. Na segunda parte, o desempenho eletroquímico destas misturas é testado em células de Supercondensadores Eletroquímicos de Dupla Camada com elétrodos de carvão ativado microporoso através das seguintes técnicas: Voltametria Cíclica, Carga-Descarga Galvanostática e Espetroscopia de Impedância Eletroquímica.

Em geral, verificou-se que o aumento da quantidade de água provoca um aumento na condutividade das misturas enquanto diminui a viscosidade das mesmas. Os voltamogramas obtidos adquirem um formato tanto mais retangular quanto maior a quantidade de água. Verificou-se ainda que a capacidade diminui com o aumento da cadeia do ácido. De entre as misturas estudadas, a mistura eutética de hexanoato de sódio e ácido hexanóico com 60% de percentagem molar deste último, apresentou os valores de condutividade mais elevados, 22.3 mS/cm (20°C), maior valor de capacidade, 71.6 F/g a 0.2 A/g, e o menor valor de resistência interna, 1.83 Ω, para 60% de composição mássica de água.

Palavras-chave: Eletrólito; Supercondensador; Sal de sódio; Ácido gordo; Mistura Eutética.

Abstract

The electrolyte is a central component of supercapacitors having a major influence on its overall performance. Eutectic systems, namely those in which the components are environmentally compatible, have received greater attention in the past years. In this work mixtures of water and eutectic mixtures of sodium hexanoate and carboxyl acids (hexanoic acid, octanoic acid, nonanoic acid and decanoic acid) were studied as potential electrolytes for Electric Double Layer Capacitors (EDLCs).

In the first part of this study, physical characterization of these mixtures was studied through measurement and exploration of several properties, namely the temperature/water-content phase diagrams, conductivity, viscosity, density, surface tension and pH. In the second part, the electrochemical performance of these mixtures was tested in EDLC cells with microporous activated carbon electrodes through Cyclic Voltammetry (CV), Galvanostatic Charge-Discharge (GCD) and Potentiostatic Electrochemical Impedance Spectroscopy (PEIS).

Overall, it was observed that the water content increases the conductivity of the eutectic systems while decreasing the viscosity. Moreover, the quasi-rectangular shape of the CV curves is obtained for higher water content. The electrode specific capacitance decreases when the acid chain increases. From this study the eutectic systems of sodium hexanoate with hexanoic acid with 60% molar composition in acid mixtures ($\text{NaC}_6:\text{C}_6(0.6)$), showed the highest conductivity, 22.3 mS/cm at 20 °C, the highest electrode specific capacitance, 71.6 F/g at 0.2 A/g, and the lowest internal resistance, 1.83 Ω for a weight water composition of 60%.

Keywords: Electrolyte; Supercapacitor; Sodium Salt; Fatty Acid; Eutectic mixture.

Contents

Resumo	iv
Abstract.....	v
List of Tables	iii
List of Abbreviations	iii
List of Symbols	iv
1. Electrolytes for Supercapacitors: State of the art	1
1.1. Supercapacitor’s fundamentals.....	1
1.1.1. Supercapacitor’s role in energy storage.....	1
1.1.2. Types of supercapacitors, Working Principles and Structure.....	4
(i) Electric Double Layer Capacitor, EDLC	5
(ii) Pseudocapacitor	8
(iii) Hybrid Supercapacitor.....	9
1.1.3. Supercapacitor performance parameters	9
Capacitance	9
Energy and Power Densities.....	10
Life cycle	11
Equivalent Series Resistance	11
Coulombic Efficiency	11
1.2. Electrolytes.....	12
1.2.1. Influence of the electrolyte in the supercapacitor.....	12
1.2.2. Types of electrolytes for EDLC supercapacitors	13
(i) Aqueous Electrolytes.....	14
(ii) Organic electrolytes	15
(iii) Ionic Liquids.....	16
(iv) Solid electrolytes and quasi-solid electrolytes	16
1.2.3. Eutectic mixtures as electrolytes for EDLC supercapacitor	16
1.3. Electrochemical Characterization Techniques	18

1.3.1.	Cyclic voltammetry	18
1.3.2.	Galvanostatic charge-discharge	20
1.3.3.	Potentiostatic Electrochemical Impedance Spectroscopy	21
2.	Motivation and Scope	23
3.	Methodology	24
3.1.	Studied Eutectic Systems	24
3.1.1.	Chemical Compounds.....	26
3.1.2.	Eutectic mixtures preparation.....	26
3.1.3.	Eutectic-water mixtures preparation	26
3.2.	Physical Characterization	26
3.2.1.	Phase diagrams.....	26
3.2.2.	Centrifuge.....	26
3.2.3.	pH	26
3.2.4.	Viscosity.....	27
3.2.5.	Density.....	27
3.2.6.	Surface Tension	27
3.2.7.	Conductivity.....	27
3.3.	Electrochemical tests	27
4.	Results	29
4.1.	Sample selection: Water composition and temperature sweep	29
4.2.	Physical Characterization	34
4.2.1.	Ionic Conductivity	34
i)	Vogel-Fulcher-Tammann	37
4.2.2.	Viscosity.....	38
i)	Vogel-Fulcher-Tammann	40
ii)	Eyring's Theory	41
iii)	Jones-Dole-Kaminsky model: Hydrodynamic radius determination.....	45
4.2.3.	Density.....	48

4.2.4.	Surface Tension	49
4.2.5.	Ionicity: Walden Plot	50
4.2.6.	pH	53
4.3.	Electrochemical Study	55
4.3.1.	Cyclic Voltammetry	55
i)	NaC ₆ :C ₆ (0.6)	55
ii)	NaC ₆ :C ₆ (0.7)	56
iii)	NaC ₆ :C ₈ (0.6)	58
iv)	NaC ₆ :C ₈ (0.7)	58
v)	NaC ₆ :C ₉ (0.7)	60
vi)	NaC ₆ :C ₁₀ (0.7)	61
4.3.2.	Galvanostatic Charge-Discharge.....	66
4.3.3.	Potentiostatic Electrochemical Impedance Spectroscopy	74
5.	Conclusions.....	79
6.	Future work.....	80
7.	Bibliography	81
8.	Supporting Information.....	86
8.1.	Sodium hexanoate preparation.....	86
8.2.	Concentration of salt.....	86
8.3.	Conductivity.....	86
8.4.	Viscosity.....	87
8.4.1.	Eyring's Theory	93
8.4.2.	Jones-Dole-Kaminsky.....	94
8.5.	Density.....	97
8.6.	Surface Tension	104
8.7.	Walden Plot	105
8.8.	pH	111
8.9.	Cyclic Voltammetry	112

8.10.	Potentiostatic Electrochemical Impedance Spectroscopy	112
8.10.1.	EIS Nyquist Plots	112
8.10.2.	Impedance Values: R_A , R_B , R_C	120
8.10.3.	Electrode Specific Capacitance <i>versus</i> Frequency plots.....	122

List of figures

Figure 1. Ragone Plot, [4].	1
Figure 2. Schematic representation of a battery (a), a capacitor (b) and a supercapacitor (c). Adapted from [6].	2
Figure 3. Publications related to supercapacitor applications released between 2011 and 2021 [7].	3
Figure 4. Brockis et al. EDL model representation [13].	6
Figure 5. Schematic representation of the charging and discharging process in an EDLC, [15].	8
Figure 6. Illustrative cyclic voltammograms of EDLC, Pseudocapacitor and battery. Source: [15].	9
Figure 7. Number of articles per year related to “Electrolytes for supercapacitors” published between 1992 and 2021 [22].	12
Figure 8. Electrolyte effect on the supercapacitor performance parameters. Adapted from [21].	13
Figure 9. Electrolyte classification for Supercapacitors, each group gives the most used respective electrolyte as example [21].	14
Figure 10. Left: Cyclic Voltammetry linear excitation signal. Right: Cyclic voltammograms at different sweep rates for an ideal capacitor [2].	18
Figure 11. Cyclic voltammetry obtained for a solid electrolyte based on Natural Polymers in a EDLC supercapacitor with activated carbon electrodes [38].	19
Figure 12. Cyclic Voltammetry for potential stability window studies at 1 mV/s for EDLC type of supercapacitors with 1M LiPF ₆ /EC:EMC 50:50 v/v electrolyte [41].	19
Figure 13. Typical charge-discharge cycle in GCD [20].	20
Figure 14. Typical Nyquist plots for EDLC supercapacitors [46].	22
Figure 15. Chemical structures and respective acronyms of the species used to prepare the eutectic mixtures.	24
Figure 16. Solid-liquid phase diagram of the sodium hexanoate salt-based eutectic solvent with each acid presented in [48]. Black outlined points refer to data collected by DSC; remaining points collected through turbidimetry.	25
Figure 17. Schematic illustration of the Swagelok® cell used in the electrochemical tests.	28
Figure 18. Eutectic-water mixtures of NaC ₆ :C ₆ (0.6) group at ambient temperature (~20 °C) identified by massic content of water.	29
Figure 19. Eutectic-water mixtures of NaC ₆ :C ₆ (0.7) group at ambient temperature (~20 °C) identified by massic content of water.	29
Figure 20. Eutectic-water mixtures of NaC ₆ :C ₈ (0.6) group at ambient temperature (~20 °C) identified by massic content of water.	30
Figure 21. Eutectic-water mixtures of NaC ₆ :C ₈ (0.7) group at ambient temperature (~20 °C) identified by massic content of water.	30
Figure 22. Eutectic-water mixtures of NaC ₆ :C ₉ (0.7) group at ambient temperature (~20 °C) identified by massic content of water.	30
Figure 23. Eutectic-water mixtures of NaC ₆ :C ₁₀ (0.7) group at ambient temperature (~20 °C) identified by massic content of water.	31

Figure 24. Phase diagram for the NaC ₆ :C ₆ (0.6) eutectic-water group.	31
Figure 25. Phase diagram for the NaC ₆ :C ₆ (0.7) eutectic-water group.	31
Figure 26. Phase diagram for the NaC ₆ :C ₈ (0.6) eutectic-water group.	32
Figure 27. Phase diagram for the NaC ₆ :C ₈ (0.7) eutectic-water group.	32
Figure 28. Phase diagram for the NaC ₆ :C ₉ (0.7) eutectic-water group.	32
Figure 29. Phase diagram for the NaC ₆ :C ₁₀ (0.7) eutectic-water group.	32
Figure 30. Mixtures of NaC ₆ :C ₈ (0.6) with 30 wt%, 40 wt%, 50 wt% and 60 wt% of water after 30 min centrifugation at 4500 rpm. Orange circle evidences the occurrence of phase separation for the mixture with 30 wt% of massic water content.	33
Figure 31. Ionic conductivity data as function of temperature for NaC ₆ :C ₆ (0.6)-water mixtures (0 wt% H ₂ O, 10 wt% H ₂ O, 20 wt% H ₂ O, 40 wt% H ₂ O (gel), 50 wt% H ₂ O and 60 wt% H ₂ O). Triangular form points identify gel mixtures.	34
Figure 32. Ionic conductivity data as function of temperature for the NaC ₆ :C ₆ (0.7)-water mixtures (0 wt%, 10 wt% H ₂ O, 20 wt% H ₂ O, 30 wt% H ₂ O, 40 wt% H ₂ O and 50 wt% H ₂ O).	34
Figure 33. Ionic conductivity data as function of temperature for NaC ₆ :C ₈ (0.6)-water mixtures (0 wt%, 10 wt% H ₂ O, 40 wt% H ₂ O (gel), 50 wt% H ₂ O (gel) and 60 wt% H ₂ O (gel)). Triangular form points identify gel mixtures.	35
Figure 34. Ionic conductivity data as function of temperature for the NaC ₆ :C ₈ (0.7)-water mixtures (0 wt%, 10 wt% H ₂ O, 20 wt% H ₂ O, 30 wt% H ₂ O, 40 wt% H ₂ O and 50 wt% H ₂ O).	35
Figure 35. Ionic conductivity data as function of temperature for the NaC ₆ :C ₉ (0.7)-water mixtures (0 wt%, 10 wt% H ₂ O, 20 wt% H ₂ O, 30 wt% H ₂ O and 40 wt% H ₂ O).	35
Figure 36. Ionic conductivity data as function of temperature for the NaC ₆ :C ₁₀ (0.7)-water mixtures (0 wt%, 10 wt% H ₂ O, 20 wt% H ₂ O, 30 wt% H ₂ O and 40 wt% H ₂ O).	35
Figure 37. Conductivity data at 20 °C organized by water massic %. “*” identifies mixtures in gel form.	36
Figure 38. Viscosity data as function of temperature for the NaC ₆ :C ₆ (0.6)-water mixtures.	38
Figure 39. Viscosity data as function of temperature for the NaC ₆ :C ₆ (0.7)-water mixtures.	38
Figure 40. Viscosity data as function of temperature for the NaC ₆ :C ₈ (0.6)-water mixtures.	39
Figure 41. Viscosity data as function of temperature for the NaC ₆ :C ₈ (0.7)-water mixtures.	39
Figure 42. Viscosity data as function of temperature for the NaC ₆ :C ₉ (0.7)-water mixtures.	39
Figure 43. Viscosity data as function of temperature for the NaC ₆ :C ₁₀ (0.7)-water mixtures.	39
Figure 44. Variation of enthalpy of activation with the water content for the NaC ₆ :C ₆ (0.6) group.	42
Figure 45. Variation of entropy of activation with the water content for the NaC ₆ :C ₆ (0.6) group.	42
Figure 46. Variation of enthalpy of activation with the water content for the NaC ₆ :C ₆ (0.7) group.	42
Figure 47. Variation of entropy of activation with the water content for the NaC ₆ :C ₆ (0.7) group.	42
Figure 48. Variation of enthalpy of activation with the water content for the NaC ₆ :C ₈ (0.7) group.	43
Figure 49. Variation of entropy of activation with the water content for the NaC ₆ :C ₈ (0.7) group.	43
Figure 50. Variation of enthalpy of activation with the water content for the NaC ₆ :C ₉ (0.7) group.	43
Figure 51. Variation of entropy of activation with the water content for the NaC ₆ :C ₉ (0.7) group.	43
Figure 52. Variation of enthalpy of activation with the water content for the NaC ₆ :C ₁₀ (0.7) group.	44

Figure 53. Variation of entropy of activation with the water content for the NaC ₆ :C ₁₀ (0.7) group	44
Figure 54. Hydrodynamic radius evolution with temperature for eutectic-water mixtures.	46
Figure 55. Schematic Proposal of organization of the species.	48
Figure 56. Density data as function of temperature for the NaC ₆ :C ₆ (0.6) group.....	48
Figure 57. Density data as function of temperature for the NaC ₆ :C ₆ (0.7) group.....	48
Figure 58. Density data as function of temperature for the NaC ₆ :C ₈ (0.6) group.....	49
Figure 59. Density data as function of temperature for the NaC ₆ :C ₈ (0.7) group.....	49
Figure 60. Density data as function of temperature for the NaC ₆ :C ₉ (0.7) group.....	49
Figure 61. Density data as function of temperature for the NaC ₆ :C ₁₀ (0.7) group.	49
Figure 62. Surface Tension as function of eutectic mixture concentration. Right: Zoom in the xx scale.	50
Figure 63. Walden plot representation for NaC ₆ :C ₆ (0.6) mixtures.	51
Figure 64. Walden plot representation for NaC ₆ :C ₆ (0.7) mixtures.	51
Figure 65. Walden plot representation for NaC ₆ :C ₈ (0.6) mixtures.	51
Figure 66. Walden plot representation for NaC ₆ :C ₈ (0.7) mixtures.	51
Figure 67. Walden plot representation for NaC ₆ :C ₉ (0.7) mixtures.	52
Figure 68. Walden plot representation for NaC ₆ :C ₁₀ (0.7) mixtures.	52
Figure 69. pH measurements at 20 °C for each eutectic-water mixture studied.	54
Figure 70. Cyclic voltammograms performed at 1 mV/s, 5 mV/s, 10 mV/s and 20 mV/s scan rates for a voltage limit of 1 volt for the NaC ₆ :C ₆ (0.6) mixture.	55
Figure 71. Cyclic voltammograms performed at 1 mV/s, 5 mV/s, 10 mV/s and 20 mV/s scan rates for a voltage limit of 1 volt for the NaC ₆ :C ₆ (0.6) +10% H ₂ O mixture.	55
Figure 72. Cyclic voltammograms performed at 1 mV/s, 5 mV/s, 10 mV/s and 20 mV/s scan rates for a voltage limit of 1 volt for the NaC ₆ :C ₆ (0.6) +20% H ₂ O mixture.	55
Figure 73. Cyclic voltammograms performed at 1 mV/s, 5 mV/s, 10 mV/s and 20 mV/s scan rates for a voltage limit of 1 volt for the NaC ₆ :C ₆ (0.6) +50% H ₂ O mixture.	55
Figure 74. Cyclic voltammograms performed at 1 mV/s, 5 mV/s, 10 mV/s and 20 mV/s scan rates for a voltage limit of 1 volt for the NaC ₆ :C ₆ (0.6) + 60% H ₂ O mixture.	56
Figure 75. Cyclic voltammograms performed at 1 mV/s, 5 mV/s, 10 mV/s and 20 mV/s scan rates for a voltage limit of 1 volt for the NaC ₆ :C ₆ (0.7).	56
Figure 76. Cyclic voltammograms performed at 1 mV/s, 5 mV/s, 10 mV/s and 20 mV/s scan rates for a voltage limit of 1 volt for the NaC ₆ :C ₆ (0.7) + 10% H ₂ O mixture.	56
Figure 77. Cyclic voltammograms performed at 1 mV/s, 5 mV/s, 10 mV/s and 20 mV/s scan rates for a voltage limit of 1 volt for the NaC ₆ :C ₆ (0.7) + 20% H ₂ O mixture.	57
Figure 78. Cyclic voltammograms performed at 1 mV/s, 5 mV/s, 10 mV/s and 20 mV/s scan rates for voltage limit of 1 volt for the NaC ₆ :C ₆ (0.7) + 30% H ₂ O mixture.	57
Figure 79. Cyclic voltammograms performed at 1 mV/s, 5 mV/s, 10 mV/s and 20 mV/s scan rates for a voltage limit of 1 volt for the NaC ₆ :C ₆ (0.7) + 40% H ₂ O mixture.	57

Figure 80. Cyclic voltammograms performed at 1 mV/s, 5 mV/s, 10 mV/s and 20 mV/s scan rates for a voltage limit of 1 volt for the NaC ₆ :C ₆ (0.7) + 50% H ₂ O mixture.	57
Figure 81. Cyclic voltammograms performed at 1 mV/s, 5 mV/s, 10 mV/s and 20 mV/s scan rates for a voltage limit of 1 volt for the NaC ₆ :C ₈ (0.6) mixture.	58
Figure 82. Cyclic voltammograms performed at 1 mV/s, 5 mV/s, 10 mV/s and 20 mV/s scan rates for a voltage limit of 1 volt for the NaC ₆ :C ₈ (0.6) + 10% H ₂ O mixture.	58
Figure 83. Cyclic voltammograms performed at 1 mV/s, 5 mV/s, 10 mV/s and 20 mV/s scan rates for a voltage limit of 1 volt for the NaC ₆ :C ₈ (0.7) mixture.	58
Figure 84. Cyclic voltammograms performed at 1 mV/s, 5 mV/s, 10 mV/s and 20 mV/s scan rates for a voltage limit of 1 volt for the NaC ₆ :C ₈ (0.7) + 10% H ₂ O mixture.	58
Figure 85. Cyclic voltammograms performed at 1 mV/s, 5 mV/s, 10 mV/s and 20 mV/s scan rates for a voltage limit of 1 volt for the NaC ₆ :C ₈ (0.7) + 20% H ₂ O mixture.	59
Figure 86. Cyclic voltammograms performed at 1 mV/s, 5 mV/s, 10 mV/s and 20 mV/s scan rates for a voltage limit of 1 volt for the NaC ₆ :C ₈ (0.7) + 30% H ₂ O mixture.	59
Figure 87. Cyclic voltammograms performed at 1 mV/s, 5 mV/s, 10 mV/s and 20 mV/s scan rates for a voltage limit of 1 volt for the NaC ₆ :C ₈ (0.7) + 40% H ₂ O mixture.	59
Figure 88. Cyclic voltammograms performed at 1 mV/s, 5 mV/s, 10 mV/s and 20 mV/s scan rates for a voltage limit of 1 volt for the NaC ₆ :C ₈ (0.7) + 50% H ₂ O mixture.	59
Figure 89. Cyclic voltammograms performed at 1 mV/s, 5 mV/s, 10 mV/s and 20 mV/s scan rates for a voltage limit of 1 volt for the NaC ₆ :C ₉ (0.7) mixture.	60
Figure 90. Cyclic voltammograms performed at 1 mV/s, 5 mV/s, 10 mV/s and 20 mV/s scan rates for a voltage limit of 1 volt for the NaC ₆ :C ₉ (0.7) + 10% H ₂ O mixture.	60
Figure 91. Cyclic voltammograms performed at 1 mV/s, 5 mV/s, 10 mV/s and 20 mV/s scan rates for a voltage limit of 1 volt for the NaC ₆ :C ₉ (0.7) + 20% H ₂ O mixture.	60
Figure 92. Cyclic voltammograms performed at 1 mV/s, 5 mV/s, 10 mV/s and 20 mV/s scan rates for a voltage limit of 1 volt for the NaC ₆ :C ₉ (0.7) + 30% H ₂ O mixture.	60
Figure 93. Cyclic voltammograms performed at 1 mV/s, 5 mV/s, 10 mV/s and 20 mV/s scan rates for a voltage limit of 1 volt for the NaC ₆ :C ₉ (0.7) + 40% H ₂ O mixture.	61
Figure 94. Cyclic voltammograms performed at 1 mV/s, 5 mV/s, 10 mV/s and 20 mV/s scan rates for a voltage limit of 1 volt for the NaC ₆ :C ₁₀ (0.7) mixture.	61
Figure 95. Cyclic voltammograms performed at 1 mV/s, 5 mV/s, 10 mV/s and 20 mV/s scan rates for a voltage limit of 1 volt for the NaC ₆ :C ₁₀ (0.7) + 10% H ₂ O mixture.	61
Figure 96. Cyclic voltammograms performed at 1 mV/s, 5 mV/s, 10 mV/s and 20 mV/s scan rates for voltage limit of 1 volt for the NaC ₆ :C ₁₀ (0.7) + 20% H ₂ O mixture.	62
Figure 97. Cyclic voltammograms performed at 1 mV/s, 5 mV/s, 10 mV/s and 20 mV/s scan rates for a voltage limit of 1 volt for the NaC ₆ :C ₁₀ (0.7) + 30% H ₂ O mixture.	62
Figure 98. Cyclic voltammograms performed at 1 mV/s, 5 mV/s, 10 mV/s and 20 mV/s scan rates for a voltage limit of 1 volt for the NaC ₆ :C ₁₀ (0.7) + 40% H ₂ O mixture.	62

Figure 99. Cyclic Voltammetry curves plotted at 5 mV/s potential scan rate for NaC ₆ :C ₆ (0.7), NaC ₆ :C ₈ (0,7), NaC ₆ :C ₉ (0,7), NaC ₆ :C ₁₀ (0.7) with 40 wt% H ₂ O.	63
Figure 100. Electrode Specific Capacitance as function of the CV scan rate for the NaC ₆ :C ₆ (0.6)-water mixtures (50 wt% H ₂ O and 60 wt% H ₂ O).	64
Figure 101. Electrode Specific Capacitance as function of the CV scan rate for the NaC ₆ :C ₆ (0.7)-water mixtures (20 wt% H ₂ O, 30 wt% H ₂ O, 40 wt% H ₂ O and 50 wt% H ₂ O).	64
Figure 102. Electrode Specific Capacitance as function of the CV scan rate for the NaC ₆ :C ₈ (0.7)-water mixtures (20 wt% H ₂ O, 30 wt% H ₂ O, 40 wt% H ₂ O and 50 wt% H ₂ O).	64
Figure 103. Electrode Specific Capacitance as function of the CV scan rate for the NaC ₆ :C ₉ (0.7)-water mixtures (20 wt% H ₂ O, 30 wt% H ₂ O and 40 wt% H ₂ O).	64
Figure 104. Electrode Specific Capacitance as function of the CV scan rate for the NaC ₆ :C ₁₀ (0.7)-water mixtures (20 wt% H ₂ O, 30 wt% H ₂ O and 40 wt% H ₂ O).	65
Figure 105. Cyclic Voltammogram for 1 mV scan rate and 1V, 1.2V, 1.4V, 1.6V, 1.8 V and 2V maximum potential of NaC ₆ :C ₆ (0.6) + 10%H ₂ O.	65
Figure 106. Capacitance, Capacitance of retention, and efficiency as function of cycle number for NaC ₆ :C ₆ (0.6) + 50%H ₂ O mixture.	67
Figure 107. Capacitance, Capacitance of retention, and efficiency as function of cycle number for NaC ₆ :C ₆ (0.6) + 60%H ₂ O mixture.	67
Figure 108. Capacitance, Capacitance of retention, and efficiency as function of cycle number for NaC ₆ :C ₆ (0.7) + 30%H ₂ O mixture.	67
Figure 109. Capacitance, Capacitance of retention, and efficiency as function of cycle number for NaC ₆ :C ₆ (0.7) + 40%H ₂ O mixture.	68
Figure 110. Capacitance, Capacitance of retention, and efficiency as function of cycle number for NaC ₆ :C ₆ (0.7) + 50%H ₂ O mixture.	68
Figure 111. Capacitance, Capacitance of retention, and efficiency as function of cycle number for NaC ₆ :C ₈ (0.7) + 20%H ₂ O mixture.	68
Figure 112. Capacitance, Capacitance of retention, and efficiency as function of cycle number for NaC ₆ :C ₈ (0.7) + 30%H ₂ O mixture.	69
Figure 113. Capacitance, Capacitance of retention, and efficiency as function of cycle number for NaC ₆ :C ₈ (0.7) + 50%H ₂ O mixture.	69
Figure 114. Capacitance, Capacitance of retention, and efficiency as function of cycle number for NaC ₆ :C ₉ (0.7) + 20%H ₂ O mixture.	69
Figure 115. Capacitance, Capacitance of retention, and efficiency as function of cycle number for NaC ₆ :C ₉ (0.7) + 30%H ₂ O mixture.	70
Figure 116. Capacitance, Capacitance of retention, and efficiency as function of cycle number for NaC ₆ :C ₉ (0.7) + 40%H ₂ O mixture.	70
Figure 117. Capacitance, Capacitance of retention, and efficiency as function of cycle number for NaC ₆ :C ₁₀ (0.7) + 20%H ₂ O mixture.	70

Figure 118. Capacitance, Capacitance of retention, and efficiency as function of cycle number for NaC ₆ :C ₁₀ (0.7) + 30%H ₂ O mixture.....	71
Figure 119. Capacitance, Capacitance of retention, and efficiency as function of cycle number for NaC ₆ :C ₁₀ (0.7) + 40%H ₂ O mixture.....	71
Figure 120. Galvanostatic charge-discharge cycles for the NaC ₆ :C ₆ (0.6) +50%H ₂ O. Right: ESR increasing with the number of cycles.....	73
Figure 121. Initial specific capacitance per electrode as a function of massic water content.	73
Figure 122. Specific capacitance per electrode after approximately 5000 cycles as a function of massic water content.....	74
Figure 123. Nyquist plot for NaC ₆ :C ₆ (0.7) +30%H ₂ O with identification of the different zone limits.....	75
Figure 124. R _A values before cycling displayed by water content.....	75
Figure 125. R _B -R _A values before cycling displayed as a function of water content.	76
Figure 126. R _C values before cycling displayed by water content.....	77
Figure 127. Electrode Specific Capacitance obtained through Potentiostatic Electrochemical Impedance Spectroscopy (PEIS) before cycling.	77
Figure 128. Electrode Specific Capacitance obtained through Potentiostatic Electrochemical Impedance Spectroscopy (PEIS) after cycling.	78
Figure 129. Nyquist plots of the NaC ₆ :C ₆ (0.6) + 50%H ₂ O electrolyte before and after cycling. Left: full scale; Right: Zoom for high frequencies.....	112
Figure 130. Nyquist plots of the NaC ₆ :C ₆ (0.6) + 60%H ₂ O electrolyte before and after cycling. Left: full scale; Right: Zoom for high frequencies.....	113
Figure 131. Nyquist plots of the NaC ₆ :C ₆ (0.7) + 20%H ₂ O electrolyte before and after cycling. Left: full scale; Right: Zoom for high frequencies.....	113
Figure 132. Nyquist plots of the NaC ₆ :C ₆ (0.7) + 30%H ₂ O electrolyte before and after cycling. Left: full scale; Right: Zoom for high frequencies.....	114
Figure 133. Nyquist plots of the NaC ₆ :C ₆ (0.7) + 40%H ₂ O electrolyte before and after cycling. Left: full scale; Right: Zoom for high frequencies.....	114
Figure 134. Nyquist plots of the NaC ₆ :C ₆ (0.7) + 50%H ₂ O electrolyte before and after cycling. Left: full scale; Right: Zoom for high frequencies.....	115
Figure 135. Nyquist plots of the NaC ₆ :C ₈ (0.7) + 20%H ₂ O electrolyte before and after cycling. Left: full scale; Right: Zoom for high frequencies.....	115
Figure 136. Nyquist plots of the NaC ₆ :C ₈ (0.7) + 30%H ₂ O electrolyte before and after cycling. Left: full scale; Right: Zoom for high frequencies.....	116
Figure 137. Nyquist plots of the NaC ₆ :C ₈ (0.7) + 40%H ₂ O electrolyte before and after cycling. Left: full scale; Right: Zoom for high frequencies.....	116
Figure 138. Nyquist plots of the NaC ₆ :C ₈ (0.7) + 50%H ₂ O electrolyte before and after cycling. Left: full scale; Right: Zoom for high frequencies.....	117

Figure 139. Nyquist plots of the $\text{NaC}_6\text{:C}_9(0.7) + 20\%\text{H}_2\text{O}$ electrolyte before and after cycling. Left: full scale; Right: Zoom for high frequencies.	117
Figure 140. Nyquist plots of the $\text{NaC}_6\text{:C}_9(0.7) + 30\%\text{H}_2\text{O}$ electrolyte before and after cycling. Left: full scale; Right: Zoom for high frequencies.	118
Figure 141. Nyquist plots of the $\text{NaC}_6\text{:C}_9(0.7) + 40\%\text{H}_2\text{O}$ electrolyte before and after cycling. Left: full scale; Right: Zoom for high frequencies.	118
Figure 142. Nyquist plots of the $\text{NaC}_6\text{:C}_{10}(0.7) + 20\%\text{H}_2\text{O}$ electrolyte before and after cycling. Left: full scale; Right: Zoom for high frequencies.	119
Figure 143. Nyquist plots of the $\text{NaC}_6\text{:C}_{10}(0.7) + 30\%\text{H}_2\text{O}$ electrolyte before and after cycling. Left: full scale; Right: Zoom for high frequencies.	119
Figure 144. Nyquist plots of the $\text{NaC}_6\text{:C}_{10}(0.7) + 40\%\text{H}_2\text{O}$ electrolyte before and after cycling. Left: full scale; Right: Zoom for high frequencies.	120
Figure 145. Specific Capacitance as function of frequency obtained from EIS for the $\text{NaC}_6\text{:C}_6(0.6) + 50\%\text{H}_2\text{O}$ mixture before and after cycling.	122
Figure 146. Specific Capacitance as function of frequency obtained from EIS for the $\text{NaC}_6\text{:C}_6(0.6) + 60\%\text{H}_2\text{O}$ mixture before and after cycling.	122
Figure 147. Specific Capacitance as function of frequency obtained from EIS for the $\text{NaC}_6\text{:C}_6(0.7) + 20\%\text{H}_2\text{O}$ mixture before and after cycling.	122
Figure 148. Specific Capacitance as function of frequency obtained from EIS for the $\text{NaC}_6\text{:C}_6(0.7) + 30\%\text{H}_2\text{O}$ mixture before and after cycling.	122
Figure 149. Specific Capacitance as function of frequency obtained from EIS for the $\text{NaC}_6\text{:C}_6(0.7) + 40\%\text{H}_2\text{O}$ mixture before and after cycling.	123
Figure 150. Specific Capacitance as function of frequency obtained from EIS for the $\text{NaC}_6\text{:C}_6(0.7) + 50\%\text{H}_2\text{O}$ mixture before and after cycling.	123
Figure 151. Specific Capacitance as function of frequency obtained from EIS for the $\text{NaC}_6\text{:C}_8(0.7) + 20\%\text{H}_2\text{O}$ mixture before and after cycling.	123
Figure 152. Specific Capacitance as function of frequency obtained from EIS for the $\text{NaC}_6\text{:C}_8(0.7) + 30\%\text{H}_2\text{O}$ mixture before and after cycling.	123
Figure 153. Specific Capacitance as function of frequency obtained from EIS for the $\text{NaC}_6\text{:C}_8(0.7) + 40\%\text{H}_2\text{O}$ mixture before and after cycling.	124
Figure 154. Specific Capacitance as function of frequency obtained from EIS for the $\text{NaC}_6\text{:C}_8(0.7) + 50\%\text{H}_2\text{O}$ mixture before and after cycling.	124
Figure 155. Specific Capacitance as function of frequency obtained from EIS for the $\text{NaC}_6\text{:C}_9(0.7) + 20\%\text{H}_2\text{O}$ mixture before and after cycling.	125
Figure 156. Specific Capacitance as function of frequency obtained from EIS for the $\text{NaC}_6\text{:C}_9(0.7) + 30\%\text{H}_2\text{O}$ mixture before and after cycling.	125
Figure 157. Specific Capacitance as function of frequency obtained from EIS for the $\text{NaC}_6\text{:C}_9(0.7) + 40\%\text{H}_2\text{O}$ mixture before and after cycling.	125

Figure 158. Specific Capacitance as function of frequency obtained from EIS for the $\text{NaC}_6\text{:C}_{10}(0.7) + 20\%\text{H}_2\text{O}$ mixture before and after cycling..... 125

Figure 159. Specific Capacitance as function of frequency obtained from EIS for the $\text{NaC}_6\text{:C}_{10}(0.7) + 30\%\text{H}_2\text{O}$ mixture before and after cycling..... 126

Figure 160. Specific Capacitance as function of frequency obtained from EIS for the $\text{NaC}_6\text{:C}_{10}(0.7) + 40\%\text{H}_2\text{O}$ mixture before and after cycling..... 126

List of Tables

Table 1. Conductivity of different electrolytes.	17
Table 2. Specific Capacitance, Potential operational window, energy and power densities for different electrolytes and respective electrode used in EDLC supercapacitors.....	17
Table 3. Eutectic mixtures acronyms and respective description.	25
Table 4. Eutectic-water mixtures of NaC ₆ :C ₆ (0.6) group and respective massic and molar compositions.....	29
Table 5. Eutectic-water mixtures of NaC ₆ :C ₆ (0.7) group and respective massic and molar compositions.....	29
Table 6. Eutectic-water mixtures of NaC ₆ :C ₈ (0.6) group and respective massic and molar compositions.....	30
Table 7. Eutectic-water mixtures of NaC ₆ :C ₈ (0.7) group and respective massic and molar compositions.....	30
Table 8. Eutectic-water mixtures of NaC ₆ :C ₉ (0.7) group and respective massic and molar compositions.....	30
Table 9. Eutectic-water mixtures of NaC ₆ :C ₉ (0.7) group and respective massic and molar compositions.....	31
Table 10. Selected mixtures for further characterization.	33
Table 11. Conductivity VTF parameters for the eutectic mixtures under study.	37
Table 12. Structure of the compounds used in the studied eutectic systems and their respective length.	46
Table 13. Critical Aggregation Concentration (CAC) in mol/L according to the number of carbons in the alkyl acid chain.....	50
Table 14. Slope and correlation coefficient obtained from the fractional Walden rule.....	53
Table 15. pK _a s of hexanoic, octanoic, nonanoic and decanoic acids.	54
Table 16. GCD operational conditions for each sample.....	66
Table 17. Specific Capacitance at the beginning of cycling and at the 5000 th cycle, % of capacitance loss and % of retained capacitance.....	72
Table 18. Conductivity of each mixture at 20 °C.....	86
Table 19. Viscosity data for the NaC ₆ :C ₆ (0.6) with water mixtures.	87
Table 20. Viscosity data for the NaC ₆ :C ₆ (0.7) with water mixtures.	88
Table 21. Viscosity data for the NaC ₆ :C ₈ (0.6) with water mixtures.	89
Table 22. Viscosity data for the NaC ₆ :C ₈ (0.7) with water mixtures.	90
Table 23. Viscosity data for the NaC ₆ :C ₉ (0.7) with water mixtures.	91
Table 24. Viscosity data for the NaC ₆ :C ₁₀ (0.7) with water mixtures.	92
Table 25. Fitting parameters from Eyring's theory for each mixture and respective enthalpy and entropy of activation.	93
Table 26. Fitting parameters of the Jones-Dole-Kaminsky model for the NaC ₆ :C ₆ : water mixtures.	94
Table 27. Fitting parameters of the Jones-Dole-Kaminsky model for the NaC ₆ :C ₈ : water mixtures.	94
Table 28. Fitting parameters of the Jones-Dole-Kaminsky model for the NaC ₆ :C ₉ : water mixtures.	95
Table 29. Fitting parameters of the Jones-Dole-Kaminsky model for the NaC ₆ :C ₁₀ : water mixtures.	95
Table 30. Hydrodynamic radius as function of temperature determined through Jones-Dole-Kaminsky model and Einstein's viscosity theory.....	96
Table 31. Density data for the NaC ₆ :C ₆ (0.6) with water mixtures.	97

Table 32. Density data for the NaC ₆ :C ₆ (0.7) with water mixtures.	98
Table 33. Density data for the NaC ₆ :C ₈ (0.6) with water mixtures.	99
Table 34. Density data for the NaC ₆ :C ₈ (0.7) with water mixtures.	100
Table 35. Density data for the NaC ₆ :C ₉ (0.7) with water mixtures.	101
Table 36. Density data for the NaC ₆ :C ₁₀ (0.7) with water mixtures.	102
Table 37. Fitting parameters from ρ vs T for NaC ₆ :C ₆ (0.6) with water mixtures.	102
Table 38. Fitting parameters from ρ vs T for NaC ₆ :C ₆ (0.7) with water mixtures.	102
Table 39. Fitting parameters from ρ vs T for NaC ₆ :C ₈ (0.6) with water mixtures.	103
Table 40. Fitting parameters from ρ vs T for NaC ₆ :C ₈ (0.7) with water mixtures.	103
Table 41. Fitting parameters from ρ vs T for NaC ₆ :C ₉ (0.7) with water mixtures.	103
Table 42. Fitting parameters from ρ vs T for NaC ₆ :C ₁₀ (0.7) with water mixtures.	103
Table 43. Surface Tension in water results for the different studied eutectic systems.	104
Table 44. Molar conductivity for NaC ₆ :C ₆ (0.6) with water mixtures.	105
Table 45. Molar conductivity for NaC ₆ :C ₆ (0.7) with water mixtures.	106
Table 46. Molar conductivity for NaC ₆ :C ₈ (0.6) with water mixtures.	107
Table 47. Molar conductivity for NaC ₆ :C ₈ (0.7) with water mixtures.	108
Table 48. Molar conductivity for NaC ₆ :C ₉ (0.7) with water mixtures.	109
Table 49. Molar conductivity for NaC ₆ :C ₁₀ (0.7) with water mixtures.	110
Table 50. pH of each mixture.	111
Table 51. Specific Capacitance (F/g) obtained from CV for the different scan-rates 1 mV/s, 5 mV/s, 10 mV/s and 20 mV/s.	112
Table 52. R _A values before cycling.	120
Table 53. R _B -R _A values before cycling.	120
Table 54. R _C values before cycling.	121
Table 55. R _B -R _A values after cycling.	121
Table 56. R _C values after cycling.	121
Table 57. Specific Capacitance from PEIS data before and after cycling.	126

List of Abbreviations

AC	Activated Carbon
ACN	Acetonitrile
C₁₀	Decanoic Acid
C₆	Hexanoic Acid
C₈	Octanoic Acid
C₉	Nonanoic Acid
CAC	Critical Aggregation Concentration
ChCl	Choline Chloride
CV	Cyclic Voltammetry
DSC	Differential Scanning Calorimetry
EDL	Electric Double Layer
EDLC	Electric Double Layer Capacitor
EIS	Electrochemical Impedance Spectroscopy
ESD	Energy Storage Devices
ESR	Equivalent Series Resistance
ETL	Electrical Triple Layer
GCD	Galvanostatic Charge-Discharge
GC-model	Gouy-Chapman model
GPS	Global Position System
HBA	Hydrogen Bond Acceptor
HBD	Hydrogen Bond Donor
HER	Hydrogen Evolution Reaction
HEV	Hybrid Electric Vehicle
IL	Ionic Liquid
JDK	Jones-Dole-Kaminsky
NaC₆	Sodium Hexanoate
OCV	Open Circuit Voltage
OER	Oxygen Evolution Reaction
PC	Propylene Carbonate
PEIS	Electrochemical Impedance Spectroscopy
TEABF₄	tetraethylammonium tetrafluoroborate
T_g	Ideal glass transition temperature
VTF	Vogel-Tamman-Fulcher

List of Symbols

σ	conductivity
η	viscosity
Λ	Molar conductivity
ρ	density
γ	Surface tension
C	Capacitance
I	Current
Φ	Phase angle
Ω	Ohm
ΔS^\ddagger	Entropy of activation
ΔH^\ddagger	Enthalpy of activation
h	Plank's constant
N_A	Avogadro's constant
V_m	Molar volume
r_s	Hydrodynamic radius

1. Electrolytes for Supercapacitors: State of the art

As a consequence of the growing of a highly technological population, the world energy demand is increasing. Since today's society mostly relies on fossil fuels to their energy needs, efficient renewable and less environmental armful energy solutions are needed. According to the Global Energy Review 2021 Report from the International Energy Agency: "the overall greenhouse emissions from energy rose to their highest ever level in 2021" [1]. Engaging sustainable, renewable, and clean energy sources is therefore urgently required. Since most of the renewable energy is intrinsically intermittent (dependent on the time of the day, geographic location, weather, etc), it is highly desirable to develop related energy storage devices to effectively harness these energy sources making their contribution to the world energy supply more relevant. The sustainable and widespread use of energy from renewable sources will depend increasingly on electrochemical energy storage technologies, like batteries and supercapacitors [2]. Along with this aspiring goal, it is important to consider that, in the development of these devices, the materials used need to be not only high-performance materials but also low-cost and environmentally friendly [3].

1.1. Supercapacitor's fundamentals

1.1.1. Supercapacitor's role in energy storage

Supercapacitors, also referred to as electrochemical capacitors, have received great attention due to their unique characteristics such as their simple configuration, long lifetime, and their capability to charge/discharge within seconds [4]. Usually compared to other energy storage devices (such as batteries, fuel cell, among others [4]), supercapacitors stand out themselves in terms of their high-power density (generally higher than 10 kW kg^{-1} [2]) and their long-life cycle (around 100 000 cycles [2]), especially when compared to batteries. They also have a higher energy density by comparison with conventional dielectric capacitors, thus supercapacitors fill in an existing gap between conventional capacitors and batteries as it can be seen in the Ragone plot, presented in **Figure 1**. In practical terms, supercapacitors restore the stored energy faster than a battery and store more energy than a conventional capacitor [2,4].

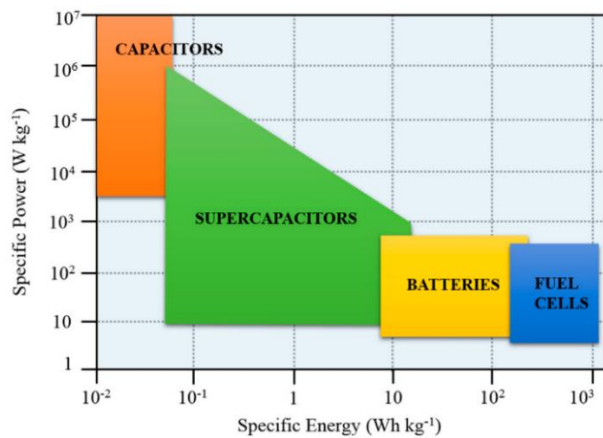


Figure 1. Ragone Plot, [4].

As a general definition, a capacitor is a device that stores energy based on the separation of charges in an electric field and that releases those stored charges (energy) in the form of electric current when necessary.

Supercapacitors are a particular type of capacitor and can be distinguished by several ways such as the charge storage mechanism, the dielectric nature, the cell structure, and the electrode material [2].

Classical **electrostatic capacitors**, often denominated as condensers, consist of two parallel electrodes, separated by a thin dielectric material (e.g., air, paper, polyester, and ceramic). When a voltage is applied between the two electrodes of the capacitor, the dielectric material becomes polarized. This means that, the positive charges of the dielectric material orient themselves towards the negative electrode and the negative ones shift towards the positive electrode, until the charges are balanced between the two electrodes, creating an internal electric field established due to the charge separation. With this polarization, the concept of capacitance arises as the energy storage through electrostatic accumulation of charges [2,5]. In **Supercapacitors**, in particular Electric Double Layer Capacitor (EDLC), the electrodes polarization leads to the accumulation and adsorption of ions in the surface and porosity of the electrodes with opposite charge (cations establish at the negative electrode and anions establish at the positive electrode). In contrast, **batteries** store energy through chemical reactions occurring at the electrode/electrolyte interface in which oxidation and reduction electrochemical reactions and intercalation/deintercalation occur, therefore it involves the conversion of chemical energy into electrical energy.

A schematic illustration of a battery (a), electrostatic capacitor (b) and supercapacitor (c) is presented in **Figure 2**.

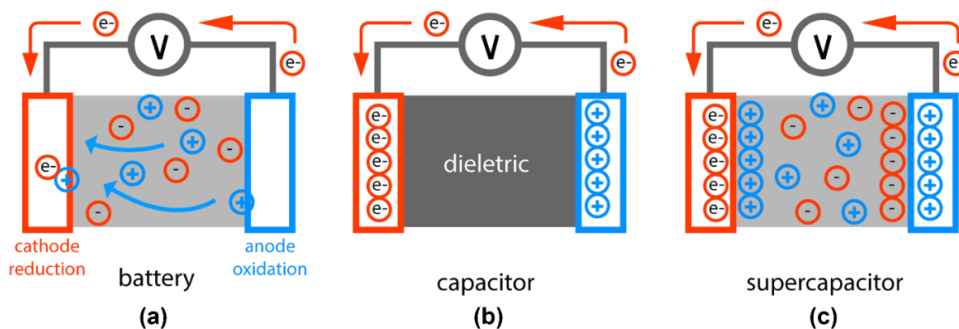


Figure 2. Schematic representation of a battery (a), a capacitor (b) and a supercapacitor (c). Adapted from [6].

As a consequence of their distinct properties, supercapacitors can be used in a large variety of applications. Applications associated with oscillating and fast power demand and delivery are favourite for supercapacitor usage. Electric transportation, renewable energy (harvest and energy storage) and electric grid (voltage regulation and microgrids) are main fields for supercapacitor application [7].

Since their first commercialization in 1971 to provide backup power for computer memory, a wide variety of fields benefit from supercapacitors for energy support. In 1970s decade, supercapacitors were essentially used for memory backup applications. However, with the improvement of electrode materials, supercapacitors started being included in military applications in the beginning of the 1980s. The continuous improvement of the supercapacitor materials and, consequently, of its performance, allowed to expand the areas of application of supercapacitors. From small devices such as photographic flashes in digital cameras, computers,

GPS, smartphones, medical defibrillators, to higher scale applications such as electric transportation, electric grid and renewable energy, supercapacitors contribute to an efficient energy storage and supply [8,9].

Navarro *et al.* [7], classified the scientific publications regarding supercapacitors in a 10 year period (2011-2021), and they obtained four main fields of study. As summarized in **Figure 3**, electric traction represents more than half of these studies, followed by power grid applications. The third more relevant application group is related to renewable energy generation and finally autonomous power systems, ships, and aircraft applications. The three above mentioned main interest applications for supercapacitors (electric transportation, renewable and electric grid) represent not only the three main fields of investigation for supercapacitor application but they also together represent almost 90% of these scientific studies [7].

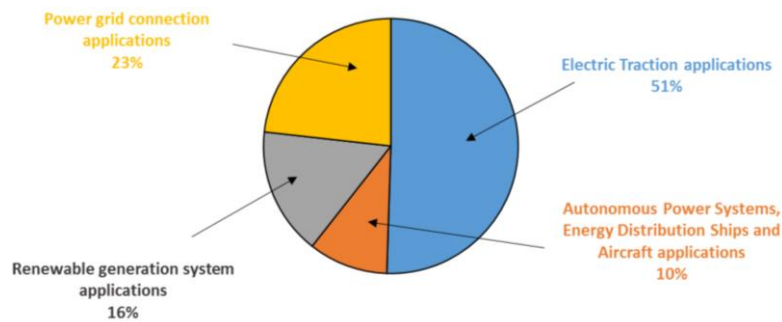


Figure 3. Publications related to supercapacitor applications released between 2011 and 2021 [7].

The transportation field is intrinsically connected to repetitive moments of acceleration and braking, which implies different energy needs in a short period of time. The same problem is associated with renewable energy, once they are dependent on climate phenomena, and, for this reason, their energy supply is unpredictable and therefore dependent of energy storage devices (ESD). When in both these cases batteries are the only ESD used, they are exposed to high-stress levels, and as a consequence their lifespan is shorten. However, if a supercapacitor is coupled with a battery, the fast response of the supercapacitor can stabilize the rapid changes of energy, providing a constant power injection to the battery, protecting it. In this way, it is possible to profit from a high specific power (fast charge/discharge) of the supercapacitor and also from the high specific energy of the battery (high amount of energy stored), lowering the cost of battery replacement and maintenance. Also, when only batteries are used, the power needs highly influence the size and weight of the battery (which is a problem specially for mobility purposes). In this way, the supercapacitor coupling allows a more compact system [5,8].

Power oscillations in the electric grid (that can arise, for example, from renewable energy sources) not only lower the grid efficiency, but they can also result in significant voltage drops and frequency fluctuations throughout the whole system. Supercapacitors can be used as a buffer at the interface between the load and the grid to solve this issue [8].

Some commercial applications of supercapacitors are listed below:

- *Ultracapbus*: In 2001 in Nuremberg, Germany had the first hybrid bus in Europe using a supercapacitor to capture energy during braking and delivering it back to start the vehicle [9];
- *Capabus*: Since 2006, electric public bus using a supercapacitor as the only power source is used in Shanghai. At the passenger pickup/drop-off station the busses are charged overhead [5];
- In 2005, *Diehl Luftfahrt Elektronik GmbH* chose supercapacitors to power emergency actuators for doors and evacuation slides in aircrafts, including the *Airbus 380* [8];
- *Toyota* came up with a hybrid racing car using a supercapacitor: the *Toyota Supra HVR* used in Hybrid Electric Vehicle (HEV) motorsport [5];
- Japan's Niigata Prefecture streetlights use supercapacitors to store solar energy and supply LED lamps overnight [9];
- *Toyota Yaris-R concept* car uses a supercapacitor to provide bursts of power [8];
- *PSA Peugeot Citroen* uses a supercapacitor as part of its stop-start fuel-saving system allowing a faster initial acceleration [9];
- *Mazda's i-ELOOP* system stores energy in a supercapacitor during deceleration and uses it to power onboard electric system [8];
- In 2014, China started to use trams powered with supercapacitors recharged in 30 seconds storing energy to run the tram for up 4 km enough to reach the next stop for the next recharge [8];
- Samsung Galaxy Note 9 S Pen stylus has a supercapacitor to charge within 40 seconds enough to be used within 30 minutes [5].

American supercapacitor manufacture, Maxwell Technologies, claims that there are more than 20 000 hybrid buses using supercapacitors to increase acceleration [8].

Although, supercapacitors have many great characteristics and a vast field of application, one of their main challenges is their low energy densities (commercial EDLCs typically have an energy density less a 10 W.h.kg^{-1} [2]) when compared with batteries and fuel cells as can be seen in **Figure 1**. Therefore, supercapacitors have their independent use limited. In order to further expand the ultracapacitors applications, a major effort needs to be done to improve their energy density, namely through the development of the new electrodes material and electrolytes [2]. In **Section 1.2** the influence of the electrolyte in the supercapacitor performance will be discussed in more detail.

1.1.2. Types of supercapacitors, Working Principles and Structure

In order to understand the influence of electrolytes in the overall supercapacitor performance, it is fundamental to firstly introduce the supercapacitors working fundamentals and structure. The most common classification of supercapacitors is based on their charge storage mechanism. According to this classification, there are three main types of supercapacitors: Electrochemical Double Layer Capacitors (EDLC), Hybrid Capacitors and Pseudocapacitors, being the EDLC the most mature technology and therefore the most commercialized one [2]. For this reason, EDLC will be covered in more detail.

(i) Electric Double Layer Capacitor, EDLC

Development of the Electric Double Layer model

The term “double-layer” was firstly introduced in the nineteenth century by von Helmholtz regarding his studies in colloidal particles. However, it was only in 1957 that EDLC was firstly described by Becker. To understand the working principle of an EDLC it is fundamental to understand the electrochemical phenomena occurring at the electrode/electrolyte interface. Considering the first proposed double layer model by Helmholtz, the Electric Double Layer (EDL) model has been developed with the contribution of Gouy and Chapman, Stern, Grahame and Bockris et al. In its pioneer theoretical attempt to explain the EDL phenomena, Helmholtz proposed that the electrode charged interface would attract the free counter-ions present in the electrolyte and repel the co-ions that will accumulate in the opposite electrode/electrolyte interface as a result of the coulombic interactions. According to Helmholtz, the distance between the electrode/electrolyte charged layers are dependent of the ion charge density (charge/size) and that there is no electron transfer between the electrode/electrolyte interface or chemical reaction [10]. The charged electrode interface along with the resulting layer of counter-ions in the electrolyte is called Electrical Double Layer (EDL) [11]. The EDL Helmholtz structure is similar to that of a conventional capacitor, and therefore the capacitance, C_H , is given by:

$$C_H = \frac{\epsilon_r \epsilon_0 A}{d} \quad (1)$$

where ϵ_r is the relative dielectric constant of the electrolyte, ϵ_0 is the dielectric constant of the vacuum ($8.854 \times 10^{-12} \text{ F/m}$), d is the thickness of the EDL and A is the surface area of the electrode.

Equation (1) demonstrates that the Helmholtz EDL theory does not consider the electrolyte concentration and the applied voltage's effects on the capacitance, which is inconsistent with the independent experimental observations made by Gouy and Chapman at the beginning of the 20th century [2]. The Gouy-Chapman model (GC model) considers the adsorption of the electrolyte ions at the surface of the electrode and considers its thermal motion and diffusion in solution, and consequently, the strictly distributed charges in the electrode side is balanced by a “diffuse layer” of counter-ions in the electrolyte [2,11,12]. The GC-model uses the Boltzmann equation to determine the concentration profiles of ions and the Poisson equation to relate the charge density with the potential, being the capacitance given by

$$C_D = \left(\frac{2 \epsilon \epsilon_0 z^2 e_0^2 c_0}{kT} \right)^{1/2} \cosh \frac{ze_0 \Psi_M}{2kT} \quad (2)$$

where z is the ionic valence (coulomb), c_0 is the ion concentration in the bulk, e_0 is the electron charge (1.6×10^{-19} Coulomb), k is the Boltzmann constant (1.38×10^{-23} J/K), T is the temperature (K), and Ψ_M is the potential at the metal surface (Volts). With this, the GC-model can explain the effect of the applied potential and the effect of temperature on the capacitance. However, this model considers that the ions are point charges (no ionic volume), meaning that near the electrode surface a greater number of charges is considered leading to an overestimation of the capacitance [11].

To overcome the limitations of the Helmholtz EDL model and the GC model, in 1924, Stern proposed a combination of the two models, suggesting that the formation of the EDL implies two distinct layers in the electrolyte side. The first layer is a stagnant compact layer of adsorbed ions with finite size (Helmholtz layer or Stern layer) and the second layer is a diffuse layer of ionic species [2,11]. Taking this into account, the overall capacitance, C_T , of the double-layer is the result of the capacitance of the Helmholtz layer, C_H , and the capacitance of the diffuse layer, C_D :

$$\frac{1}{C_T} = \frac{1}{C_H} + \frac{1}{C_D} \quad (3)$$

Considering equation (3) the smallest capacitance will determine the overall capacitance, and therefore, C_H will determine the overall capacitance at high potentials or high electrolyte concentrations while the contribution of C_D for the total capacitance is more significant less concentrated solutions [2].

In 1947, Grahame added to the Stern EDL model the effect of cations/anions and solvent in the formation of the EDL, since as most cations are generally smaller than anions, cations have a propensity to have a larger solvation shell. For this reason, cations and anions exhibit different distances to the electrodes surface. This led Grahame to separate the Helmholtz layer into an inner Helmholtz layer, where ions are adsorbed, and an outer Helmholtz layer, where ions are solvated, and thus Grahame EDL model is also referred to as electrical triple layer model (ETL). Bockris et al. further proposed the presence of the solvent in the inner Helmholtz layer, since these molecules are strongly oriented as a consequence of the proximity to the charged electrode surface [2,11]. This model representation is shown in **Figure 4**.

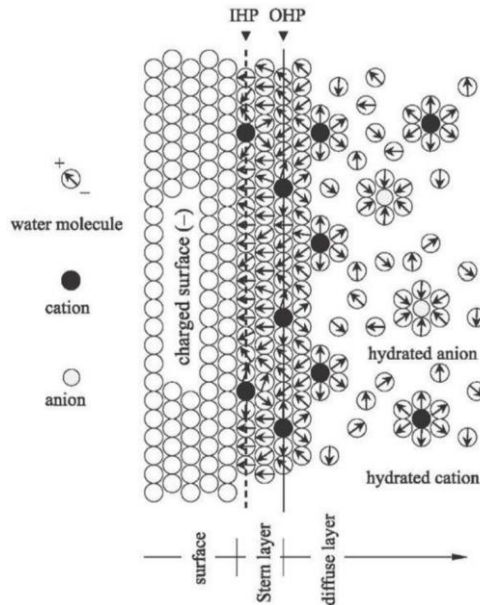


Figure 4. Brockis et al. EDL model representation [13].

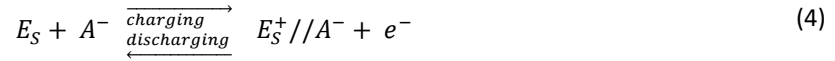
As described until now the EDL structure and formation is dependent of several factors, and therefore this model is still under discussion and development. Although the described EDL models provide a fundamental insight for the development of high-performance EDLC supercapacitors, they are all based on planar electrodes.

Typical EDLCs use porous carbon with high specific surface area (SSA) in order to maximize the contact between the electrode and the electrolyte.

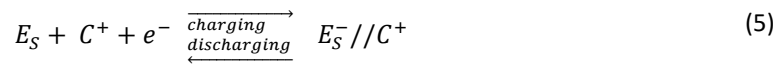
EDLC working principle and structure

The following equations (equations (4) to (6)) represent the charging/discharging processes of an EDLC.

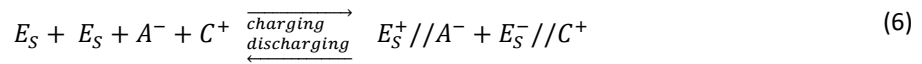
Negative Electrode



Positive Electrode



Overall



E_S represents one electrode surface, // represents the electric double layer (EDL), A^- represents the anions of the electrolyte and C^+ represents the cations of the electrolyte [14].

During the charging process, electrons flow from the positive electrode to the negative electrode via an external energy source. Simultaneously in the electrolyte, cations move to the negatively charged electrode while the anions move to the positive electrode, forming an EDL near each electrode, balancing charges, and storing energy. The charging process implies an increase in the cell voltage [14,15]. The process of discharging implies the release of the stored energy through the opposite order of events that occurs in the charging process. Therefore, during the discharging process, electrons flow from the negative electrode to the positive electrode through an external circuit and the adsorbed ions on the electrode surface return to the bulk electrolyte [14,15].

Figure 5 illustrates the typical structure of an EDLC and the respective previously described charging/discharging processes. Beyond the electrodes, respective current collectors, and electrolyte, an EDLC cell structure presents a separator (membrane) that separates the two electrodes preventing short circuit but allowing ion migration.

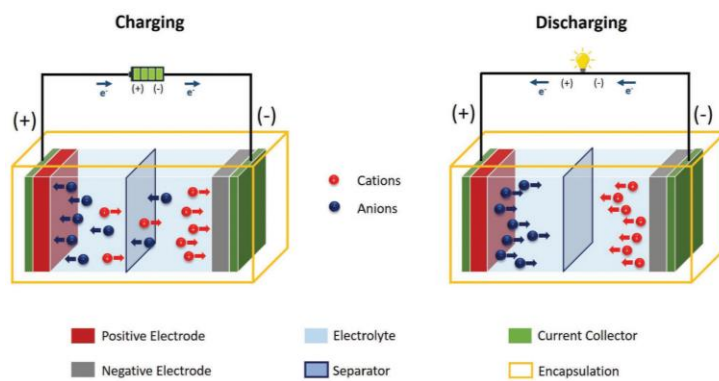


Figure 5. Schematic representation of the charging and discharging process in an EDLC, [15].

The electrostatic mechanism of an EDLC implies that, ideally there is no charge transfer across the electrode/electrolyte (non-faradaic mechanism) and, for this reason, there is almost no structural or volume change in an EDLC cell [2]. The EDLC charging and discharging processes are not as kinetically restricted as chemical reactions, and hence they are highly reversible, and the storage and release of charges is very fast, leading to a high-power density ($> 500 \text{ W/kg}$) and long-life cycles (usually between 10^5 and 10^6). However, since the charge storage occurs through a physical process and is limited by the available electrode/electrolyte interface, EDLCs have much lower energy densities ($<10 \text{ Wh/kg}$) than batteries ($35\text{-}150 \text{ Wh/kg}$) [2]. To address this limitation, more recent types of supercapacitors, such as Pseudocapacitors and Hybrid Capacitors, have shown an improvement in the energy density.

(ii) Pseudocapacitor

Pseudocapacitors, also known as faradaic or redox supercapacitors, store energy not through the separation of charges as occurs on the EDLC but mainly through fast and reversible redox reactions on the surface or near the surface of electroactive materials [16]. In this type of supercapacitors, the active material of the electrodes is usually metal oxides and hydroxides, being ruthenium oxide (RuO_2) the first and most extensively studied pseudocapacitive material used. However, Ru is an expensive and rare metal, thus less expensive alternatives such as manganese oxide, nickel oxide have been studied as possible alternatives [2].

Electrode materials that display faradaic behaviour can be classified as either pseudocapacitive or battery-type materials based on differences in kinetics. For electrodes with pseudocapacitive behaviour, the charge storage mechanism is confined to the electrode surface (or near) and, therefore, it is not a diffusion-controlled process as it is in battery type materials. For this reason, although a pseudocapacitor working principle is similar to those of a battery, as it requires charge transfer across the electrode/electrolyte interface, the voltage response in pseudocapacitors is faster exhibiting capacitor-type characteristics, such as rectangular cyclic voltammetry curves and charge/discharge curves similar to EDLC [15,16].

Since the origin of the capacitance in pseudocapacitors does not arise from electrostatic charge separation, often the capacitance in pseudocapacitors is referred to as pseudocapacitance [2]. Pseudocapacitors present a capacitance that can be 10 to 100 times greater than that obtained in conventional EDLCs, leading to an enhancement of the energy density. However, because faradaic processes are often slower than purely

electrostatic processes, pseudocapacitors typically have lower power densities when compared to EDLCs. [2]. Additionally, the frequent oxidation and reduction processes on pseudocapacitors have a propensity to modify the structure of the electrode and the electrolyte, which reduces the cycle stability [16].

(iii) Hybrid Supercapacitor

The above mentioned electrochemical capacitors consist of two electrodes of the same type (capacitive materials in the case of the EDLC or pseudocapacitive material in the case of Pseudocapacitors) having a symmetrical configuration. In contrast, hybrid supercapacitors are composed of electrodes of dissimilar material, some common electrode combinations are: one EDL electrode with a pseudocapacitive electrode; an EDL electrode with a battery-type electrode and a pseudocapacitive electrode with a battery-type electrode.

A schematic representation of the electrochemical signature of the different types of supercapacitors is presented in **Figure 6**. This voltammograms demonstrate that for an EDLC supercapacitor, a rectangular shape voltammogram is obtained and no redox peaks are obtained as in the case of batteries.

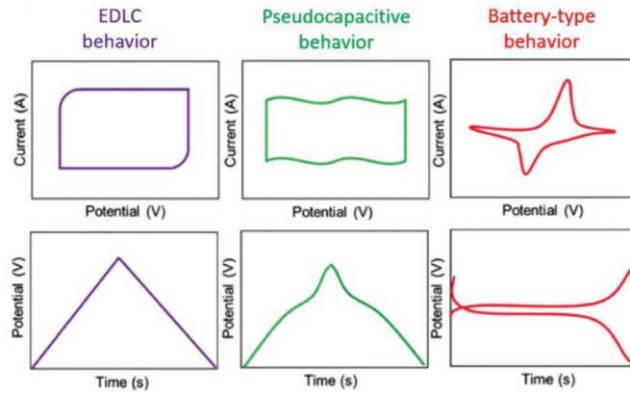


Figure 6. Illustrative cyclic voltammograms of EDLC, Pseudocapacitor and battery. Source: [15].

1.1.3. Supercapacitor performance parameters

Despite the general definitions of the performance parameters, these can be adjusted depending on the type of supercapacitor (EDLC, pseudocapacitor or hybrid), and even on the cell assembly (two or three electrodes). The following description of the performance parameter considers EDLC supercapacitor type (symmetric) and two-electrode testing cell.

Capacitance

As previously mentioned, capacitance is a measurement of the amount of energy stored in the form of accumulated charges at a given voltage. For conventional capacitors the capacitance, C , is proportional to the number of charges accumulated at each electrode (Q) and is inversely proportional to the voltage applied between the negative and positive electrodes [2]:

$$C = \frac{Q}{V} \quad (7)$$

However, for EDL and pseudocapacitance, the capacitance may not be constant with the variation of the voltage and therefore often the capacitance for one electrode is given as [2]:

$$C = \frac{dQ}{dV} \quad (8)$$

In industry, galvanostatic charge discharge (GCD) is the main method to determine the capacitance, however, it can also be determined through cyclic voltammetry (CV) and Electrochemical Impedance Spectroscopy (EIS). The determination of capacitance from each technique will be explain ahead in each corresponding section.

For a typical EDLC, the whole cell can be considered as two capacitors in series in which each electrode/electrolyte interface corresponds to a capacitor, and thus the overall capacitance is given by:

$$\frac{1}{C_T} = \frac{1}{C_+} + \frac{1}{C_-} \quad (9)$$

where C_+ and C_- correspond to the capacitances of the negative and positive electrode, respectively.

More often, the capacitance is given as specific capacitance which can be defined as gravimetric specific capacitance (C_g), volumetric capacitance (C_V) or normalized by the electrode surface area (C_A), being C_g the most commonly used and is given in Farad per gram (F/g) [2]. For one electrode the specific capacitance, C_{ge} , is given by

$$C_{ge} = \frac{C_{ie}}{m_e} \quad (10)$$

where m_e is the weight of the active material in one electrode and C_{ie} is the electrode capacitance.

For the whole system, the gravimetric capacitance, C_g , is given by merging equations (9) and (10)

$$C_g = \frac{C_{g+}m_+C_{g-}m_-}{(C_{g+}m_+ + C_{g-}m_-)(m_+ + m_-)} \quad (11)$$

where C_{g+} and C_{g-} are the gravimetric capacitances of the positive and negative electrode respectively, and m_+ and m_- are their respective weight [19]. Considering a symmetric cell in which both electrodes have the same weight and specific capacitance ($m_- = m_+ = m$) and ($C_{g+} = C_{g-} = C_{ge}$) [19], equation (11) rearranges to give

$$C_g = \frac{C_{ge}}{4} \quad (12)$$

For a two-electrode assembled cell, the cell capacitance is usually collected, C_T , and often in literature the specific capacitance is given per electrode, and therefore it can be calculated through the following equation

$$C_{ge} = 4 \frac{C_T}{m_{cell}} \quad (13)$$

where m_{cell} is the mass of the active material in both electrodes.

Energy and Power Densities

For supercapacitors the energy (E) and power densities (P) are theoretically given by equations (14) and (15) respectively [2]

$$E = \frac{1}{2} CV^2 = \frac{QV}{2} \quad (14)$$

$$P = \frac{1}{4R_s} V^2 \quad (15)$$

where V is the voltage applied across the two electrodes, Q is the total charge stored in the supercapacitor, C the overall capacitance and R_s is the equivalent series resistance (ESR). The energy density is usually expressed per mass Wh/kg or per volume Wh/m³ and the power density expressed in W/kg or W/m³.

From these equations, it can be seen that to increase the performance of a supercapacitor is fundamental to increase the applied voltage and the capacitance and decrease the resistance. From these parameters, the applied voltage has a dominant effect (proportional to the square of the operational voltage). Moreover, the resistance is highly dependent on the electrolyte because the conductivity of the electrolyte has a major effect on its resistance. Therefore, once that the maximum working voltage of the supercapacitor is determined by the electrochemical stability of the electrolyte [2] and the resistance is also largely influenced by the electrolyte, the performance of the supercapacitor is highly dependent on the electrolyte as it will be discussed in **Section 1.2**.

Life cycle

Life cycle of supercapacitors is an important parameter to evaluate its stability. Through several charging discharging cycles (Galvanostatic Charge-Discharge test) it is possible to compare the capacitance in the first cycles with the capacitance of the last cycles and evaluate how the performance was affected. EDLC using carbon electrodes tend to have at least 80% of the initial capacitance (capacitance of retention) after 10⁵-10⁶ cycles [2]. For pseudocapacitors and hybrid supercapacitors, the life cycle tends to be smaller because of the electrolyte/electrode interactions that lead to faster degradation, as mentioned above. Thus, the life cycle of supercapacitors is not only affected by the type of supercapacitor but also by the electrode and electrolyte materials and working conditions (temperature, voltage, scan rate and current) [2].

Equivalent Series Resistance

The Equivalent Series Resistance (ESR) is a combination of the various types of resistance present in the supercapacitor, namely the intrinsic resistance of the electrode material current collector and electrolyte, diffusion resistance of the ions, the contact resistance between the electrode and the current collector, and the ion transport resistance across the electrolyte [20]. As discussed earlier, the ESR will mainly affect the supercapacitor power density (equation (15)), the lower the ESR the higher the power density. Higher ESR values slows the charging/discharging process. For this reason, for applications that require fast response (high power density), ESR is a pivotal parameter. The bulk electrolyte resistance and the resistance between the electrode and the electrolyte tend to dominate the overall ESR, this effect is more critical for organic electrolytes, Ionic Liquids (ILs) and solid-state electrolytes [21]. Usually Electrochemical impedance spectroscopy (EIS) is a technique used to determinate the ESR.

Coulombic Efficiency

The coulombic efficiency is given by the ratio between the times of galvanostatic discharging and charging

$$\eta = \frac{t_D}{t_C} \times 100\% \quad (16)$$

t_D and t_C are the times of galvanostatic discharging and charging, respectively.

1.2. Electrolytes

The electrolyte choice for a certain supercapacitor highly depends on the working principle of this device (EDL, pseudocapacitive or hybrid), because this will determine if the electrolyte participates in faradaic processes. This subsection mainly focuses on the role of electrolytes in the EDLC supercapacitor type.

1.2.1. Influence of the electrolyte in the supercapacitor

In a supercapacitor, the electrolyte is a central component (by the nature of adsorbed ions), and therefore, its characteristics and interaction with the other components have an important effect in the overall supercapacitor performance. Even though the reported literature on electrolytes for supercapacitor application has suffered a large growth, especially in the last ten years, (**Figure 7**), the research on supercapacitor electrodes is more developed in comparison to that of electrolytes [2,22]

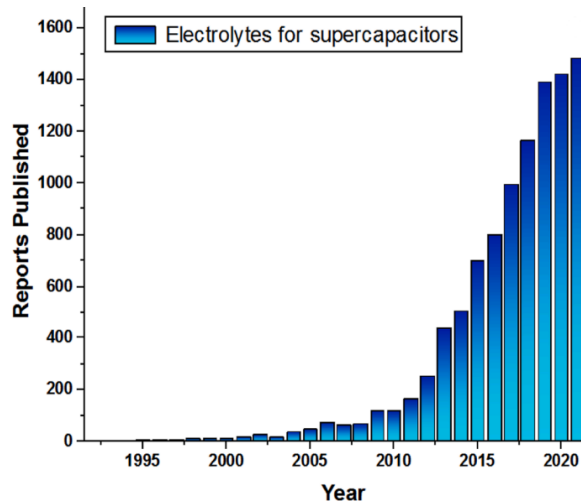


Figure 7. Number of articles per year related to “Electrolytes for supercapacitors” published between 1992 and 2021 [22].

The general design requirements of a supercapacitor electrolyte that need to be considered are: chemical and electrochemical stability, inertness to the other supercapacitor components (electrodes, current collectors, etc), affordability, high ionic conductivity, wide temperature operational range (thermal stability), safety (low volatility and flammability), and environmental friendliness [2,22]. However, it is challenging to find an electrolyte that fully satisfies all these requirements. As a result, a compromise between those requirements must be made in accordance with the final supercapacitor application.

The above described supercapacitor performance parameters (capacitance, equivalent series resistance (ESR), power density, energy density, operational temperature range and life cycling), **Section 1.1.3**, are largely influenced by the electrolyte used [2]. The formation of the EDL depends on the electrolyte ions (charge density, polarizability, size, and concentration), the solvent used, the interaction between the ion and solvent and the overall interaction between the electrolyte and electrode. Thus, all these aspects will influence the

supercapacitor performance, namely, the capacitance obtained [21], that as a consequence will affect the energy density (see equation (14)). On the other hand, the operational voltage of a supercapacitor is dependent on the electrochemical stability window of the electrolyte. Moreover, the energy and power densities will be also affected (see equations (14) and (15)) [2,23]. The ionic transport (related with mobility of the ions and viscosity of the electrolyte) affects the ESR of the supercapacitor, that as a consequence will also affect the power density (see equation (15)). Furthermore, the thermal stability of the supercapacitor is also highly dependent on the electrolyte once the operational window is limited by the boiling and freezing points of the electrolyte. Also, if the electrolyte is a salt solution the temperature will influence its solubility and transport properties.

The overall operational conditions (voltage, temperature, current, etc) and interaction between the electrolyte and electrode materials (for example side chemical reactions and wettability), have an effect on the supercapacitor performance and lifetime.

The electrolyte influence on the performance parameters of a supercapacitor is summarized in **Figure 8**.

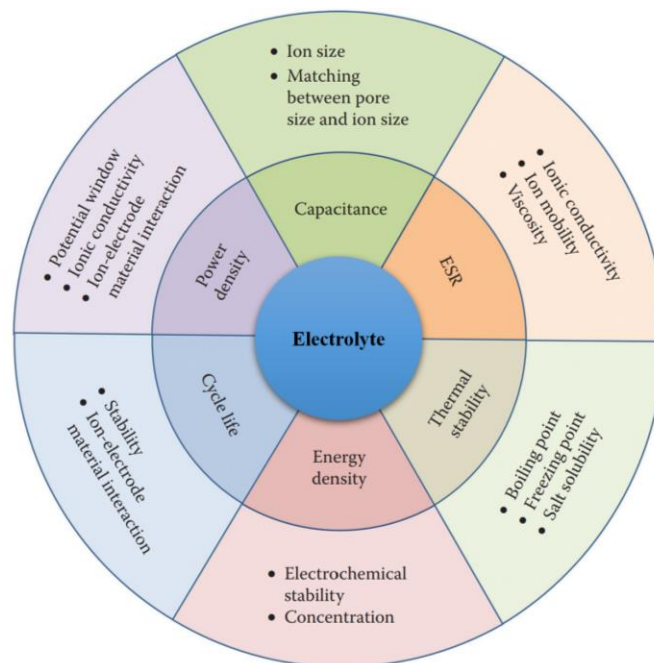


Figure 8. Electrolyte effect on the supercapacitor performance parameters. Adapted from [21].

To improve supercapacitors performance and variety, different types of electrolytes have been developed (each presenting its advantages and drawbacks), allowing supercapacitors to further penetrate the energy storage applications and market.

1.2.2. Types of electrolytes for EDLC supercapacitors

There is an enormous variety of electrolytes for supercapacitor application, from different physical states to wide chemical composition range, and thus a wide classification of electrolytes is presented in **Figure 9** [21].

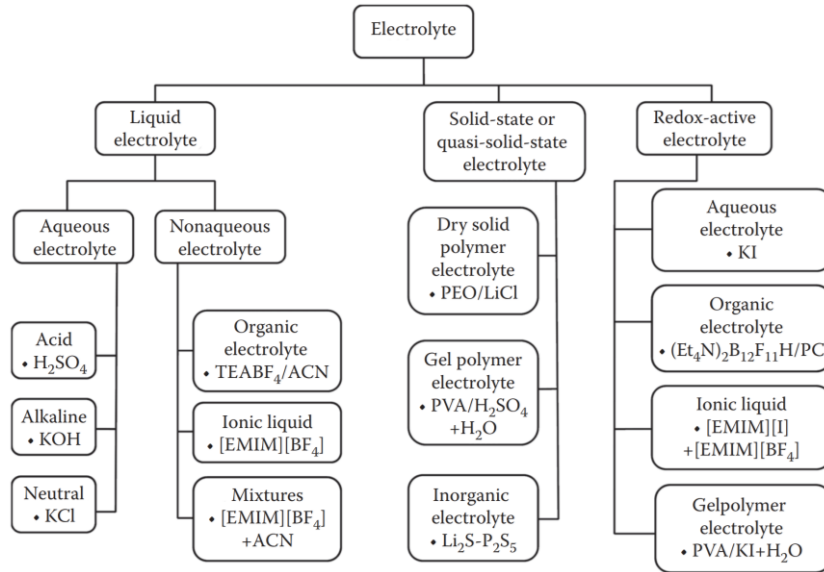


Figure 9. Electrolyte classification for Supercapacitors, each group gives the most used respective electrolyte as example [21].

Among the three main groups (Liquid, solid/quasi-solid-state and redox active electrolytes) presented in **Figure 9**, aqueous, organic, and ionic liquids (ILs) electrolytes are presented in two of these categories. Actually, this three groups (aqueous, organic and ILs) are considered the “traditional” electrolyte classification [22].

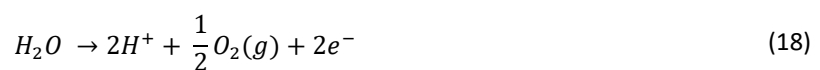
(i) Aqueous Electrolytes

Aqueous electrolytes were the originally used electrolytes in supercapacitors. However, nowadays organic electrolytes lead the supercapacitors market [22]. Aqueous electrolytes gather great characteristics such as their high ionic conductivity, low internal resistance (resulting on higher power density), they are generally more affordable, they are easy to handle once they do not need special conditions to be prepared (for example an inert atmosphere to avoid moisture), which greatly simplifies the assembly of supercapacitors. These electrolytes generally exhibit higher specific capacitance because of the small size of the solvated ions, allowing them to easily penetrate the carbon pores of the traditional electrodes [21,22].

The main drawback of aqueous electrolytes is their limited operating potential window due to the water hydrolysis potential (1.23 Volts), which as previously discussed, limits the energy and power densities [3,24]. Water hydrolysis consists in the water decomposition in hydrogen and oxygen:



This reaction is the result of two electrochemical reactions occurring in each of the electrodes of an electrochemical cell. At the positive electrode, occurs the oxygen evolution reaction (OER):



And at the negative electrode, the hydrogen evolution reaction (HER):



The minimum applied voltage (ΔE^0) that would trigger these reactions can be calculated by the following thermodynamic approach,

$$\Delta G = -nF\Delta E^0 \quad (20)$$

where ΔG process Gibbs free energy change, n is the number of transferred electrons and F is the Faraday constant. For the water decomposition process at 1 atm and 25 °C, the ΔE^0 calculated through equation (20) is 1.23 volts.

However, at the electrode/electrolyte interface, these electrochemical processes are more complex and the HER and OER reactions may involve other phenomena. For example, processes involving the adsorption of the species will require an additional applied potential (to overcome the additional free energy) for the reaction to proceed. Then the potential needed is higher than the original predicted by the thermodynamic approach. This excess potential is denominated as overpotential, η . The values of the overpotential vary with the electrode and electrolyte used. Furthermore, the interaction between the solvated ions and the water molecules will also contribute to further increase the overpotential for water composition. This interaction may be more significant for more concentrated solutions [24].

Thus, in practical terms a voltage higher than 1.23 V is required for water electrolysis to occur in aqueous electrolytes because of two main reasons:

- The hydrogen/oxygen evolution reactions need an overpotential on every electrode surface, and the overpotential magnitude varies greatly for various electrode materials.
- The process of water decomposition becomes more challenging due to the interaction of ions and solvents in electrolytes.

Taking advantages of these two mechanisms it is possible to develop water-based electrolytes operating at higher operational voltages [24].

The research on aqueous electrolytes is essentially divided on acidic, alkaline and neutral solutions, being the aqueous electrolytes of 5M H₂SO₄ and 6 M KOH and ~2M Na₂SO₄ the most used [19,22]. The alkaline aqueous electrolytes are the most widely used aqueous electrolyte type once, in comparison with acidic electrolytes, alkaline electrolytes allow the use of cheaper metallic materials (for example Ni) as current collectors. When compared with extreme pH electrolytes, neutral electrolytes have lower H⁺ and OH⁻ concentrations, which results in a higher overpotential for the OER and HER at activated carbon (AC), therefore neutral aqueous electrolytes have higher electrochemical stability than acid and alkaline aqueous electrolytes [2]. Moreover, neutral electrolytes provide greater safety and less corrosion [21]. Neutral electrolytes typically use salts that include Lithium (e.g. LiCl, Li₂SO₄), Sodium (e.g. NaCl, Na₂SO₄ and NaNO₃), Potassium e.g. (KCl, K₂SO₄ and KNO₃), Calcium (Ca(NO₃)₂) and Magnesium (e.g. MgSO₄) salts [21].

(ii) Organic electrolytes

Organic electrolytes for supercapacitors typically consist in conducting salts dissolved in organic solvents. Currently, commercially available supercapacitors use organic electrolytes because of their high voltage

window (typically 2.5-2.8 volts) that represents higher energy and power density [23]. Despite this, there are still many limitations associated with organic electrolytes, namely safety concerns related to their flammability, volatility, and toxicity when compared to aqueous electrolytes. Regarding some technical aspects, comparing organic and aqueous electrolytes, the first generally they present lower specific capacitance and conductivity, higher cost and they require the supercapacitor assembly to take place under controlled atmosphere to avoid impurities, especially moisture [2,22]. Typical commercial organic electrolytes are tetraethylammonium tetrafluoroborate (TEABF₄) dissolved in acetonitrile (ACN) or propylene carbonate (PC) [2].

(iii) Ionic Liquids

Ionic Liquids (ILs), often denominated as liquid at room temperature salts, are usually defined as compounds that are solely composed of ions (usually a large asymmetric cation and an organic or inorganic anion) resulting in a melting point lower 100 °C [2,25]. A large variety of cations and anions combinations make the physical and chemical properties of ILs highly tunable, and thus ILs can be designed to meet certain requirements of supercapacitors, some of them not possible to achieve using aqueous or organic electrolytes [25]. Generally, ILs have a highly ionized environment, negligible volatility, broad liquid temperature ranges, and a wide operating voltage window (around 4 volts). However, they usually present high viscosity, poor conductivity, and high costs [21]. One of the main drawbacks of ILs for supercapacitor application is that some are solid or highly viscous at room temperature, therefore room temperature ILs are more interesting for energy storage application. A solution to overcome this limitation consist of binary mixtures of ionic liquids that lead to the formation of a eutectic system allowing their use at room temperature [23]. The role of eutectic systems as electrolytes for supercapacitor application will further develop on **Section 1.2.3**. ILs used in supercapacitors are often Imidazolium, pyrrolidinium, ammonium, sulfonium, phosphonium as cations and tetrafluoroborate (BF₄⁻), hexafluorophosphate (PF₆⁻), bis(trifluoromethanesulfonyl)imide (TFSI⁻), bis(fluorosulfonyl)imide (FSI⁻), and dicyanamide (DCA⁻) as anions [2].

(iv) Solid electrolytes and quasi-solid electrolytes

New types of supercapacitors such as micro-supercapacitors, stretchable and flexible supercapacitors require the development of new electrolytes, namely semi-solid or solid-state. This new type of electrolytes, allows to expand the supercapacitor applications and addresses the problem of electrolyte leakage risk related to liquid electrolytes [2].

1.2.3. Eutectic mixtures as electrolytes for EDLC supercapacitor

Eutectic systems consist of combinations of at least two compounds, that through the establishment of hydrogen bonds form a new eutectic point with a melting point lower than those of each its individual components [26]. Therefore, eutectic mixtures allow benefiting from the properties of the pure compounds at room temperature. Since a large amount of compound combinations form a eutectic system, eutectic solvents are often denominated as “designer solvents”.

Recently eutectic mixtures have gained attention as potential candidates for supercapacitor electrolyte [27]. To the best of my knowledge, the first paper that studies eutectic mixtures as potential electrolytes for

supercapacitors was published in 2005 [28]. In this paper, eutectic mixtures of LiTFSI (lithium bis(trifluoromethane-sulfonyl) imide) with acylamino group compounds (acetamide; ethylurea; urea; methyl urea; 1,3-dimethylurea; 1,3-imidazolidinone) were studied as potential supercapacitor electrolytes.

Choline Chloride (ChCl)-based eutectic mixtures are one of the most studied eutectic systems as electrolyte for supercapacitor (for example ChCl-urea [29–31] and ChCl-Ethylene Glycol [32]), this mixtures are particularly interesting as their components are environment-friendly. Lithium salt-based eutectic mixtures have also been explored as electrolytes (for example LiTFSI:NMA(N-methyl-acetamide) [33]), however the problems associated with lithium scarcity turn this electrolytes less viable. Eutectic mixtures of ILs (for example pyrrolidinium nitrate [Pyr][NO₃] with pyrrolidinium bis(trifluoromethanesulfonyl)imide [Pyr][TFSI] [23]) are interesting electrolyte options as they may allow to expand the operating temperature of ILs which is usually pointed as one of their main drawbacks.

Table 1 and **Table 2** summarize pivotal performance parameters for different types of electrolytes.

Table 1. Conductivity of different electrolytes.

Electrolyte	Conductivity (mS/cm) at 25 °C	Ref
Aqueous, H ₂ SO ₄ (30 wt%)	750	[2,27]
Aqueous, KOH (6M)	510	[2]
Organic, TEABF ₄ in PC (1M)	13	[2]
Organic, TEABF ₄ in ACN (1M)	59.9	[2,27]
IL, EMIMBF ₄	14	[2]
Eutectic Mixture, ChCl:Urea (1:2)	1.3	[30]
Eutectic Mixture, ChCl:Urea (1:2) + 5wt%H ₂ O	16.8	[30]
Eutectic Mixture, LiFSI:Formamide (1:9)	11.5	[34]
Eutectic Mixture, NaNO ₃ : N-methyl-acetamide (1:9)	3.17	[33]

Table 2. Specific Capacitance, Potential operational window, energy and power densities for different electrolytes and respective electrode used in EDLC supercapacitors.

Electrolyte	Electrode	Specific Capacitance (F/g)	Operational Voltage (Volts)	Energy density (Wh/kg)	Power density (W/kg)	Ref
Aqueous, H ₂ SO ₄ (1 M, RT)	Activated Carbon	83 at 1 A/g	1	2.9	250	[35]
Aqueous, KOH (6M)	Activated Carbon	67 at 1 A/g	1	2.3	250	[35]
Organic, TEABF ₄ in ACN (1M)	Activated Carbon	124	2.5	28	-	[2]

IL, EMIMBF ₄	Porous carbon	147 at 1 A/g	3	11.4	98000	[35]
Eutectic Mixture, ChCl:Urea (1:2)	Three dimensional graphene like electrode	96 at 0.2 A/g	2.2	16	-	[30]
Eutectic Mixture, LiFSI:Formamide (1:9)	Activated Carbon	139 at 0.2 A/g	2.4	~30	~200	[34]

1.3. Electrochemical Characterization Techniques

A series of electrochemical techniques such as Cyclic voltammetry (CV), Galvanostatic charge/discharge (GCD) and Electrochemical Impedance Spectroscopy (EIS) have been used to extensively characterize and evaluate supercapacitors performance. These methods allow to determine key parameters such as capacitance, energy and power densities, life cycling, operating voltage, and equivalent series resistance (ESR).

1.3.1. Cyclic voltammetry

Cyclic voltammetry is a widely used technique for battery and supercapacitor research. In most common cyclic voltammetry tests, for a two-electrode (symmetrical configuration), a voltage is linearly applied between the positive and negative electrode and cycled inside a specific range (potential window) at a specific rate (speed at which the potential changes in mV/s) [36], then the resulting current flowing through the cell is measured. The data obtained through these tests are more often plotted as current (I , mili Amperes) as function of the voltage E (Volts), however it can be also plotted as the current (mA) or potential (V) as function of time (s) [36].

For an ideal supercapacitor, a constant sweep rate ($\pm E$) results in a constant and equivalent current ($\pm I$), hence the cyclic voltammogram has rectangle-shape pattern as presented in **Figure 10**.

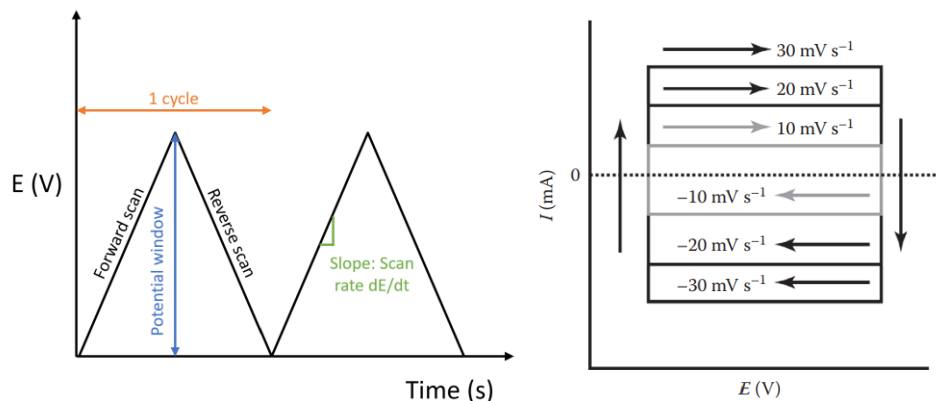


Figure 10. Left: Cyclic Voltammetry linear excitation signal. Right: Cyclic voltammograms at different sweep rates for an ideal capacitor [2].

Analysing the CV curves shape is an important approach to firstly evaluate qualitatively the performance of the electrolyte. Under real conditions, the CV curves deviate from the ideal case, [23,37], an example of real CV curve is presented in **Figure 11**.

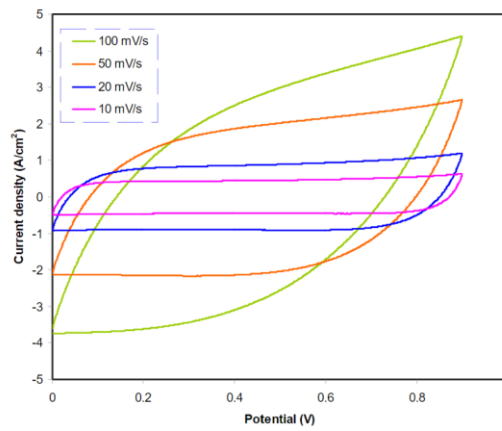


Figure 11. Cyclic voltammetry obtained for a solid electrolyte based on Natural Polymers in a EDLC supercapacitor with activated carbon electrodes [38].

As can be seen in **Figure 11**, the CV response of a supercapacitor is scan-rate dependent. For smaller scan rates, a plateau region is observed indicating that the ions move at slow and nearly constant rate and therefore, the ion insertion in the electrode porosity and the ion accumulation near the electrode surface develops without a significant influence of the ohmic resistance. As the scan rate increases, the plateau region gets smaller and CV curves tend to assume a “leaf-like” shape, revealing that the voltage is changing faster than the ions response to establish at the electrode surface [38,39]. Thus, the influence of ohmic resistance in the ion motion reflects as distortion of the rectangular shape [40].

Cyclic Voltammetry also allows to evaluate the electrolyte electrochemical stability through the variation of the voltage window. When a bump arises in the voltammogram indicating that the electrolyte started to degrade, **Figure 12** illustrates this phenomenon.

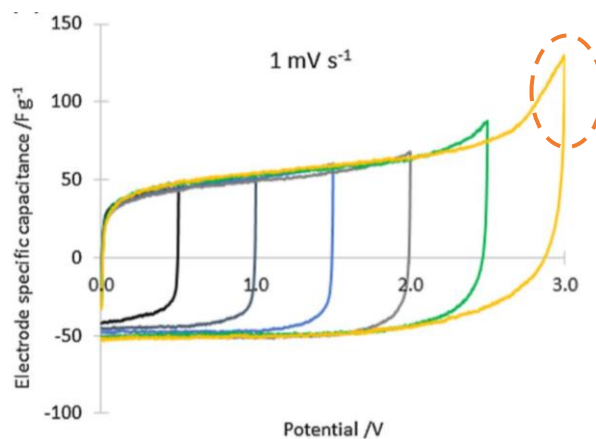


Figure 12. Cyclic Voltammetry for potential stability window studies at 1 mV/s for EDLC type of supercapacitors with 1M LiPF₆/EC:EMC 50:50 v/v electrolyte [41].

From cyclic voltammetry the capacitance can also be determined through the integration of the curve Current vs Potential:

$$C = \frac{\int I dV}{\Delta V \times \nu} \quad (21)$$

or using the curve Current vs time:

$$C = \frac{\int I dt}{\Delta V} \quad (22)$$

where I is the measured current (Ampere), ΔV the potential window (Volts), m the mass of the active material (g) and ν the scan rate (V/s) [2].

1.3.2. Galvanostatic charge-discharge

Galvanostatic charge-discharge (GCD) method is performed by charging and discharging the electrochemical cell at a certain current density, therefore the current ($I = \frac{dQ}{dt}$) is held constant and the voltage is measured. GCD method is often used to test the electrolyte and supercapacitor performance, it allows to determine the capacitance, the energy and power densities, the ESR and the life cycle [2]. The testing voltage range should be in accordance with the electrolyte electrochemically stable window, previously tested through CV [42].

As previously mentioned, in industry GCD is the main used technique to quantify the capacitance. For a two-electrode system the capacitance can be obtained by GCD through the following equation,

$$C = \frac{2I}{m \left(\frac{dV}{dt} \right)} = 2I \frac{\Delta t}{m \Delta V} \quad (23)$$

where I is the constant discharge current (A), $\frac{dV}{dt}$ is the slope of the GCD discharge curve and m is the mass of the active material (electrodes) [33].

The ESR can be calculated through the voltage drop occurring when the current changes from charging to discharging [43]. A typical charge-discharge cycle obtained in GCD is presented in **Figure 13**.

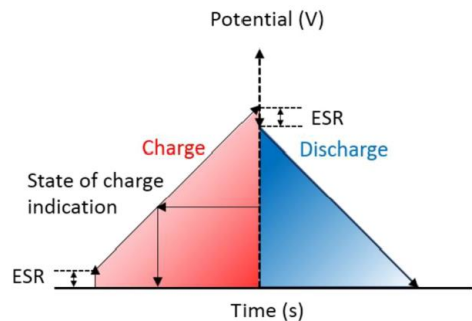


Figure 13. Typical charge-discharge cycle in GCD [20].

1.3.3. Electrochemical Impedance Spectroscopy

Electrochemical impedance spectroscopy (EIS) has been used for the characterization of the electrode, electrolyte, and interface between them. This technique is operated at an open-circuit voltage (OCV) imposing a time harmonic oscillating electric potential of small amplitude, $E(t)$, (usually less than 10 mV) applied over a wide range of frequencies (for example from 500 kHz to 5 mHz) and a resulting harmonic current density is measured, $I(t)$. The resulting current has the same angular frequency (ω) as the applied potential, however its signal as phase shift given by a phase angle, Φ [44].

$$E(t) = E_0 \sin(\omega t) \quad (24)$$

$$I(t) = I_0 \sin(\omega t - \Phi) \quad (25)$$

Transforming equations (24) and (25) into complex numbers through Euler's notation ($e^{j\omega t} = \cos(\omega t) + j\sin(\omega t)$), and applying the Re operator $E(t)$ and $I(t)$ are given by:

$$E(t) = \text{Re}[E_0 e^{j\omega t}] \quad (26)$$

$$I(t) = \text{Re}[I_0 e^{j\omega t} e^{-j\Phi}] \quad (27)$$

Impedance, Z , is the resistance obtained in an alternating potential/current system and is given by the ratio between potential and the current (analogous to ohms law), equation (28).

$$Z = \frac{E(t)}{I(t)} = \frac{E_0}{I_0} e^{j\Phi} = |Z|(\cos\Phi + j\sin\Phi) \quad (28)$$

This rearrangement allows to determine the real and imaginary of the impedance, equation (29), plotting the negative of the imaginary and the real impedance values, a Nyquist plot is obtained, **Figure 14**.

$$Z = \frac{E(t)}{I(t)} = Z_r + jZ_i \quad (29)$$

The Nyquist plot is the most common graphical representation of EIS technique. Once the measured current is result of different electrochemical phenomena, and since these processes occur with different time scales, they will have characteristic frequencies associated, represented in the Nyquist plot as different shapes at specific frequencies. The Nyquist plot for an ideal EDLC would be a vertical line corresponding to the double layer capacitance [43]. However, in real experimental conditions, three distinct zones are usually identified. At high frequencies, a semicircle is exhibited, followed by a 45° sloping line (Warburg region) at medium frequencies and finally in the low frequency region, a quasi-vertical line is observed [45]. In **Figure 14** a schematic representation of a typical (EIS) Nyquist plot is presented.

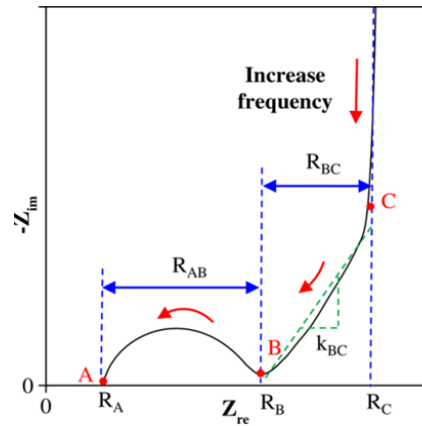


Figure 14. Typical Nyquist plots for EDLC supercapacitors [46].

The interception at the xx axis (R_A) represents the internal resistance, also called ESR (combination of various types of resistance in the supercapacitor, namely the intrinsic resistance of the current collector, bulk electrolyte resistance, among others) [43]. The origin of the semi-circle has been attributed to the electrode porous structures of the AC electrode, and to the resistance to polarization of the electrode and of the ions [45]. The Warburg zone (R_{BC}) is usually the resistance associated with the species diffusion resistance in the electrode porosity [33,47] The vertical shape at lower frequencies indicates a pure capacitive behaviour, representing the formation of the of the electrical double layer [3,43].

2. Motivation and Scope

Energy has been a major topic of active research in the past years as a consequence of the need to find solutions to an increasing energy world demand. The energy production paradigm has an urgent necessity of evolution towards higher efficiency and less environmental impact. Supercapacitors are presented as elite energy storage devices, whose unique characteristics bring new possibilities to attain the energy world demand. This being said, it is fundamental to study the supercapacitor components, namely the electrolyte, in order to optimize their performance. Moreover, studying electrolyte alternatives that are not only high performance but in which the components are environmentally compatible is a major goal. Eutectic mixtures, known for their high compound tunability, give the opportunity to search for environmentally compatible compounds with promising performance.

One of most studied eutectic mixture used in supercapacitor electrolytes is the Choline Chloride:Urea in a 1:2 molar ratio. These systems are particularly advantageous regarding its environmental friendliness, which is of major interest once the currently commercially available supercapacitors rely on organic electrolytes. In this study, mixtures of water and eutectic systems of sodium hexanoate with different carboxylic acids (hexanoic, octanoic, nonanoic and decanoic) are physically and electrochemical characterized in order to explore their possible use as electrolytes for supercapacitor. Analogous to the Choline Chloride: Urea eutectic systems, the studied eutectic mixture here presented are also constituted by environmentally compatible compounds. Moreover, since supercapacitors are increasingly included in applications of final consumer gadgets, solid and quasi-solid electrolytes are important to avoid leakage of the electrolyte. The eutectic systems here proposed, when mixed with water at certain compositions form gel mixtures as a consequence of their hydrophobic nature, making them candidates for a quasi-solid electrolyte without needing an additional supporting matrix as the case of Choline Chloride: Urea.

The following sections reunite in a first part a physicochemical study, including the phase-diagrams, conductivity, viscosity, density, surface tension and pH. In the second part, an electrochemical study is performed through Cyclic Voltammetry, Galvanostatic Charge-Discharge and Potentiostatic Electrochemical Impedance Spectroscopy techniques.

3. Methodology

3.1. Studied Eutectic Systems

Four types of eutectic solvents based on the mixture of an organic salt as Hydrogen Bond Acceptor (HBA) (sodium hexanoate) with a long alkyl chain carboxylic acid as Hydrogen Bond Donor (HBD) (hexanoic, octanoic, nonanoic and decanoic acids) were prepared through heating and stirring. When a clear liquid was obtained it was slowly cooled until ambient temperature, after this, new nine mixtures of each eutectic solvent combined with water were prepared, varying the water content from 10% to 90% of water in weight. The structures of the compounds used to prepare the eutectic solvents are presented in **Figure 15**.

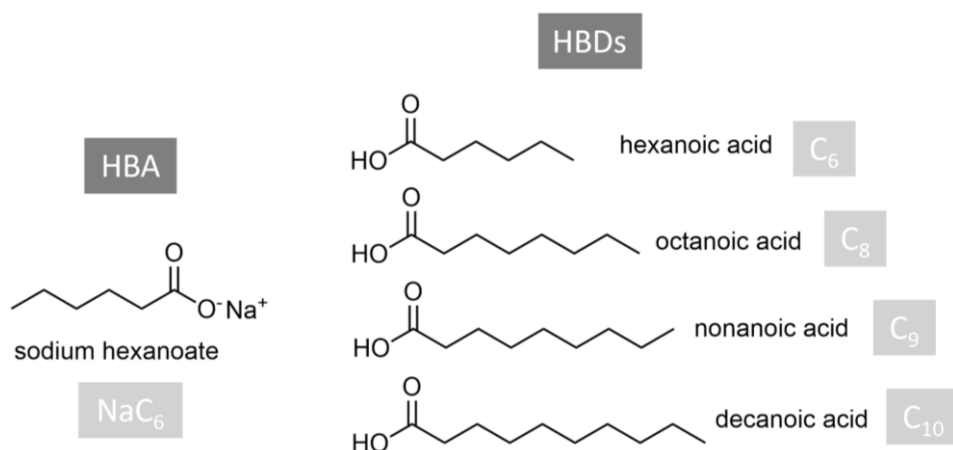


Figure 15. Chemical structures and respective acronyms of the species used to prepare the eutectic mixtures.

In a previous study developed with my collaboration [48], sodium hexanoate (NaC₆) with long chain fatty acids eutectic solvents, namely, octanoic acid (C₈), nonanoic acid (C₉) and decanoic acid (C₁₀), were characterized. The solid-liquid phase diagrams of these mixtures were built at ambient pressure allowing to determine the composition window in which these solvents are homogeneous liquids at ambient temperature.

To choose the composition (acid/salt ratio) of the starting eutectic mixtures for this work two aspects were considered: At room temperature, the initial eutectic mixture is liquid, and they contain the maximum amount of salt possible to benefit from the presence of the sodium ion for ionic conductivity purposes.

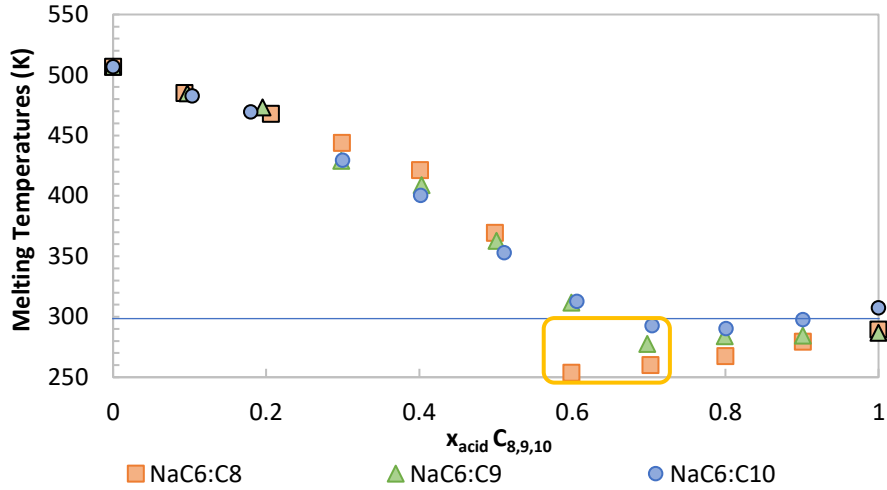


Figure 16. Solid-liquid phase diagram of the sodium hexanoate salt-based eutectic solvent with each acid presented in [48]. Black outlined points refer to data collected by DSC; remaining points collected through turbidimetry.

Figure 16 shows the solid-liquid phase diagram presented in [48], the blue line highlights the approximate ambient temperature (around 25°C). That said, it is possible to see that for these types of mixtures the eutectic point occurs between 0.6 and 0.7 molar of acid, occurring by order of length of acid chain (octanoic, nonanoic and decanoic), being the corresponding temperature as lower as smaller the acid chain.

Therefore, the eutectic point does not change greatly with the carboxylic acid (HBD), being the effect of the sodium hexanoate (HBA) predominant as stated in [48].

Considering that the length of the acid chain does not have a major effect on the eutectic composition occurrence and that, as previously stated, the size of the electrolyte ions can have a major effect in the overall supercapacitor performance, the combination of sodium hexanoate with hexanoic acid (NaC₆:C₆) was also studied for 0.6 and 0.7 molar composition in acid.

Taking this into account, the starting mixtures used were NaC₆:C₆ with $x_{\text{acid}}=0.6$ and $x_{\text{acid}}=0.7$, NaC₆:C₈ with $x_{\text{acid}}=0.6$ and $x_{\text{acid}}=0.7$, NaC₆:C₉ with $x_{\text{acid}}=0.7$ and NaC₆:C₁₀ with $x_{\text{acid}}=0.7$.

The eutectic mixtures used, and their respective acronyms are summarized in **Table 3**.

Table 3. Eutectic mixtures acronyms and respective description.

Eutectic mixture acronyms	Description
NaC ₆ :C ₆ (0.6)	Sodium hexanoate with hexanoic acid with 60% molar in acid
NaC ₆ :C ₆ (0.7)	Sodium hexanoate with hexanoic acid with 70% molar in acid
NaC ₆ :C ₈ (0.6)	Sodium hexanoate with octanoic acid with 60% molar in acid
NaC ₆ :C ₈ (0.7)	Sodium hexanoate with octanoic acid with 70% molar in acid
NaC ₆ :C ₉ (0.7)	Sodium hexanoate with nonanoic acid with 70% molar in acid
NaC ₆ :C ₁₀ (0.7)	Sodium hexanoate with decanoic acid with 70% molar in acid

3.1.1. Chemical Compounds

The sodium hexanoate ($C_6H_{11}NaO_2$) used to prepare the eutectic mixtures was synthesized through a saponification reaction using a sodium hydroxide in methanol solution and hexanoic acid also in methanol, the synthesis process is described in **Section 8.1** from Supporting Information.

The sodium hydroxide (NaOH) (CAS 1310-73-2) used in the sodium hexanoate synthesis was purchased from Eka, and the methanol (CH_3OH) (CAS 67-56-1) with 99.8% of purity was purchased from Sigma-Aldrich.

The hexanoic acid ($C_6H_{12}O_2$) (CAS 142-62-1) with 99% of purity was purchased from Aldrich, the octanoic acid ($C_8H_{16}O_2$) (CAS 124-07-2) with 99% purity was purchased from Acros Organics, the nonanoic acid ($C_9H_{18}O_2$) (CAS 607-197-00-8) with 97% of purity was purchased from Sigma and decanoic acid ($C_{10}H_{20}O_2$) with 99% of purity was purchased from Alpha Aesar.

3.1.2. Eutectic mixtures preparation

The eutectic mixtures of sodium hexanoate with long alkyl chain carboxylic acids were prepared adding the acid to the sodium hexanoate in a glass vial. Each compound was weighted in an analytical high precision Mettler Toledo (MS205DU) balance with an uncertainty of $\pm 10^{-4}$ g. Each mixture was slowly heated up with constant stirring using a Heidolph MR Hei-Tec heating-stirring plate, until a clear liquid phase was obtained. Then the heating was turned off allowing the mixtures to rest and slowly cool down until ambient temperature.

3.1.3. Eutectic-water mixtures preparation

The mixtures of eutectic and water were also prepared in glass vials adding to the eutectic mixture the water and weighted in the above mentioned balance. Then using a Labnet vortex mixer each water-eutectic combination was agitated. The water used to prepare these mixtures was ultrapure, double distilled water passed through a reverse osmosis system and further treated with a Milli-Q plus water purification apparatus.

3.2. Physical Characterization

Viscosity, density, surface tension, conductivity and pH data were collected for each sample, the technical aspects, equipment, and experimental conditions used for each technique will be described in the respective subsection.

3.2.1. Phase diagrams

Using a VWR thermostatic bath, the physical aspect of the samples was registered between -10°C and 60°C ($\pm 0.01^\circ\text{C}$).

3.2.2. Centrifuge

The centrifugation of the gel mixtures was carried out in a VWR CompactStar CS 4 centrifuge at 4500 rpm.

3.2.3. pH

The pH data was collected at 20°C using a *Consort SP28X* pH electrode connected to a *Consort multiparameter C3010 analyser*.

3.2.4. Viscosity

The viscosity measurements were carried out between 10°C and 60°C ($\pm 0.02^\circ\text{C}$) using an automatic Anton Paar® rolling-ball viscometer (*Lovis 2000 M/ME*). The viscometer was pre-calibrated with ultra-pure water. The uncertainty of the measurements was 2%.

3.2.5. Density

The density measurements were carried out between 10°C and 60°C ($\pm 0.02^\circ\text{C}$) using an Anton Paar® densimeter equipped with a digital vibrating tube densimeter. The densimeter was pre-calibrated with ultra-pure water. The uncertainty of the measurements was $2 \times 10^{-5} \text{ g}\cdot\text{cm}^{-3}$.

3.2.6. Surface Tension

Surface tension measurements were carried out by Du Noüy method using a K10ST Krüss digital tensiometer at ambient temperature with an 0.1 mN/m accuracy.

3.2.7. Conductivity

The ionic conductivity measurements were performed with a multichannel conductivity meter (*BioLogic*®, France) based on a frequency response analyzer (MCM 10) connected to a Peltier-based temperature control unit with ten slots (WTSH 10, Biologic). The measurements were conducted between -20°C and 50°C ($\pm 0.02^\circ\text{C}$) in sealed cells with Pt parallel-plate electrodes protecting the samples from air exposure.

3.3. Electrochemical tests

The electrodes used in the electrochemical tests were prepared with activated carbon (AC) from *Blue solution, France*, coated on aluminum, having a composition of AC/polyvinylidene difluoride/carbon black with an 80/10/10 wt ratio (wt: weight). The AC (*Blue Solution, France*) has a specific area of $1500 \text{ m}^2 \text{ g}^{-1}$ (BET) with an average pore size 1.17 nm. The average loading of AC per unit area is 5 mg cm^{-2} and the bulk density reaches $0.7 \text{ cm}^3 \text{ g}^{-1}$.

The cells were assembled in *Swagelok*® cells comprising two AC electrodes (diameter: 10 mm) and a *Whatman*® GF/C glass microfiber filter (thickness of 0.67 mm) as the separator as illustrated in **Figure 17**. The quantity of electrolyte added to each cell was approximately 150 μL .

Cyclic voltammetry (CV), Galvanostatic charge-discharge cycling (GCD), and potentiostatic impedance spectroscopy (PEIS) were conducted in cells by a computer-controlled multichannel potentiostat/galvanostat (VMP3, *Biologic*®, France).

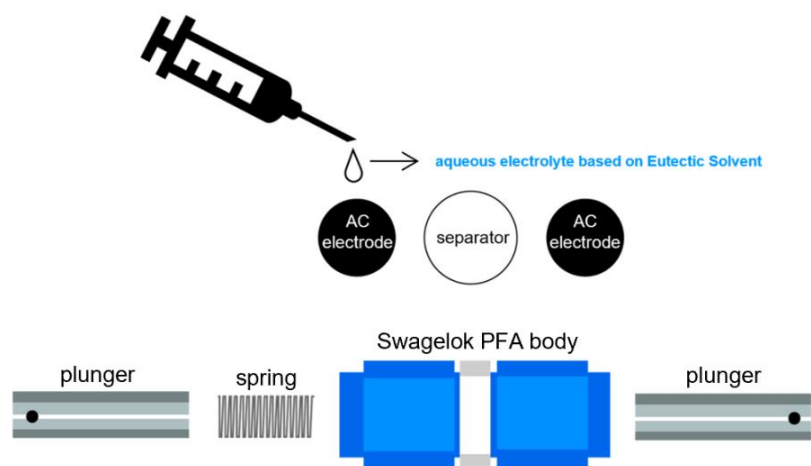


Figure 17. Schematic illustration of the Swagelok® cell used in the electrochemical tests.

The long-term cycling protocol by GCD cycles is performed at a normalized current density of 0.2 A g^{-1} or 0.1 A g^{-1} (normalized with respect to the mass of the activated carbon, 5.0 mg per electrode) for 5000 cycles. The CV was performed at 1, 5, 10 and 20 mV/s scan rates. PEIS was conducted between 500 kHz and 5 mHz (ten points per decade) at open-circuit voltage with an oscillating amplitude fixed at 5 mV. All EDLC devices were cycled under ambient conditions.

4. Results

4.1. Sample selection: Water composition and temperature sweep

As previously indicated, a supercapacitor's electrolyte has a significant impact in the operating temperature, and thus it is critical to monitor any changes, namely phase changes, occurring in the studied mixtures. Taking into consideration the hydrophobic nature of the initial eutectic systems, the water composition and temperature are crucial variables to consider ensuring the presence of a homogeneous media.

For each eutectic mixture, nine eutectic-water mixtures were prepared with a massic water composition ranging from 10wt% to 90wt% with an increment of 10%. From **Table 4** to **Table 9**, a summary of the analysed eutectic-water solutions along with the corresponding massic and molar composition in water is presented.

Table 4. Eutectic-water mixtures of $\text{NaC}_6:\text{C}_6(0.6)$ group and respective massic and molar compositions.

Eutectic Combination	massic water %	molar water %
$\text{NaC}_6:\text{C}_6(0.6)$	10	43.6
	20	63.5
	30	74.9
	40	82.2
	50	87.4
	60	91.2
	70	94.2
	80	96.5
	90	98.4

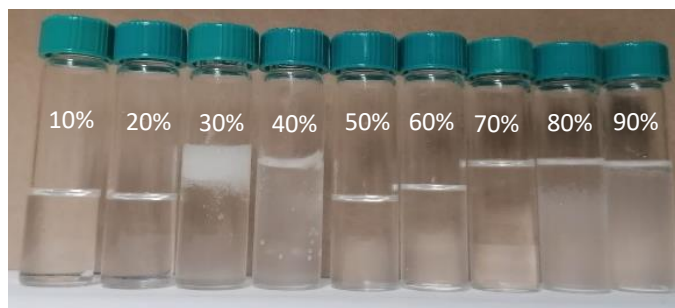


Figure 18. Eutectic-water mixtures of $\text{NaC}_6:\text{C}_6(0.6)$ group at ambient temperature ($\sim 20^\circ\text{C}$) identified by massic content of water.

Table 5. Eutectic-water mixtures of $\text{NaC}_6:\text{C}_6(0.7)$ group and respective massic and molar compositions.

Eutectic Combination	massic water %	molar water %
$\text{NaC}_6:\text{C}_6(0.7)$	10	43.3
	20	63.2
	30	74.6
	40	82.1
	50	87.2
	60	91.1
	70	94.1
	80	96.5
	90	98.4



Figure 19. Eutectic-water mixtures of $\text{NaC}_6:\text{C}_6(0.7)$ group at ambient temperature ($\sim 20^\circ\text{C}$) identified by massic content of water.

Table 6. Eutectic-water mixtures of $\text{NaC}_6:\text{C}_8(0.6)$ group and respective massic and molar compositions.

Eutectic Combination	massic water %	molar water %
$\text{NaC}_6:\text{C}_8(0.6)$	10	46.3
	20	65.9
	30	76.8
	40	83.7
	50	88.5
	60	92
	70	94.2
	80	96.9
	90	98.6

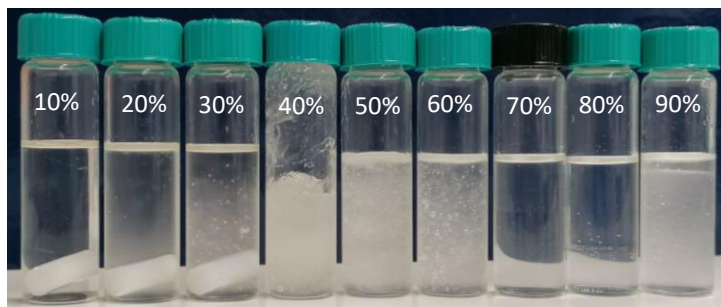


Figure 20. Eutectic-water mixtures of $\text{NaC}_6:\text{C}_8(0.6)$ group at ambient temperature ($\sim 20^\circ\text{C}$) identified by massic content of water.

Table 7. Eutectic-water mixtures of $\text{NaC}_6:\text{C}_8(0.7)$ group and respective massic and molar compositions.

Eutectic Combination	massic water %	molar water %
$\text{NaC}_6:\text{C}_8(0.7)$	10	46.7
	20	66.3
	30	77.3
	40	84.0
	50	88.7
	60	92.2
	70	94.8
	80	96.9
	90	98.6

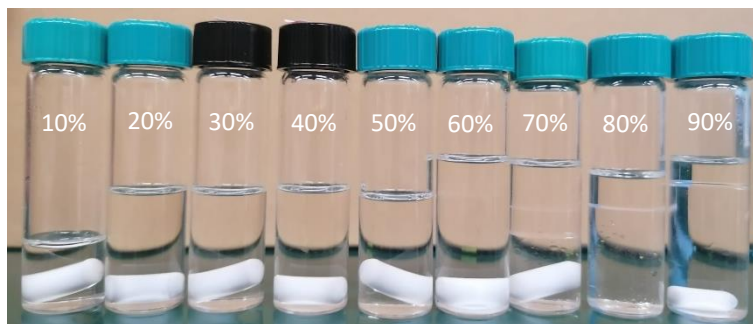


Figure 21. Eutectic-water mixtures of $\text{NaC}_6:\text{C}_8(0.7)$ group at ambient temperature ($\sim 20^\circ\text{C}$) identified by massic content of water.

Table 8. Eutectic-water mixtures of $\text{NaC}_6:\text{C}_9(0.7)$ group and respective massic and molar compositions.

Eutectic Combination	massic water %	molar water %
$\text{NaC}_6:\text{C}_9(0.7)$	10	48.7
	20	68
	30	78.4
	40	84.9
	50	89.5
	60	92.7
	70	95.2
	80	97.1
	90	98.7

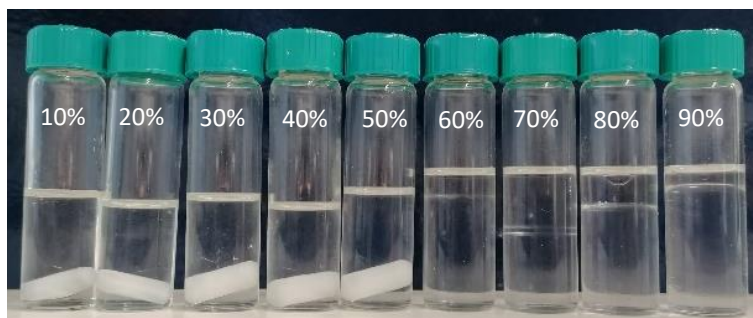


Figure 22. Eutectic-water mixtures of $\text{NaC}_6:\text{C}_9(0.7)$ group at ambient temperature ($\sim 20^\circ\text{C}$) identified by massic content of water.

Table 9. Eutectic-water mixtures of $\text{NaC}_6\text{:C}_9(0.7)$ group and respective massic and molar compositions.

Eutectic Combination	massic water %	molar water %
$\text{NaC}_6\text{:C}_{10}(0.7)$	10	50.6
	20	69.6
	30	79.6
	40	85.9
	50	90.1
	60	93.2
	70	95.5
	80	97.3
	90	98.8

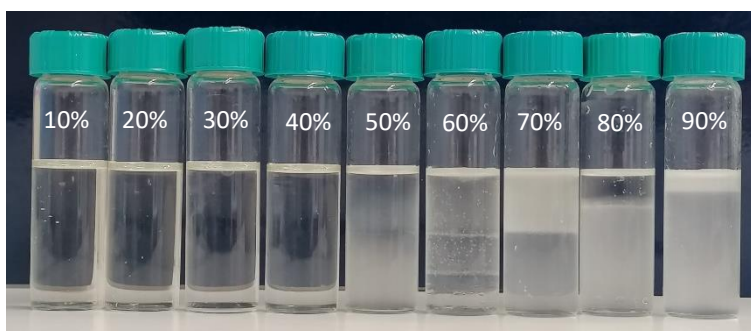


Figure 23. Eutectic-water mixtures of $\text{NaC}_6\text{:C}_{10}(0.7)$ group at ambient temperature ($\sim 20^\circ\text{C}$) identified by massic content of water.

During the preparation of each aqueous eutectic mixture it was observed that these mixtures can have various physical aspect as function of the water content and temperature, as it can be observed in **Figure 18** to **Figure 23**. Given this, the physical aspect of each mixture was investigated as a function of temperature from -10°C to 60°C with a sweep rate of 5°C . The observed physical aspect was registered at each temperature step (-10°C , -5°C , 0°C , 5°C , 10°C , 15°C , 20°C , 25°C , 30°C , 35°C , 40°C , 45°C , 50°C , 55°C and 60°C) after mixing and after about 10 minutes of resting at the corresponding temperature. With the collected observations it was possible to build drafts of sol-gel diagrams **Figure 24** to **Figure 29** and different physical state areas are proposed (1 phase, 2 phases, 3 phases, turbid gel and solid).

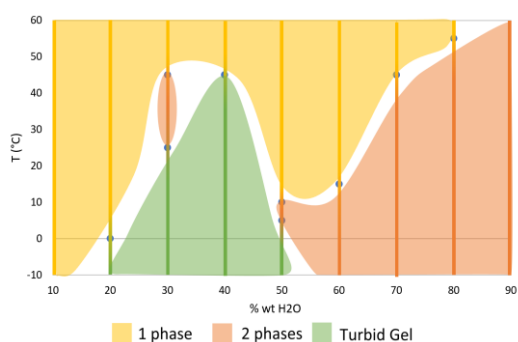


Figure 24. Phase diagram for the $\text{NaC}_6\text{:C}_6(0.6)$ eutectic-water group.

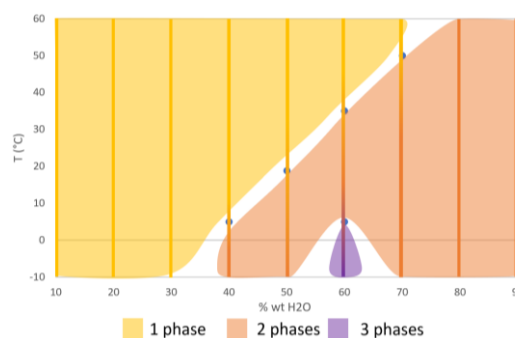


Figure 25. Phase diagram for the $\text{NaC}_6\text{:C}_6(0.7)$ eutectic-water group.

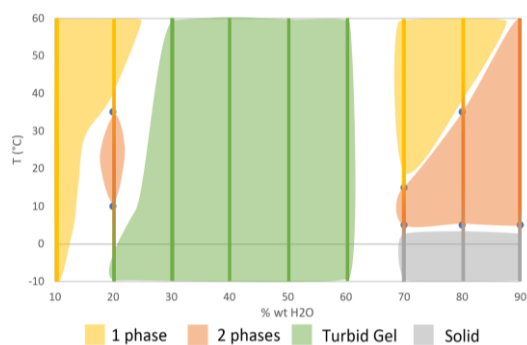


Figure 26. Phase diagram for the $\text{NaC}_6:\text{C}_8(0.6)$ eutectic-water group.

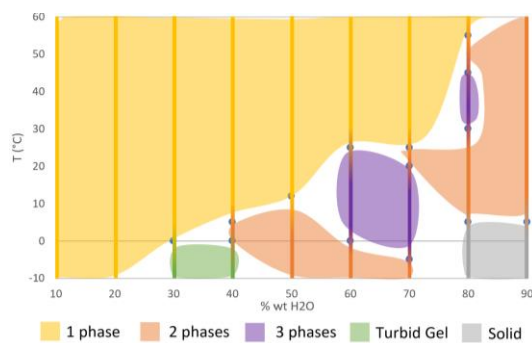


Figure 27. Phase diagram for the $\text{NaC}_6:\text{C}_8(0.7)$ eutectic-water group.

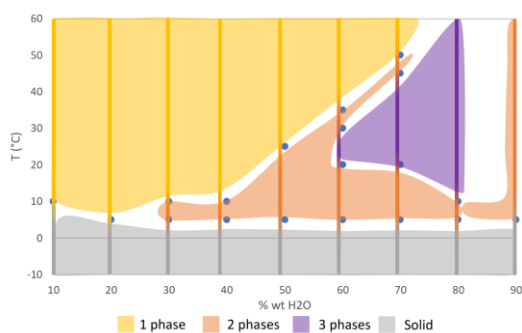


Figure 28. Phase diagram for the $\text{NaC}_6:\text{C}_9(0.7)$ eutectic-water group.

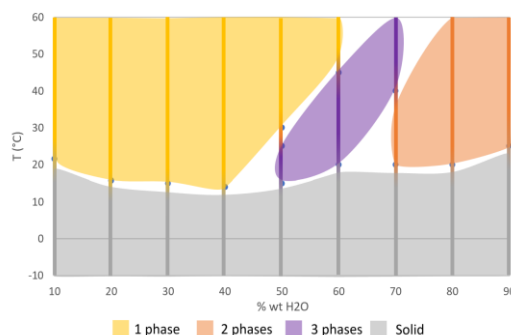


Figure 29. Phase diagram for the $\text{NaC}_6:\text{C}_{10}(0.7)$ eutectic-water group.

After the temperature sweeping for each water composition is possible to conclude that for groups in which the eutectic composition is 0.7 molar in acid, the occurrence of one liquid phase (yellow region) is wider. Also, for those eutectic compositions, 3 phases are observed when the water content ranges from 50% to 80%. On the other hand, the occurrence of a gel phase (green region) has a predominance in mixtures where the eutectic has a larger quantity of salt (0.6 molar composition in acid). Also, the longer the acid chain is, the larger is the solid phase (grey region) which compromises the possibility to have an electrolyte at low temperatures. As can be observed in **Figure 28** and **Figure 29**, for all water compositions, a solid phase occurs up to 5 °C and 20 °C, respectively. In general, the larger the water content and the lower the temperature, the greater is the probability to have phase separation and the use of these mixtures as electrolytes is compromised.

Considering the aforementioned considerations, the mixtures chosen to be studied were those that exhibited a homogenous phase (liquid or gel) in a high range of temperature. For gel mixtures, it was important to centrifuge them to evaluate their stability. The mixtures of $\text{NaC}_6:\text{C}_8(0.6)$ with 30 wt%, 40 wt%, 50 wt% and 60 wt% and $\text{NaC}_6:\text{C}_8(0.6)$ with 40 wt% of water where centrifuged at 4500 rpm (rotations per minute) for 30 minutes, only for 30 wt% of water phase separation was observed has shown in **Figure 30**.

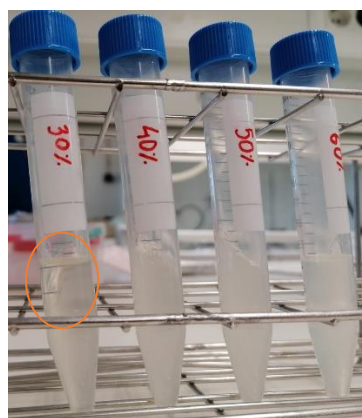


Figure 30. Mixtures of $\text{NaC}_6:\text{C}_8(0.6)$ with 30 wt%, 40 wt%, 50 wt% and 60 wt% of water after 30 min centrifugation at 4500 rpm. Orange circle evidences the occurrence of phase separation for the mixture with 30 wt% of massic water content.

The following table gives a summary of the mixtures that were selected to proceed with physical and electrochemical characterisation.

Table 10. Selected mixtures for further characterization.

Eutectic Combination	massic water %	molar water %	Salt concentration (M)	Physical aspect at 20 °C
$\text{NaC}_6:\text{C}_6(0.6)$	10	43.6	2.92	One liquid phase
	20	63.5	2.61	One liquid phase
	40	82.2	-	Turbid gel
	50	87.4	1.63	One liquid phase
	60	91.2	1.30	One liquid phase
$\text{NaC}_6:\text{C}_6(0.7)$	10	43.3	2.19	One liquid phase
	20	63.2	1.96	One liquid phase
	30	74.6	1.72	One liquid phase
	40	82.1	1.46	One liquid phase
	50	87.2	1.24	One liquid phase
$\text{NaC}_6:\text{C}_8(0.6)$	10	46.3	1.84	One liquid phase
	40	83.7	-	Turbid gel
	50	88.5	-	Turbid gel
	60	92.0	-	Turbid gel
$\text{NaC}_6:\text{C}_8(0.7)$	10	46.7	1.85	One liquid phase
	20	66.3	1.70	One liquid phase
	30	77.3	1.50	One liquid phase
	40	84.0	1.30	One liquid phase
	50	88.7	1.10	One liquid phase
$\text{NaC}_6:\text{C}_9(0.7)$	10	48.7	1.72	One liquid phase

	20	68.0	1.54	One liquid phase
	30	78.4	1.35	One liquid phase
	40	84.9	1.17	One liquid phase
NaC ₆ :C ₁₀ (0.7)	10	50.6	1.60	One liquid phase
	20	69.6	1.43	One liquid phase
	30	79.6	1.26	One liquid phase
	40	85.9	1.08	One liquid phase

4.2. Physical Characterization

The viscosity, density, surface tension, conductivity and pH were properties measured in this work that are key parameters for the determination of thermodynamic and transport properties of solutions allowing a better understanding of the studied mixtures.

4.2.1. Ionic Conductivity

Ionic conductivity, σ , is a property that allows to evaluate the capacity of an electrolyte to conduct electricity through the presence of ions. For this reason, ionic conductivity can be used as a first test to evaluate the potential application of a solution as electrolyte. Considering that ionic conductivity is highly dependent on ion dissociation and mobility, thus it can depend on the size of ions and on the interaction between them. Generally, a limited number of free charges and/or high viscosities strongly influence the conductivity results. [23,26]. From **Figure 31** to **Figure 36** the ionic conductivity data collected for each mixture is presented.

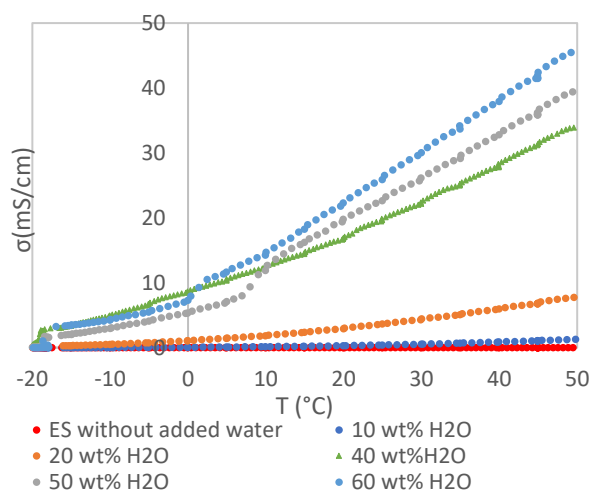


Figure 31. Ionic conductivity data as function of temperature for NaC₆:C₆(0.6)-water mixtures (0 wt% H₂O, 10 wt% H₂O, 20 wt% H₂O, 40 wt% H₂O (gel), 50 wt% H₂O and 60 wt% H₂O). Triangular form points identify gel mixtures.

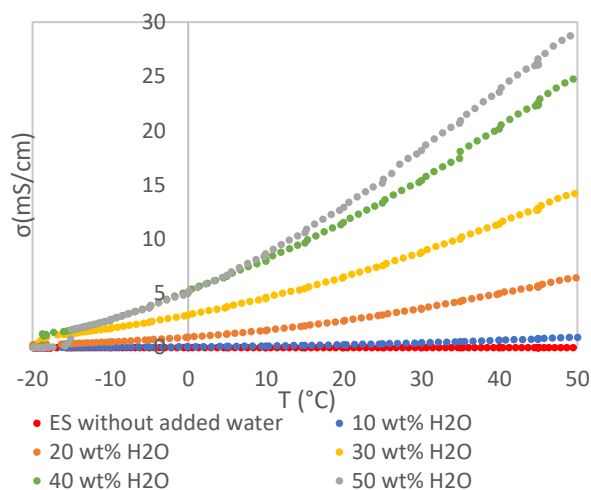


Figure 32. Ionic conductivity data as function of temperature for the NaC₆:C₆(0.7)-water mixtures (0 wt%, 10 wt% H₂O, 20 wt% H₂O, 30 wt% H₂O, 40 wt% H₂O and 50 wt% H₂O).

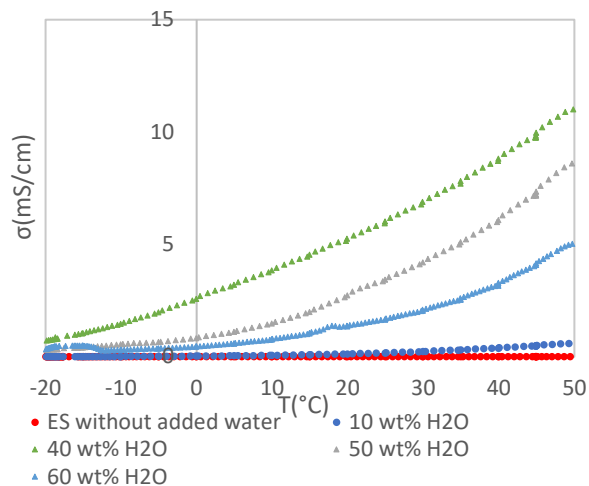


Figure 33. Ionic conductivity data as function of temperature for $\text{NaC}_6:\text{C}_8(0.6)$ -water mixtures (0 wt%, 10 wt% H_2O , 40 wt% H_2O (gel), 50 wt% H_2O (gel) and 60 wt% H_2O (gel)). Triangular form points identify gel mixtures.

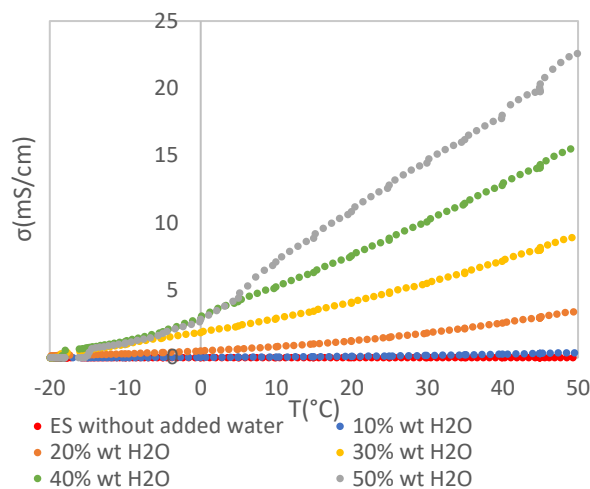


Figure 34. Ionic conductivity data as function of temperature for the $\text{NaC}_6:\text{C}_8(0.7)$ -water mixtures (0 wt%, 10 wt% H_2O , 20 wt% H_2O , 30 wt% H_2O , 40 wt% H_2O and 50 wt% H_2O).

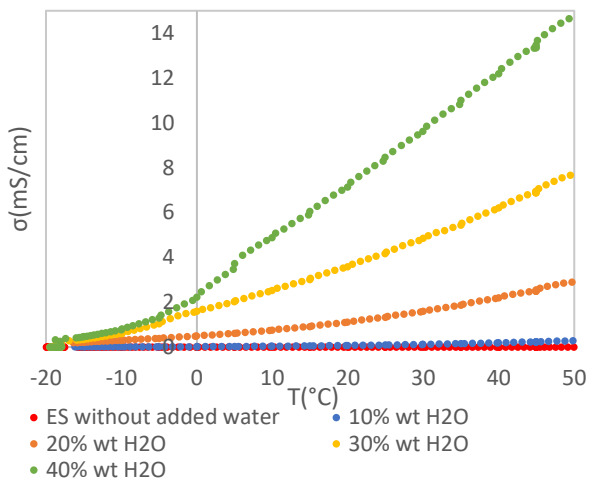


Figure 35. Ionic conductivity data as function of temperature for the $\text{NaC}_6:\text{C}_9(0.7)$ -water mixtures (0 wt%, 10 wt% H_2O , 20 wt% H_2O , 30 wt% H_2O and 40 wt% H_2O).

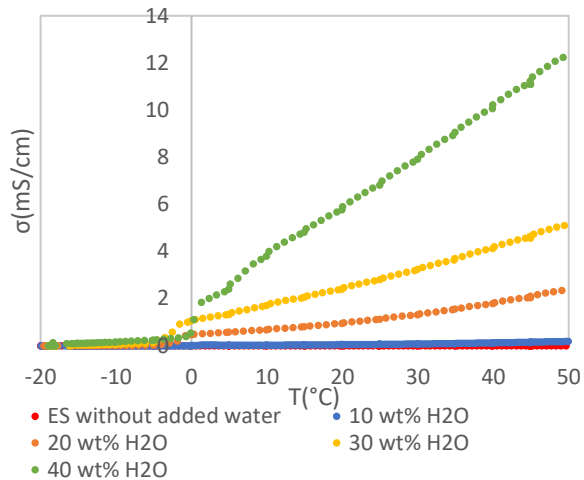


Figure 36. Ionic conductivity data as function of temperature for the $\text{NaC}_6:\text{C}_{10}(0.7)$ -water mixtures (0 wt%, 10 wt% H_2O , 20 wt% H_2O , 30 wt% H_2O and 40 wt% H_2O).

It can be observed from the analysis of figures **Figure 31** to **Figure 36** that, for all mixtures, conductivity increases with temperature as expected. The temperature rise weakens the intermolecular interactions between the species providing them higher mobility resulting in a higher conductivity.

In **Figure 37**, a summary of the conductivity results for all the aqueous eutectic mixtures at 20 °C is presented.

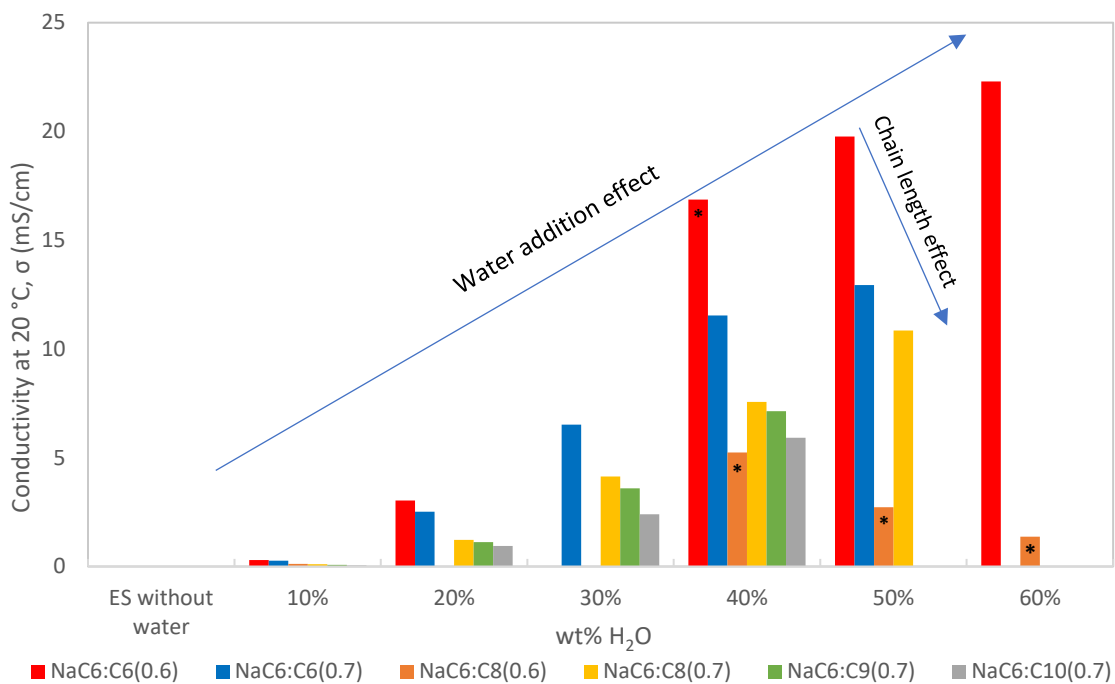


Figure 37. Conductivity data at 20 °C organized by water massic %. “*” identifies mixtures in gel form.

From **Figure 37** it is possible to conclude that, in general, the conductivity increases with the water content and that it decreases with the acid chain. As will be discussed in **Subsection 4.2.2**, the water addition to the eutectic mixture affects the eutectic original H-bond network, improving the mobility of the species (including the ionic species, namely the sodium (Na^+), the C_xCOO^- (where x can stand for 6, 8, 9 or 10) and the proton (H^+)) resulting in the enhancement of the solution conductivity. Moreover, the size of the ions compromises their mobility, and therefore the conductivity is smaller for the mixtures with the larger acid chain (decanoic acid, C_{10}). However, for mixtures containing the same acid (i.e. $\text{NaC}_6:\text{C}_6(0.6)$ and $\text{NaC}_6:\text{C}_6(0.7)$) and with similar molar water composition, for example $\text{NaC}_6:\text{C}_6(0.6) + 50 \text{ wt}\% \text{H}_2\text{O}$ (87.4 molar% H_2O) and $\text{NaC}_6:\text{C}_6(0.7) + 50 \text{ wt}\% \text{H}_2\text{O}$ (87.2 molar% H_2O), the conductivity for the $\text{NaC}_6:\text{C}_6(0.6)$ mixture is much higher than it is for $\text{NaC}_6:\text{C}_6(0.7)$ (19.8 mS/cm and 12.9 mS/cm, respectively). Therefore, the amount of salt present in the mixture has a significant effect on the conductivity, which can be associated with the presence of a larger amount of sodium cation (Na^+) that due to its smaller size, shows greater mobility.

Moreover, for the $\text{NaC}_6:\text{C}_8(0.6)$ group the gel formation greatly decreases the conductivity. However, for the $\text{NaC}_6:\text{C}_6(0.6)$, the gel formation does not seem to affect the tendency of conductivity to rise with the water content. Thus, mixtures with small acid chains, high water content and high amount of salt, namely $\text{NaC}_6:\text{C}_6(0.6) + 60\% \text{H}_2\text{O}$, gather the best conditions to achieve the highest conductivity 22.3 mS/cm at 20 °C.

The water effect in the conductivity of eutectic systems has been reported in literature for electrolytes containing $\text{ChCl}:\text{Urea}$ (1:2) eutectic mixtures [30]. Similar to the behaviour depicted by the eutectic mixtures under study, the $\text{ChCl}:\text{Urea}$ eutectic mixtures have their conductivity improved with the water content. Pure $\text{ChCl}:\text{Urea}$ (1:2) presents a conductivity of 1.3 mS/cm, while by adding 5 wt% H_2O the conductivity rises to 16.78 mS/cm.

i) **Vogel-Fulcher-Tammann**

Since the temperature dependence on the conductivity of mixtures does not follow the Arrhenius' law, the Vogel-Tamman-Fulcher (VTF) law (equation (30)) was used [23].

$$\sigma = \sigma_0 \exp \left[\frac{-B'_\sigma}{T - T_0} \right] \quad (30)$$

Where σ_0 , B'_σ and T_0 are the fitting parameters, where T_0 is the ideal glass transition temperature (Tg). The B'_σ allows to determine the pseudo-energy of activation multiplying by the universal gas constant ($R=8.314 \text{ J mol}^{-1} \text{ K}^{-1}$). The VFT parameters for the conductivity of the studied eutectic systems are shown in **Table 11**.

Table 11. Conductivity VTF parameters for the eutectic mixtures under study.

Eutectic Mixture	wt% H ₂ O	σ_0 (mS/cm)	T_0 (K)	$B'_\sigma \times R$ (kJ/mol)	R ²
NaC₆:C₆(0.6)	10	672.6	165.7	8.2	0.9998
	20	191.0	192.6	3.5	0.9998
	40*	255.5	199.8	2.1	0.9991
	50	175.9	229.4	1.2	0.9991
	60	289.3	218.2	1.6	0.9993
NaC₆:C₆(0.7)	10	341.9	155.5	8.2	0.9998
	20	462.3	162.0	5.7	0.9999
	30	300.5	175.4	3.7	0.9999
	40	178.6	210.0	1.9	0.9993
	50	352.1	202.3	2.5	0.9998
NaC₆:C₈(0.6)	10	278.8	167.9	8.0	0.9994
	40*	550.3	134.6	6.1	0.9996
	50*	7347.5	114.0	11.7	0.9989
	60*	11767.6	140.0	11.8	0.9966
NaC₆:C₈(0.7)	10	351.4	138.0	10.5	0.9997
	20	769.4	132.1	8.6	0.9998
	30	194.5	175	3.8	0.9998
	40	117.7	209	1.9	0.9979
	50	99.2	229.3	1.2	0.9979
NaC₆:C₉(0.7)	10	1321.3	106.3	15.2	0.9997
	20	1158.3	104.7	10.9	0.9998
	30	99.45	191.3	2.8	0.9998
	40	85.9	219	1.5	0.9996
NaC₆:C₁₀(0.7)	10	1185.1	97.4	16.4	0.9995
	20	522.7	114.0	9.4	0.9985

	30	124.0	165.6	4.16	0.9993
	40	77.5	219.1	1.6	0.9994

From the conductivity VTF fitting it is possible to see that, generally, the pseudo energy of activation decreases with the water composition, which is consistent with the fact that this activation energy can be seen as the energy that is needed for the molecules to pass each other. The $\text{NaC}_6\text{:C}_8(0.6)$ -water group is an exception to this tendency, as for the gel mixtures the pseudo-energy of activation increases with the amount of water (40%, 50%, 60%). However, this is in accordance with the conductivity of these mixtures as it decreases with the water content (orange bars identified with “*” in **Figure 37**).

4.2.2. Viscosity

Viscosity has a considerable interest as it is related to other transport properties such as mass and heat transfer and it has the advantage of being relatively easy to access [49]. Especially in the study of electrolytes, viscosity reveals to be an important parameter once it is related to the mobility of ionic species and, therefore, it has an influence in the performance of the supercapacitor. For this reason, the viscosity can provide information on a molecular basis, since it is a direct consequence of the intermolecular interactions, and it is an important parameter to establish the operational conditions of the electrolyte/supercapacitor [49].

For each eutectic-water mixtures, the viscosity data is presented from **Figure 38** to **Figure 43**. In agreement with the previously shown temperature versus water content diagrams (**Figure 24** to **Figure 29**), only temperatures where a liquid homogeneous phase occurs were selected to acquire viscosity data. The viscosity of gel mixtures cannot be acquired with the used viscosimeter, and therefore their viscosity is not presented.

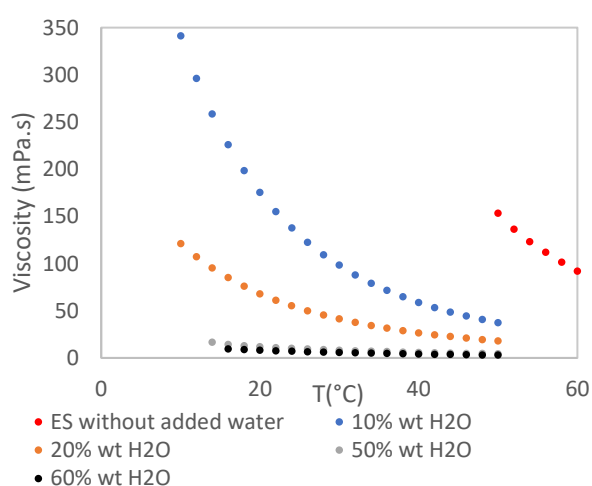


Figure 38. Viscosity data as function of temperature for the $\text{NaC}_6\text{:C}_6(0.6)$ -water mixtures.

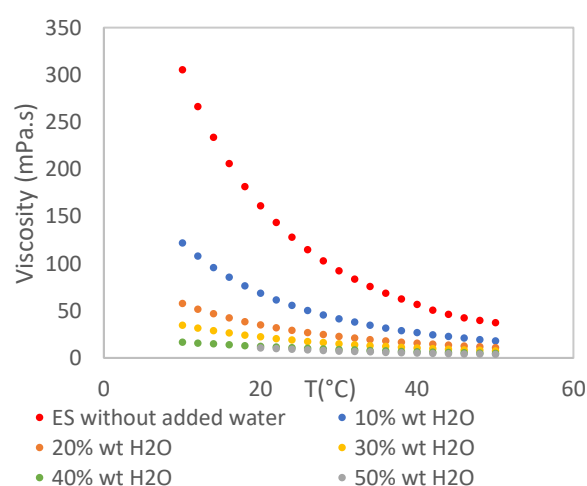


Figure 39. Viscosity data as function of temperature for the $\text{NaC}_6\text{:C}_6(0.7)$ -water mixtures.

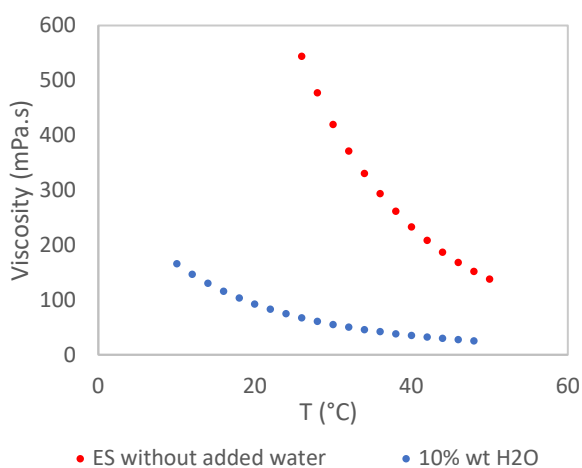


Figure 40. Viscosity data as function of temperature for the $\text{NaC}_6:\text{C}_8(0.6)$ -water mixtures.

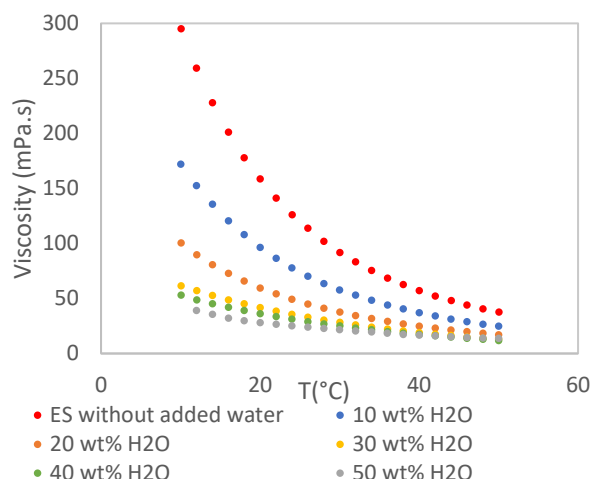


Figure 41. Viscosity data as function of temperature for the $\text{NaC}_6:\text{C}_8(0.7)$ -water mixtures.

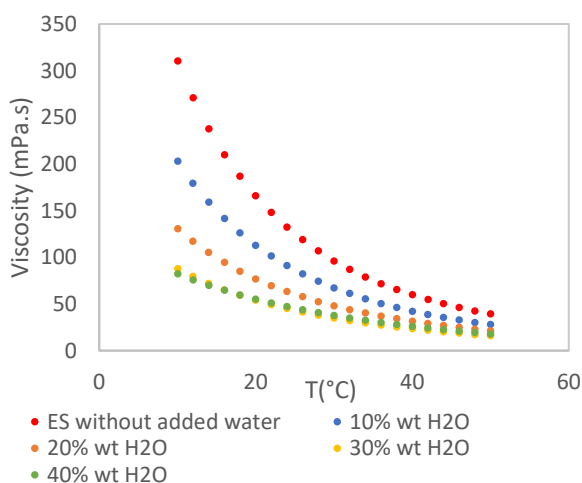


Figure 42. Viscosity data as function of temperature for the $\text{NaC}_6:\text{C}_9(0.7)$ -water mixtures.

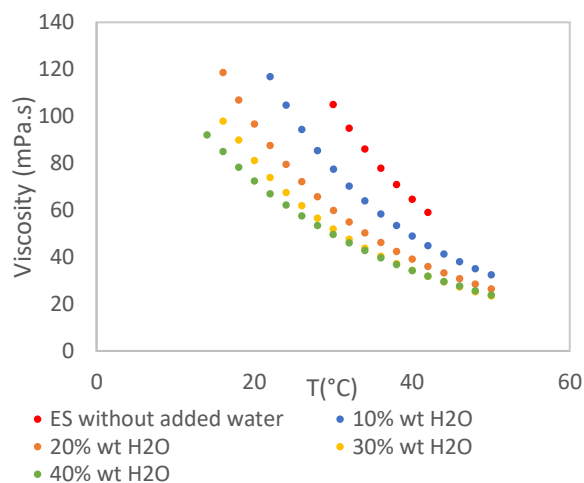


Figure 43. Viscosity data as function of temperature for the $\text{NaC}_6:\text{C}_{10}(0.7)$ -water mixtures.

From the collected data is possible to see that the viscosity greatly decreases with the water content and with temperature. Moreover, the effect of water on viscosity is more prominent at low water content and low temperature. The addition of water in eutectic mixtures interferes with the pre-established hydrogen bonding within the eutectic system compounds resulting in higher mobility of the species and therefore decreasing the viscosity and, consequently, increasing conductivity as discussed above. The decrease in viscosity with the increasing temperature is due to the weakening of the intermolecular forces in the mixture that also results on a high mobility of the species.

i) **Vogel-Fulcher-Tammann**

Since all mixtures exhibit a non-Arrhenius behaviour, the Vogel-Fulcher-Tammann equation (equation (31)) was used to represent the temperature dependence of viscosity [23]. The VFT parameters for the viscosity of the studied eutectic systems are shown in **Table 12**.

$$\eta = \eta_0 \exp \left[\frac{B'_\eta}{T - T_0} \right] \quad (31)$$

Table 12. Viscosity VTF parameters for the eutectic mixtures under study.

Eutectic Mixture	wt% H ₂ O	η_0 (Pa. s)	T_0 (K)	$B'_\eta \times R$ (kJ/mol)	R ²
NaC₆:C₆(0.6)	10	2.2E-05	148.2	10.8	1.0000
	20	3.2E-05	150.1	5.4	1.0000
	50	2.0E-04	197.8	3.3	0.9986
	60	1.7E-05	127.0	8.6	0.9999
NaC₆:C₆(0.7)	10	3.8E-05	152.7	8.8	1.0000
	20	4.4E-05	147.6	8.1	1.0000
	30	1.8E-05	120.3	10.2	1.0000
	40	1.9E-05	123.8	9.2	1.0000
	50	2.4E-05	140.9	7.7	1.0000
NaC₆:C₈(0.6)	10	1.9E-05	142.2	12.0	1.0000
NaC₆:C₈(0.7)	10	2.8E-05	142.6	10.2	1.0000
	20	1.2E-05	117.8	12.4	1.0000
	30	1.2E-05	114.1	12.2	1.0000
	40	-	-	-	-
	50	-	-	-	-
NaC₆:C₉(0.7)	10	1.6E-05	131.5	11.9	1.0000
	20	1.3E-05	119.0	12.5	1.0000
	30	2.6E-06	75.0	18.0	1.0000
	40	-	-	-	-
NaC₆:C₁₀(0.7)	10	2.2E-05	134.9	11.4	1.0000
	20	8.4E-06	106.4	14.5	1.0000
	30	1.9E-06	65.0	20.2	1.0000
	40	-	-	-	-

For the mixtures containing acids with longer alkyl chain (octanoic, nonanoic e decanoic) and higher water content the VTF model was not adequate to describe the temperature influence in viscosity. Generally, compared to the pseudo-activation energy obtained from conductivity, the pseudo-activation energy obtained for viscosity presents higher values. This difference between the pseudo-activation energy parameters is expected once conductivity relates essentially to the ionic species and the viscosity directly describes the interaction of all species in the mixture, this difference has been reported on literature for a variety of electrolyte studies (for example in [50]).

ii) Eyring's Theory

The determination of thermodynamic activation parameters, namely enthalpy, ΔH^\ddagger and entropy, ΔS^\ddagger , of viscous flow through Eyring's equation allows to better understand intermolecular interactions [49]. Through this theory, the viscosity relation with the thermodynamic activation parameters (ΔH^\ddagger , ΔS^\ddagger) is given by:

$$\eta = \left(\frac{h \cdot N_A}{V_m}\right) \times \exp\left(\frac{-\Delta S^\ddagger}{R}\right) \times \exp\left(\frac{\Delta H^\ddagger}{RT}\right) \quad (32)$$

where h is the Plank's constant, V_m is the molar volume, N_A is the Avogadro's' number and R is the ideal gas constant. In order to extract the enthalpy and entropy of activation from viscosity data, the equation (32) was linearized resulting in equation (33).

$$\ln(\eta) = \ln\left(\frac{h \cdot N_A}{V_m}\right) - \frac{\Delta S^\ddagger}{R} + \frac{\Delta H^\ddagger}{RT} \quad (33)$$

From the representation of the logarithm of viscosity with the inverse of temperature, the enthalpy of activation is obtained multiplying the slope by the universal gas constant and the entropy is obtained by the following relation:

$$\Delta S^\ddagger = [-b + \ln\left(\frac{h \cdot N_A}{V_m}\right)] \times R \quad (34)$$

The obtained values of both enthalpy and entropy of activation are present in **Figure 44** to **Figure 53**.

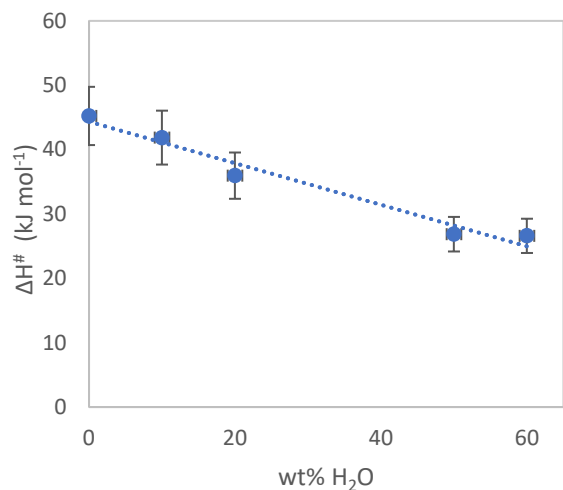


Figure 44. Variation of enthalpy of activation with the water content for the NaC₆:C₆(0.6) group.

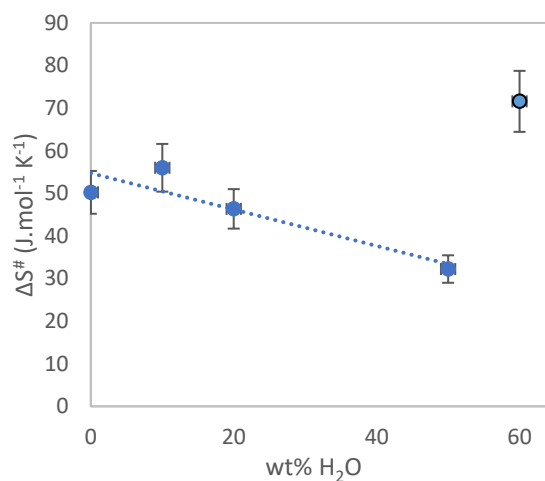


Figure 45. Variation of entropy of activation with the water content for the NaC₆:C₆(0.6) group.

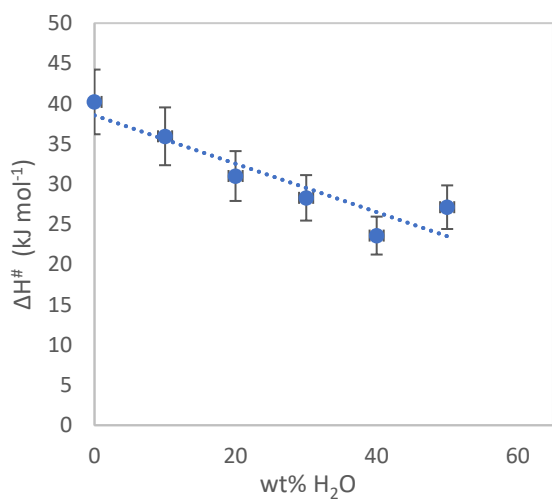


Figure 46. Variation of enthalpy of activation with the water content for the NaC₆:C₆(0.7) group.

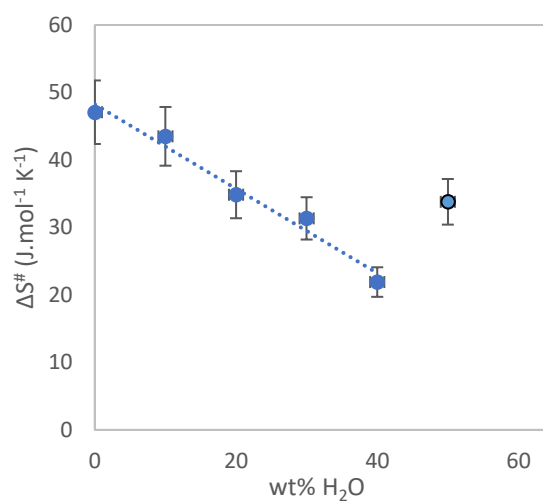


Figure 47. Variation of entropy of activation with the water content for the NaC₆:C₆(0.7) group.

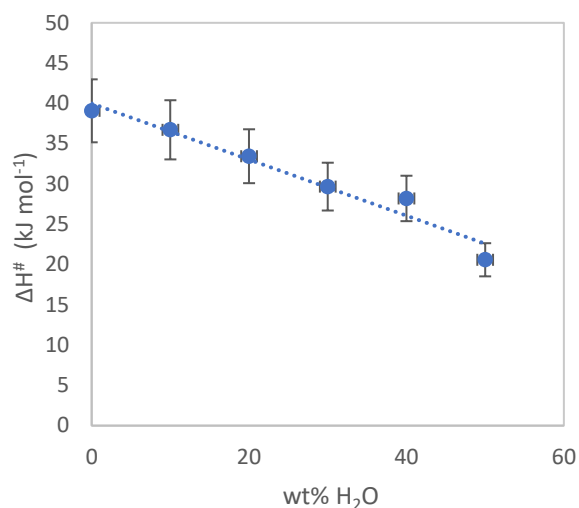


Figure 48. Variation of enthalpy of activation with the water content for the $\text{NaC}_6:\text{C}_8(0.7)$ group.

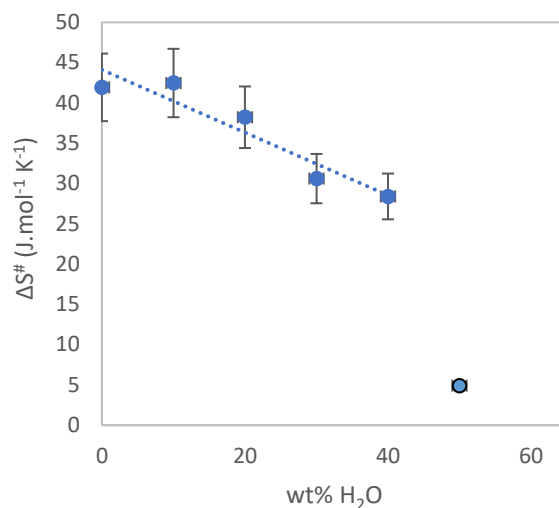


Figure 49. Variation of entropy of activation with the water content for the $\text{NaC}_6:\text{C}_8(0.7)$ group.

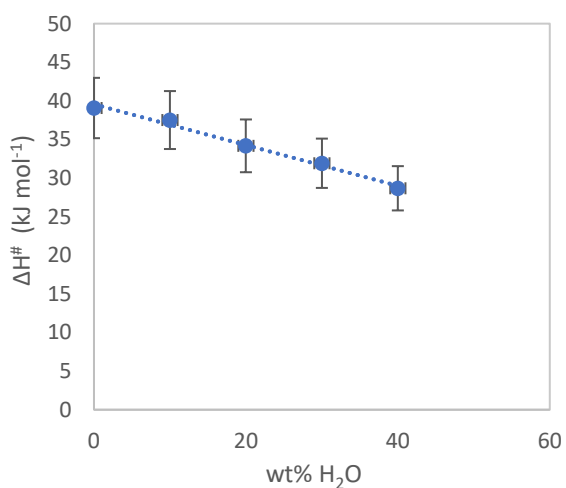


Figure 50. Variation of enthalpy of activation with the water content for the $\text{NaC}_6:\text{C}_9(0.7)$ group.

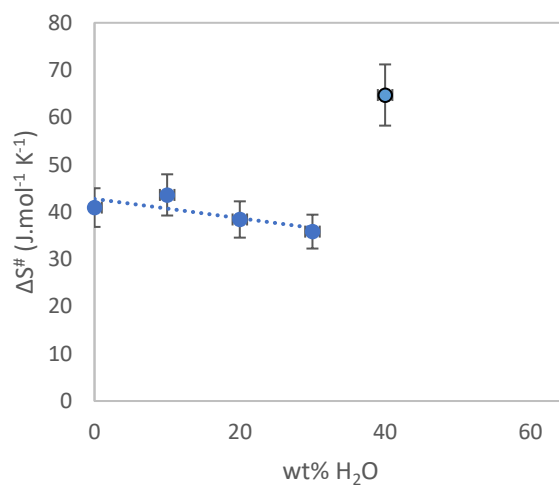


Figure 51. Variation of entropy of activation with the water content for the $\text{NaC}_6:\text{C}_9(0.7)$ group.

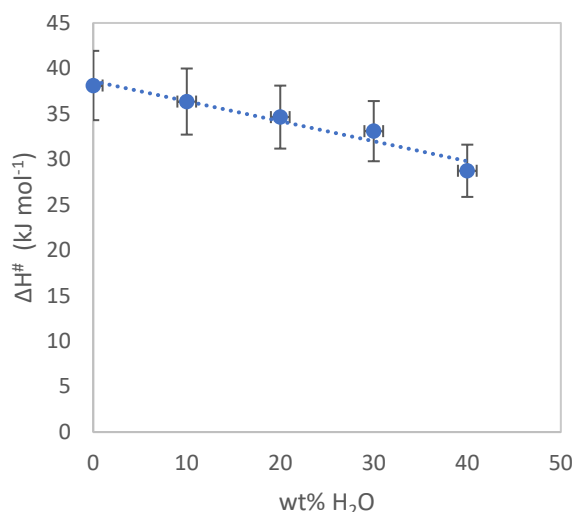


Figure 52. Variation of enthalpy of activation with the water content for the $\text{NaC}_6:\text{C}_{10}(0.7)$ group.

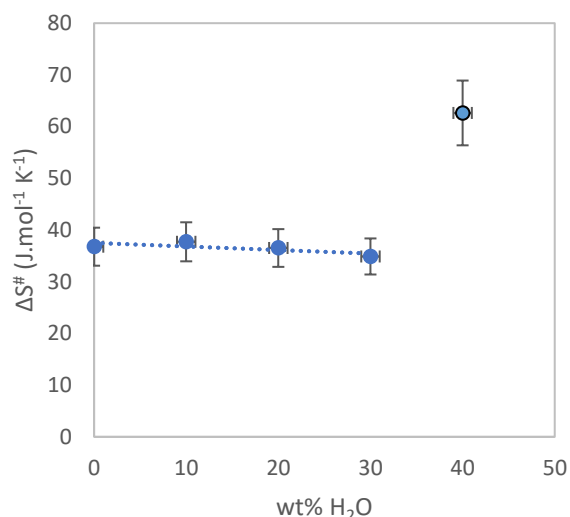


Figure 53. Variation of entropy of activation with the water content for the $\text{NaC}_6:\text{C}_{10}(0.7)$ group

From the previous **Figure 44** to **Figure 53** it is observed that, generally, the enthalpy values decrease with the water content in the same range of values (between 20 kJ/mol and 45 kJ/mol) for the different NaC_6 : Acid mixtures. In Eyring's theory, the enthalpy of activation yields the interaction strength between adjacent species (namely solvent-solvent, ion-solvent and ion-ion) [51]. Therefore, since the enthalpy values decrease with water content, it is reasonable to say that the presence of water weakens the species interaction, namely the hydrogen bond network of the original eutectic mixture. This is consistent with the conductivity results discussed above. The enthalpy values of the original eutectic mixtures have similar enthalpy values, which may be associated with the fact that these analogous mixtures rely in the same type of interaction, namely the hydrogen bonds (between the sodium salt and the fatty acid) characteristic of eutectic solvents.

Additionally, the entropy values tend to decrease with the water content until a certain water composition (40, 50 or 60 wt% H₂O depending on the mixture). The entropy of activation in Eyring's theory is related to an empty space availability in the media ("hole") to receive another species [51], and generally, to the overall system organization. Taking this into consideration, the decrease of entropy with water suggests that the water addition to the mixture causes a reorganization that leads to a more organized system (possibly related to the formation of aggregates as concluded in surface tension results discussed ahead) with a higher number of available "holes". The entropy increasing observed for the highest water composition, may be related to the fact that these compositions are close to the limit of miscibility of the eutectic/water system (as can be observed in **Figure 24** to **Figure 29**) which may reflect a different organization of the system.

Moreover, the variation of enthalpy (kJ/mol variation) is more significant than the variation of entropy ($\text{J}\cdot\text{mol}^{-1}\cdot\text{K}^{-1}$ variation), which can indicate that the weakening of the species interactions with the water content is more significant than the overall mixture organization.

iii) Jones-Dole-Kaminsky model: Hydrodynamic radius determination

It is possible to gather essential aspects about the interactions between the components and ion hydration by evaluating how viscosity for aqueous electrolytes changes with temperature and concentration. In 1929, Jones and Dole proposed an empirical equation, equation (35), for the variation of the relative viscosity, η_r , with electrolyte concentration, C , where η_0 is the viscosity of the pure solvent, in this study, water. The coefficient A is related to the long-range coulombic forces and B is related with the interactions between the solvent and the ions. The B value can assume positive or negative values depending on the degree of solvent structuring. Usually, a positive B value is associated with structure-making (i.e. ordering) ions, and, on the other hand, a negative B value is associated with structure-breaking (disordering) ions [50]. However, this equation is only valid for solutions with concentration lower than 0.1 mol/L [52,53].

$$\eta_r = \frac{\eta}{\eta_0} = 1 + AC^{1/2} + BC \quad (35)$$

For more concentrated solutions (beyond 1-3 molar according to [54]), a quadratic term (DC^2) was added by Kaminsky to the original Jones-Dole equation to introduce a temperature correction associated with the large increase of viscosity with temperature for these mixtures. However, the physical meaning of the D coefficient in the Jones-Dole-Kaminsky (JDK) equation remains unclear [52]. Often, equation (36), is adjusted to a second order polynomial, equation (37), once that for concentrations higher than 0.1 mol/L the coefficient A is negligible [50].

$$\frac{\eta}{\eta_0} - 1 = \eta_r - 1 = \eta_{sp} = AC^{1/2} + BC + DC^2 \quad (36)$$

$$\eta_{sp} = A' + BC + DC^2 \quad (37)$$

The coefficient B of the JDK equation is linked to the hydrodynamic radius, r_s , through Einstein's viscosity theory based on the model of solid spheres in solution and crown of solvent around solvated ions. The relation between B and r_s , equation (38), enables us to estimate the hydration sphere's dimension around the solvated ion [50], equation (39), in which N_A is the Avogadro's constant.

$$B = 2.5 \left(\frac{4}{3} \pi \times r_s^3 \times N_A \right) \quad (38)$$

$$r_s = \sqrt[3]{\frac{3B}{10\pi \times N_A}} \quad (39)$$

Based on the collected viscosity data, the specific viscosity, η_{sp} , for each salt concentration and temperature was calculated. For each temperature, the specific viscosity and respective salt concentration were fitted to the second order polynomial, equation (37), and the B coefficient was obtained. As shown in **Table 10** the concentrations of the studied eutectic-water solutions range between 1 and 3 mol/L, therefore according to [54], this corresponds to the limit of applicability of the JDK equation. For this reason, the more concentrated samples (10% wt H₂O) were excluded from the polynomial fitting.

The variation of the estimated hydrodynamic radius with temperature for the different studied systems is presented in **Figure 54**.

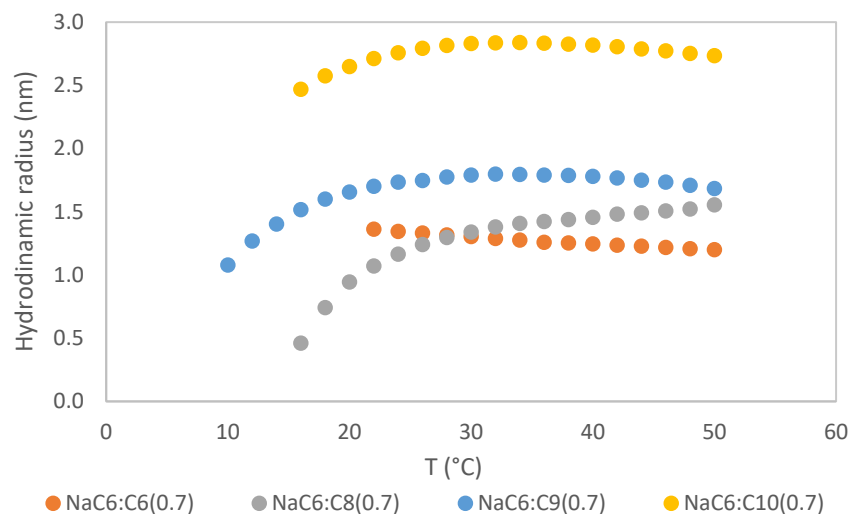
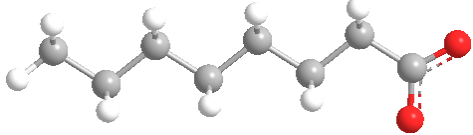
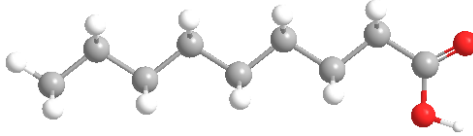
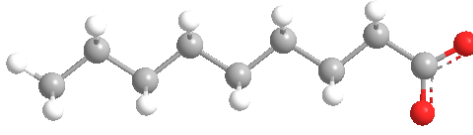
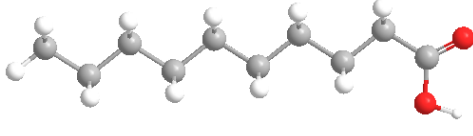
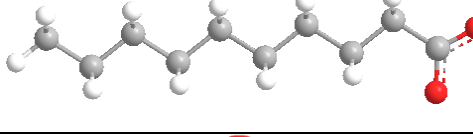
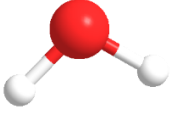


Figure 54. Hydrodynamic radius evolution with temperature for eutectic-water mixtures.

With the exception of the NaC₆:C₆ system, in which the estimated hydrodynamic radius does not vary significantly with temperature, all the other systems present a low value of hydrodynamic radius for low temperatures, increasing with temperature until they reach an approximately constant value (plateau in the graph). Generally, the estimated hydrodynamic radius increases with the acid chain. In order to compare the obtained results with the length of the species (protonated and deprotonated forms) in the mixtures, their length was extracted from *Chem 3D*[®] and are presented on **Table 12**.

Table 12. Structure of the compounds used in the studied eutectic systems and their respective length.

Species	Length (Angstroms)	Structure
Hexanoic acid	8.218	
Hexanoate	8.257	
Octanoic acid	10.704	

Octanoate	10.743	
Nonanoic acid	11.945	
Nonanoate	11.983	
Decanoic acid	13.191	
Decanoate	13.230	
Water	1.482	

Associating the length of the deprotonated forms (predominant forms according to the pH of the mixture, **Section 3.2.3**) with the water, the following lengths are obtained: ~ 1 nm for the $\text{NaC}_6:\text{C}_6$; ~ 1.2 nm for the $\text{NaC}_6:\text{C}_8$; ~ 1.4 nm for the $\text{NaC}_6:\text{C}_9$; 1.5 nm for the $\text{NaC}_6:\text{C}_{10}$. Comparing these values with the obtained radius extracted with the JDK theory, they seem to be in accordance, except for the $\text{NaC}_6:\text{C}_{10}$ -water mixtures, for which the JDK theory predicts higher values. This can be related to the fact that the working concentrations are in the limit of applicability of the JDK theory, leading to an overestimation of the values. Further tests to corroborate this molecular level organization would be needed, for example using X-ray scattering.

Based on these results, **Figure 55** illustrates a schematic proposal of the orientation of the species.

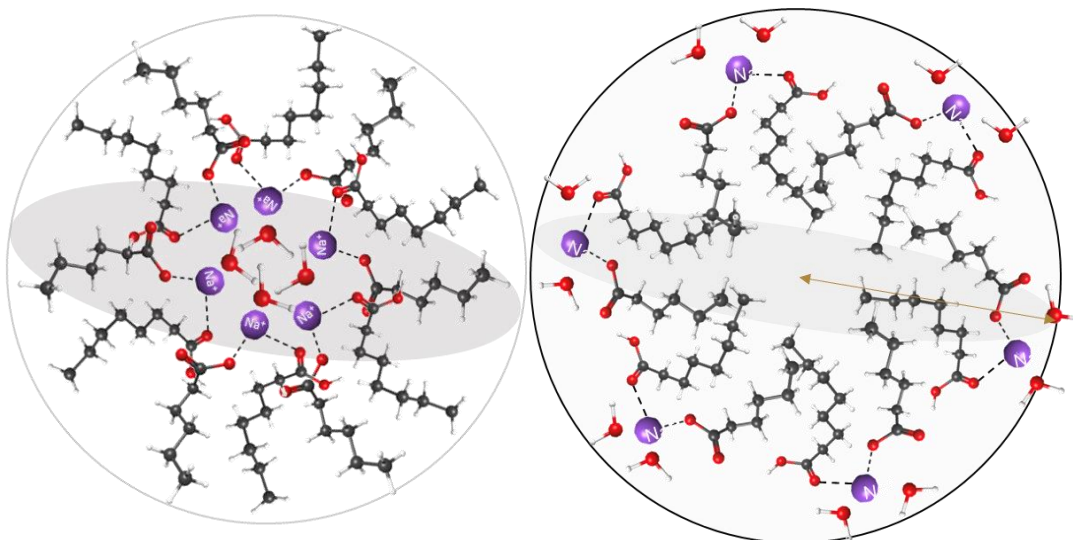


Figure 55. Schematic Proposal of organization of the species.

4.2.3. Density

The density measurements for each mixture are presented in **Figure 56** to **Figure 61** collected for the same range temperatures used for viscosity.

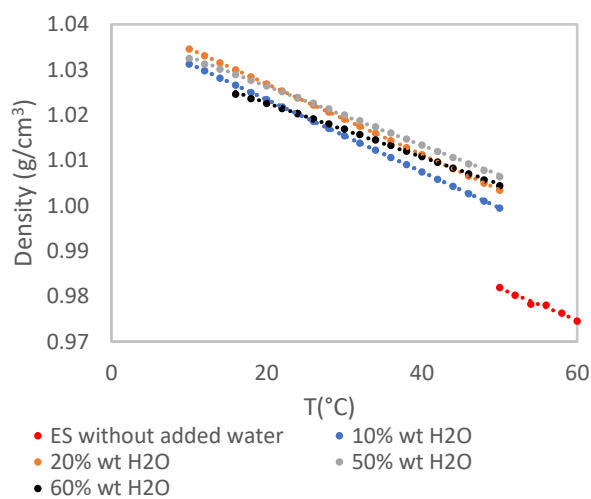


Figure 56. Density data as function of temperature for the $\text{NaC}_6:\text{C}_6(0.6)$ group.

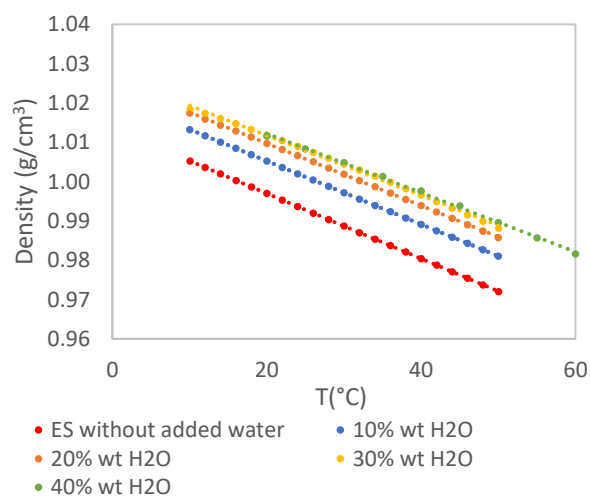


Figure 57. Density data as function of temperature for the $\text{NaC}_6:\text{C}_6(0.7)$ group.

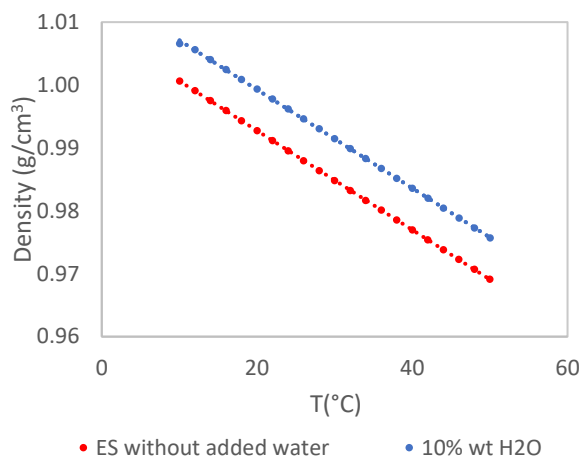


Figure 58. Density data as function of temperature for the $\text{NaC}_6:\text{C}_8(0.6)$ group.

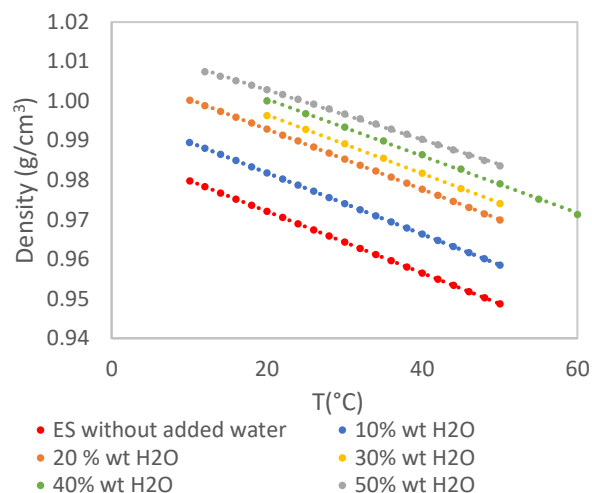


Figure 59. Density data as function of temperature for the $\text{NaC}_6:\text{C}_8(0.7)$ group.

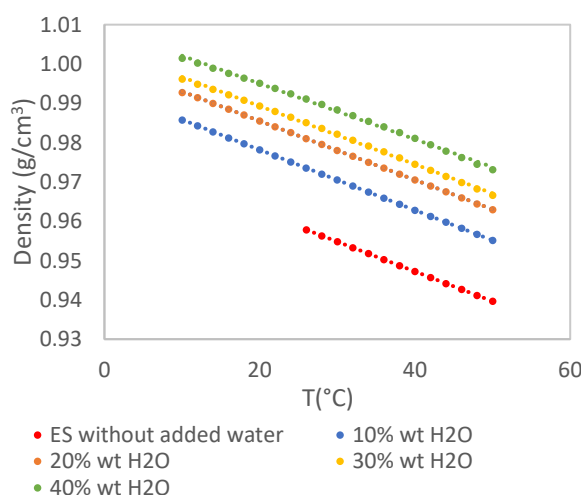


Figure 60. Density data as function of temperature for the $\text{NaC}_6:\text{C}_9(0.7)$ group.

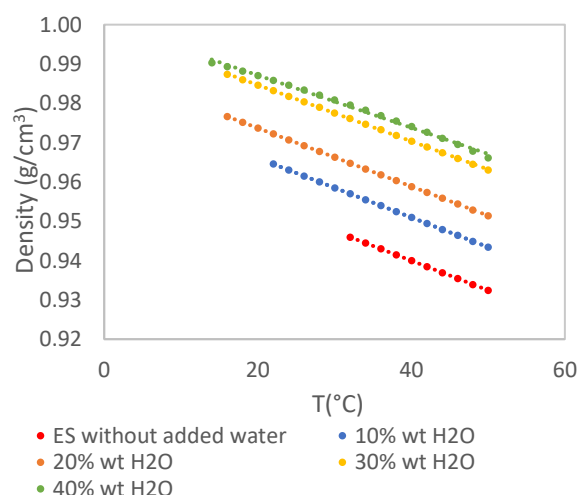


Figure 61. Density data as function of temperature for the $\text{NaC}_6:\text{C}_{10}(0.7)$ group.

From the previous figures it is observed that the density of the mixtures increases with the water composition. Once the density of pure water is higher than the density of the eutectic system, a direct evolution of the density values is observed with the increase of the water composition. As expected, a linear temperature dependence was also observed for all mixtures, $\rho = a + bT$, where a and b are fitting parameters (in Supporting information, Section 8.5).

4.2.4. Surface Tension

The sodium hexanoate and fatty acids have amphiphilic nature once the polar carboxyl group will have water affinity and, in contrast, the apolar long alkyl chain is hydrophobic. For this reason, in presence of water these compounds will self-assemble forming aggregates, where the carboxyl group will orientate to the water molecules and the carbon chain will avoid it. For each sodium hexanoate-fatty acid combination type ($\text{NaC}_6:\text{C}_6$,

NaC₆:C₈, NaC₆:C₉ and NaC₆:C₁₀) the surface tension was measured as function of their molar concentration in water and the results are presented in **Figure 62**.

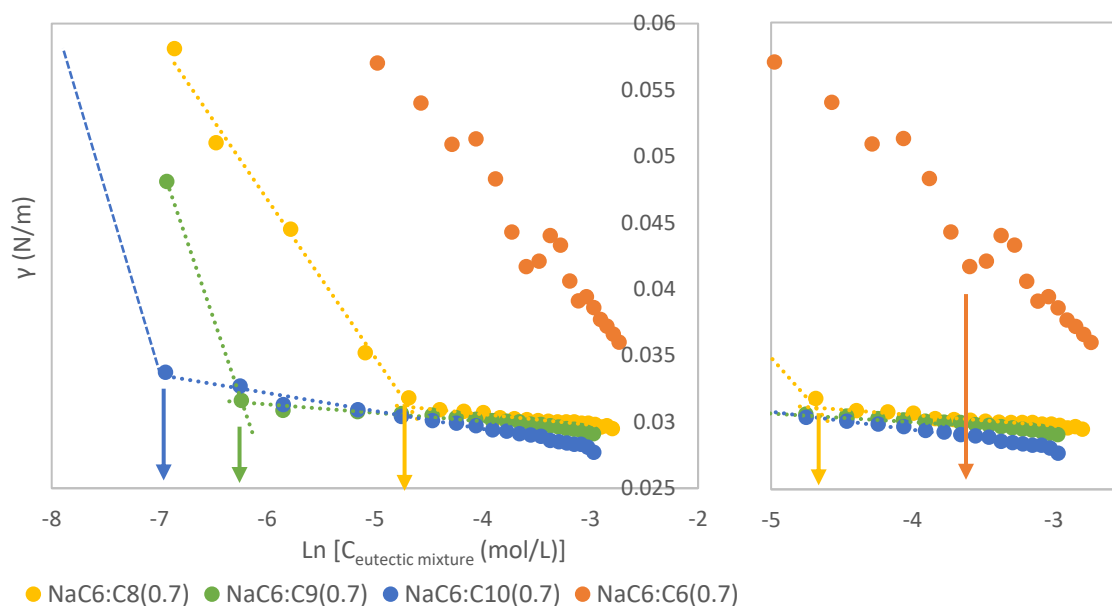


Figure 62. Surface Tension as function of eutectic mixture concentration. Right: Zoom in the xx scale.

As expected, the surface tension decreases with the concentration of the eutectic mixture until the critical aggregation concentration (CAC) is reached, and after the CAC a plateau region is observed. The CAC value decreases as the carbon acid chain increases once the hydrophobicity rises with the hydrocarbon chain. The influence of the hydrocarbon chain length on the CAC has been largely reported on literature (for example for protic ionic liquids of diisopropylethylamine alkyl carboxylates [DIPEA][C_nH_{2n+1}COO] [55]). Moreover, it is possible to say that the water-eutectic mixtures under study are likely to have a high level of organization since they have considerably larger concentrations than their corresponding determined CACs. The determined CACs for each type of mixture are presented in the following table.

Table 13. Critical Aggregation Concentration (CAC) in mol/L according to the number of carbons in the alkyl acid chain.

Number of carbons in the acid chain	CAC (mol/L)
6	2.75×10^{-2}
8	9.24×10^{-3}
9	1.96×10^{-3}
10	9.65×10^{-4}

4.2.5. Ionicity: Walden Plot

Walden plot is a qualitative/semi-qualitative method to study the ionicity (fraction of ions that participate in conduction) of electrolytic solutions, and it consists of a representation of the logarithm of the molar conductivity (Λ , S.mol⁻¹.cm²) as function of the logarithm of the reciprocal viscosity (or fluidity, η^{-1}) [26].

The bisector represented in Walden plot is used as a reference and it represents the theoretical behaviour of 0.01 mol/L KCl aqueous solution, in which ions are known to be fully dissociated having equal mobility [23,26,56]. The distance to the KCl ideal line allows to quantify the ionicity of a solution and classify it as being non-ionic, poorly ionic, good ionic or superionic [30].

The Walden plots of each NaC₆: Acid and water mixtures are presented from **Figure 63** to **Figure 68**. The molar conductivity, Λ , was calculated using the relationship $\Lambda = V_m \times \sigma$, where V_m is the molar volume determined through density data.

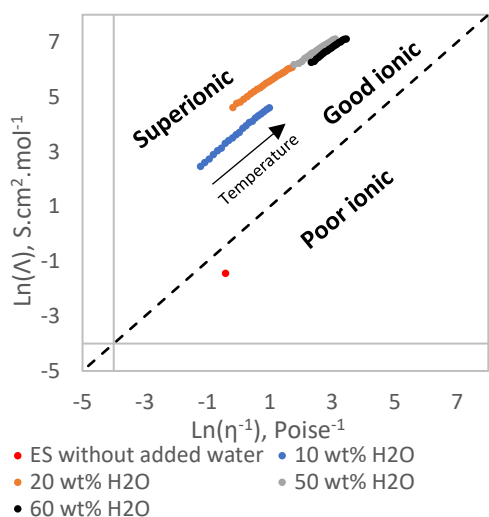


Figure 63. Walden plot representation for NaC₆:C₆(0.6) mixtures.

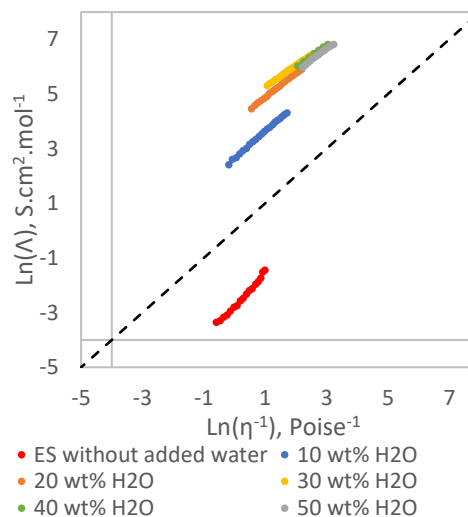


Figure 64. Walden plot representation for NaC₆:C₆(0.7) mixtures.

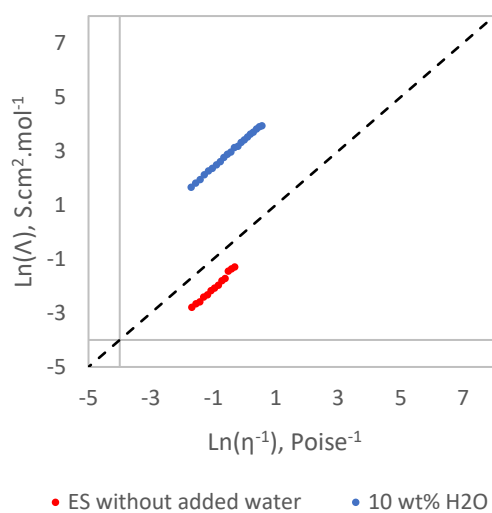


Figure 65. Walden plot representation for NaC₆:C₈(0.6) mixtures.

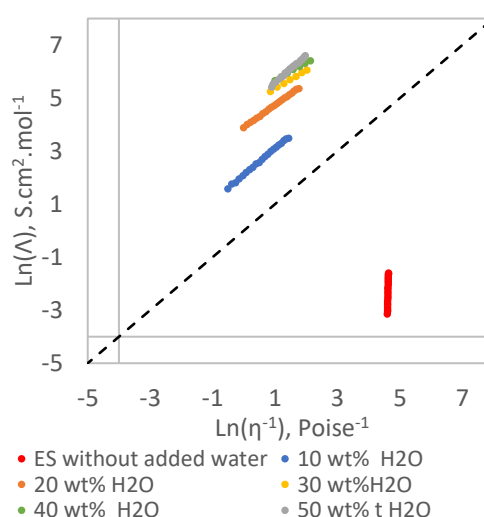


Figure 66. Walden plot representation for NaC₆:C₈(0.7) mixtures.

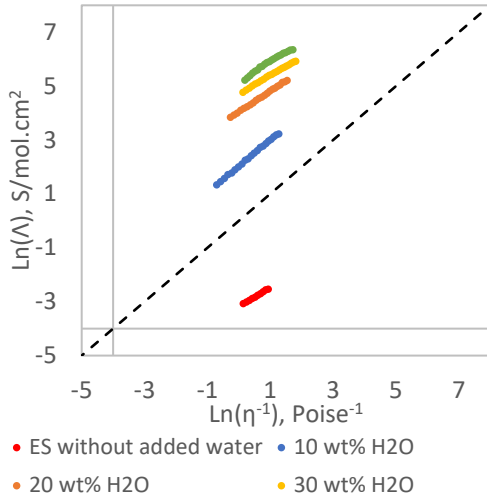


Figure 67. Walden plot representation for $\text{NaC}_6:\text{C}_9(0.7)$ mixtures.

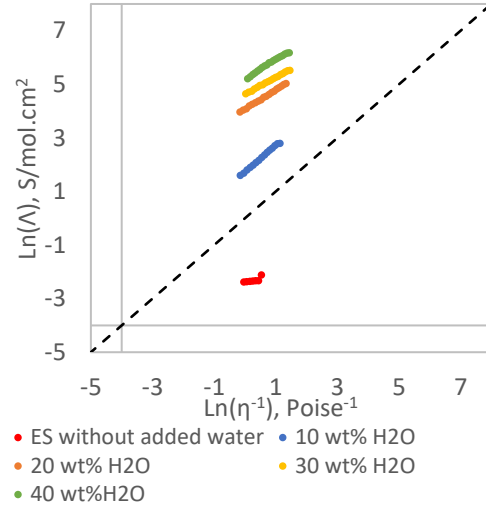


Figure 68. Walden plot representation for $\text{NaC}_6:\text{C}_{10}(0.7)$ mixtures.

From the above Walden plot representations, it is observed that for all NaC_6 : Acid mixtures, the water addition turns the original poorly ionic eutectic mixture into a good ionic liquid and superionic.

The Walden rule is an empirical rule that was originally proposed for diluted solutions, and it states that the product of molar conductivity with viscosity is constant with temperature,

$$\Lambda \cdot \eta = \text{constant}(k) \quad (40)$$

In the Walden plot, the Walden rule reflects as a parallel line to the ideal KCl diagonal line (slope equal to 1, equation (41)), meaning that the temperature influences the conductivity and viscosity in the same extent.

$$\text{Ln}(\Lambda) = \text{Ln}(k) + \text{Ln} \eta^{-1} \quad (41)$$

However, for some mixtures the linear variation of conductivity and viscosity with temperature is not verified (for example for ionic liquids [56]), and the Walden rule is not satisfied. For these mixtures, a derivation of the Walden rule is used, the fractional Walden rule, equation (42).

$$\text{Ln}(\Lambda) = \text{Ln}(k) + \alpha \text{Ln} \eta^{-1} \quad (42)$$

$$\Lambda \cdot \eta^\alpha = \text{constant} \quad (43)$$

In the Walden plot, this can be seen as a non-parallel line to the KCl ideal line (slope different from 1). For the studied mixtures, it is possible to see in the Walden plot that for some compositions the plotted points are not parallel to the KCl line revealing the temperature effect. Therefore, the fractional Walden rule was applied and the α values were extracted and are presented in **Table 14**.

Table 14. Slope and correlation coefficient obtained from the fractional Walden rule.

Mixture	wt% H2O	Slope (α)	R ²
NaC₆:C₆(0.6)	0	-	-
	10	0.98	0.998
	20	0.77	0.998
	50	0.75	0.997
	60	0.80	0.995
NaC₆:C₆(0.7)	0	1.21	0.989
	10	0.99	0.999
	20	0.88	0.999
	30	0.78	0.999
	40	0.84	0.997
	50	1.19	0.997
NaC₆:C₈(0.6)	0	1.11	0.990
	10	1.02	0.999
NaC₆:C₈(0.7)	0	47.95	0.996
	10	1.00	0.999
	20	0.84	0.999
	30	0.73	0.783
	40	0.66	0.997
	50	1.02	0.997
NaC₆:C₉(0.7)	0	0.70	0.996
	10	0.98	0.999
	20	0.77	0.999
	30	0.68	0.998
	40	0.74	0.987
NaC₆:C₁₀(0.7)	0	0.034	0.556
	10	0.98	0.998
	20	0.72	0.999
	30	0.63	0.998
	40	0.73	0.728

For the mixtures with 10 % of water, the temperature influences the conductivity and viscosity in the same extent as their associated slope (α) is almost 1. For all the aqueous mixtures, the α values decrease with the water content until the penultimate composition (50% for NaC₆:C₆(0.6), 40% for NaC₆:C₆(0.7), NaC₆:C₈(0.7), and 30% for the NaC₆:C₉(0.7) and NaC₆:C₁₀(0.7)), reflecting that the temperature effect in the fluidity of the mixture is more prominent than in its molar conductivity.

4.2.6. pH

The concentration of free protons in a solution, [H⁺], determines the pH of that solution. It is possible to predict the degree of acid dissociation of an acid by comparing the pH with the corresponding acid's dissociation constant, pK_a. If the pH is greater than the pK_a, the deprotonated form is predominant in solution, if in the

contrary the pH is lower than the pK_a , the protonated form is predominant and less free protons are available in solution.

Monitoring the pH in electrolytes where acids are present is crucial for better understanding the role of free proton contribution to conductivity. The pK_a s of the solutions used in this study are displayed in **Table 15**.

Table 15. pK_a s of hexanoic, octanoic, nonanoic and decanoic acids.

Acid	pK_a
Hexanoic, C ₆	4.88 [57]
Octanoic, C ₈	4.89 [58]
Nonanoic, C ₉	4.95 [58]
Decanoic, C ₁₀	4.90 [58]

The pH measured for each mixture are presented in **Figure 69** as function of water content.

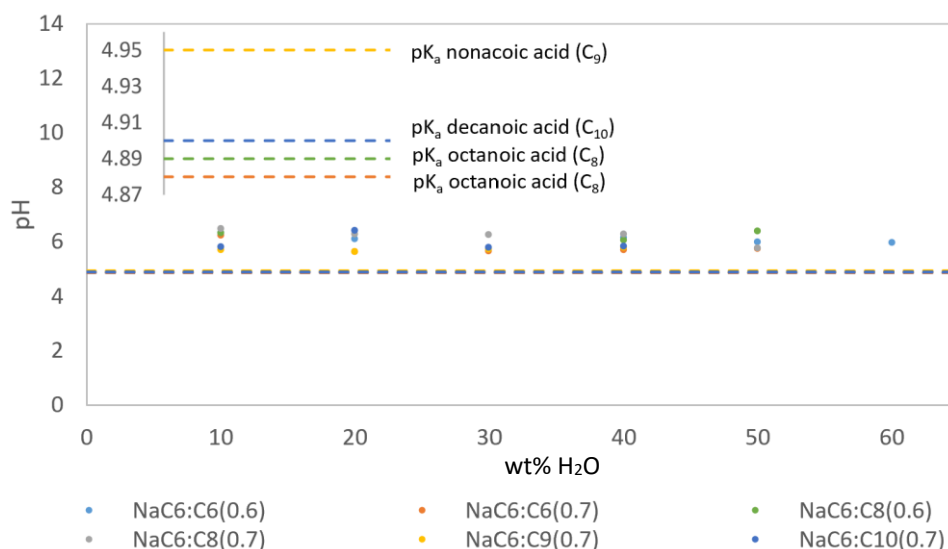


Figure 69. pH measurements at 20 °C for each eutectic-water mixture studied.

Since the pH of every mixture exceeds the corresponding pK_a , the deprotonated form of the acid predominates. As shown in **Figure 69**, each group's pH is maintained at a constant level with the addition of water, therefore the number of free protons in solution is not considerably altered. As was earlier observed, the presence of water significantly affects each group's conductivity, since the number of free protons is not affected by the water content, this means that the increase of conductivity with the water content is not due to a larger amount of free protons in solution.

4.3. Electrochemical Study

4.3.1. Cyclic Voltammetry

Cyclic voltammetry tests were performed for each mixture at four different scan rates, 1 mV/s, 5 mV/s; 10 mV/s and 20 mV/s and for a voltage range from 0 to 1 volt, all at room temperature ($\sim 20^\circ\text{C}$). Cyclic Voltammetry was performed for all the mixtures summarized in **Table 10**, excepting the gel mixtures ($\text{NaC}_6:\text{C}_6(0.6) + 40\%$; $\text{NaC}_6:\text{C}_8(0.6) + 40\%\text{H}_2\text{O}$; $\text{NaC}_6:\text{C}_8(0.6) + 50\%\text{H}_2\text{O}$; $\text{NaC}_6:\text{C}_8(0.6) + 60\%\text{H}_2\text{O}$), for these mixtures it was not possible to perform cyclic voltammetry adequately. The collected CV curves are presented from **Figure 70** to **Figure 98**.

i) $\text{NaC}_6:\text{C}_6(0.6)$

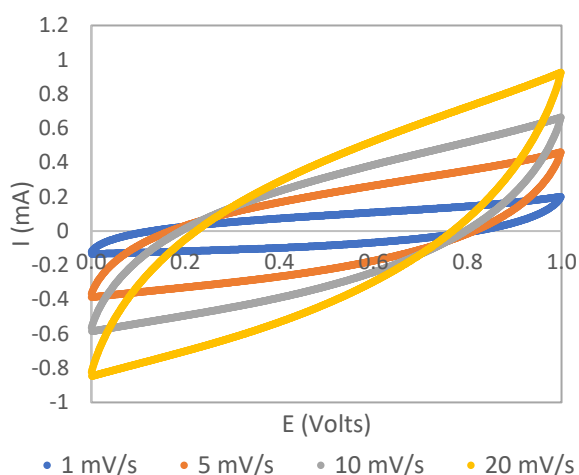


Figure 70. Cyclic voltammograms performed at 1 mV/s, 5 mV/s, 10 mV/s and 20 mV/s scan rates for a voltage limit of 1 volt for the $\text{NaC}_6:\text{C}_6(0.6)$ mixture.

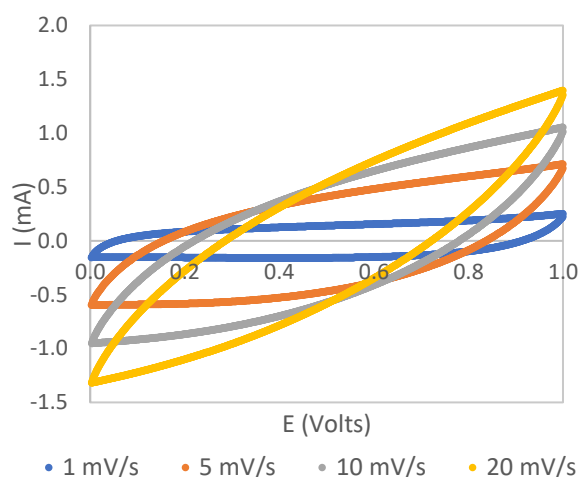


Figure 71. Cyclic voltammograms performed at 1 mV/s, 5 mV/s, 10 mV/s and 20 mV/s scan rates for a voltage limit of 1 volt for the $\text{NaC}_6:\text{C}_6(0.6) + 10\% \text{H}_2\text{O}$ mixture.

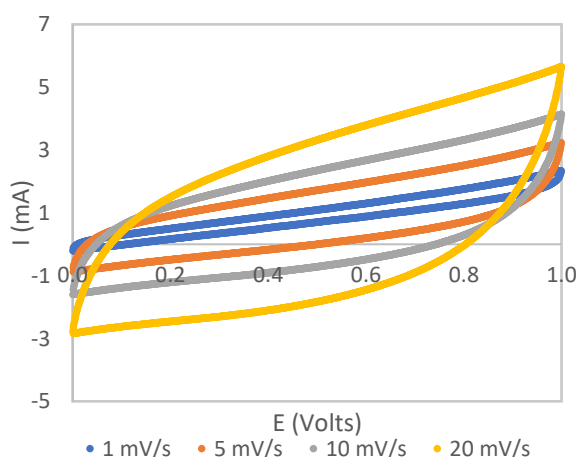


Figure 72. Cyclic voltammograms performed at 1 mV/s, 5 mV/s, 10 mV/s and 20 mV/s scan rates for a voltage limit of 1 volt for the $\text{NaC}_6:\text{C}_6(0.6) + 20\% \text{H}_2\text{O}$ mixture.

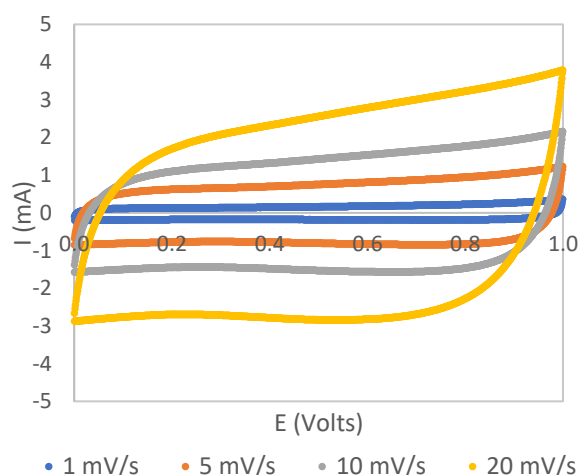


Figure 73. Cyclic voltammograms performed at 1 mV/s, 5 mV/s, 10 mV/s and 20 mV/s scan rates for a voltage limit of 1 volt for the $\text{NaC}_6:\text{C}_6(0.6) + 50\% \text{H}_2\text{O}$ mixture.

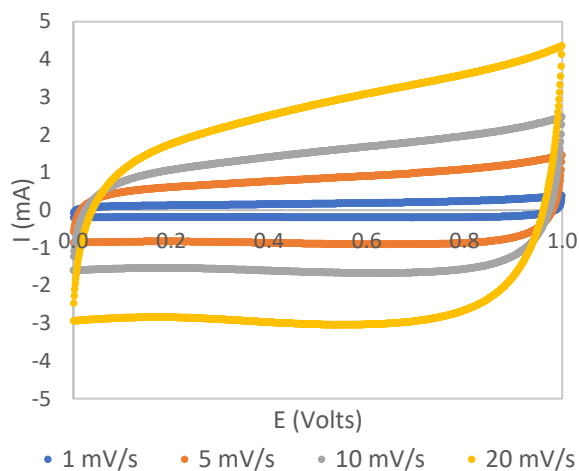


Figure 74. Cyclic voltammograms performed at 1 mV/s, 5 mV/s, 10 mV/s and 20 mV/s scan rates for a voltage limit of 1 volt for the $\text{NaC}_6:\text{C}_6(0.6)$ + 60% H_2O mixture.

ii) $\text{NaC}_6:\text{C}_6(0.7)$

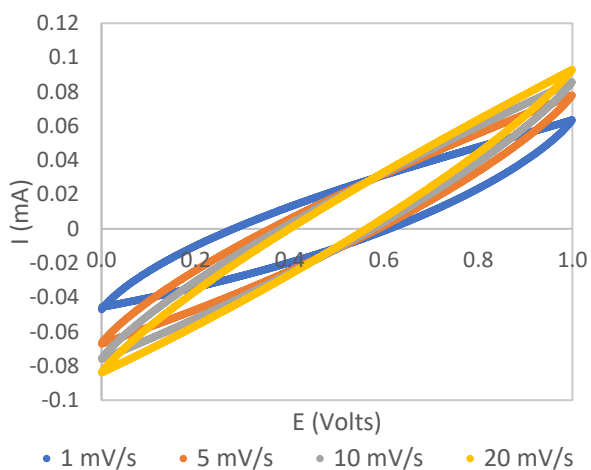


Figure 75. Cyclic voltammograms performed at 1 mV/s, 5 mV/s, 10 mV/s and 20 mV/s scan rates for a voltage limit of 1 volt for the $\text{NaC}_6:\text{C}_6(0.7)$.

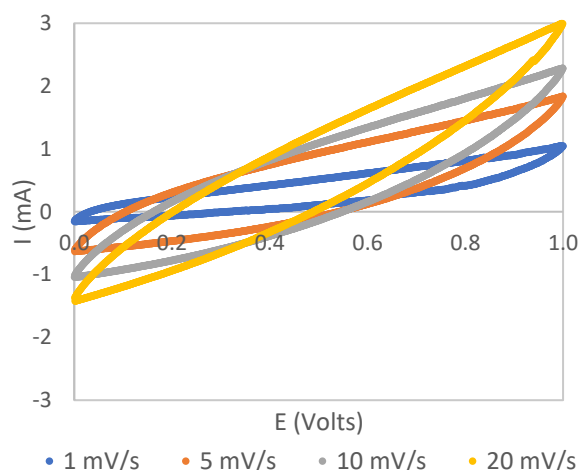


Figure 76. Cyclic voltammograms performed at 1 mV/s, 5 mV/s, 10 mV/s and 20 mV/s scan rates for a voltage limit of 1 volt for the $\text{NaC}_6:\text{C}_6(0.7)$ + 10% H_2O mixture.

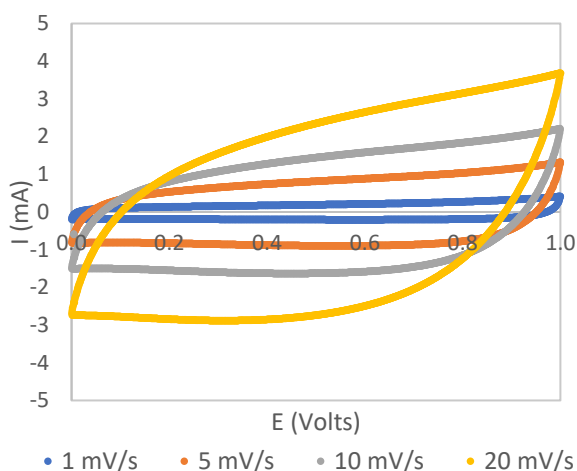


Figure 77. Cyclic voltammograms performed at 1 mV/s, 5 mV/s, 10 mV/s and 20 mV/s scan rates for a voltage limit of 1 volt for the NaC₆:C₆(0.7) + 20% H₂O mixture.

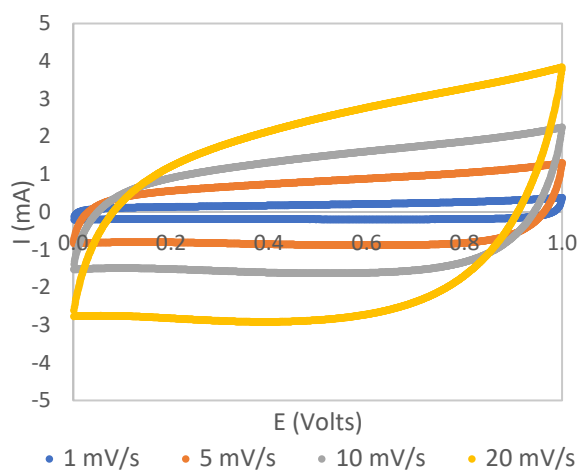


Figure 78. Cyclic voltammograms performed at 1 mV/s, 5 mV/s, 10 mV/s and 20 mV/s scan rates for a voltage limit of 1 volt for the NaC₆:C₆(0.7) + 30% H₂O mixture.

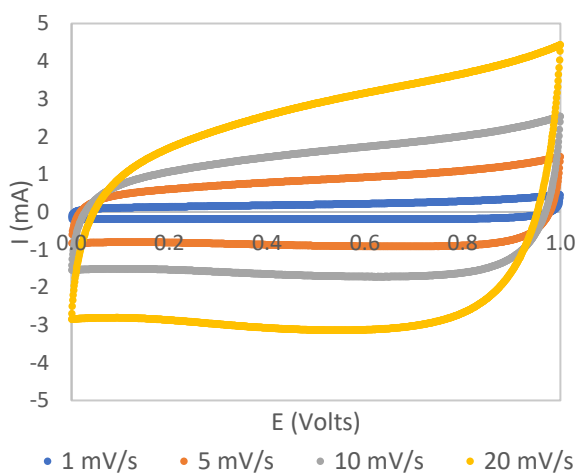


Figure 79. Cyclic voltammograms performed at 1 mV/s, 5 mV/s, 10 mV/s and 20 mV/s scan rates for a voltage limit of 1 volt for the NaC₆:C₆(0.7) + 40% H₂O mixture.

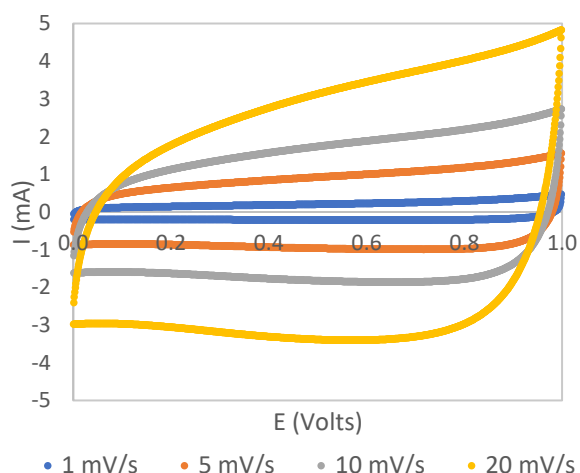


Figure 80. Cyclic voltammograms performed at 1 mV/s, 5 mV/s, 10 mV/s and 20 mV/s scan rates for a voltage limit of 1 volt for the NaC₆:C₆(0.7) + 50% H₂O mixture.

iii) $\text{NaC}_6:\text{C}_8(0.6)$

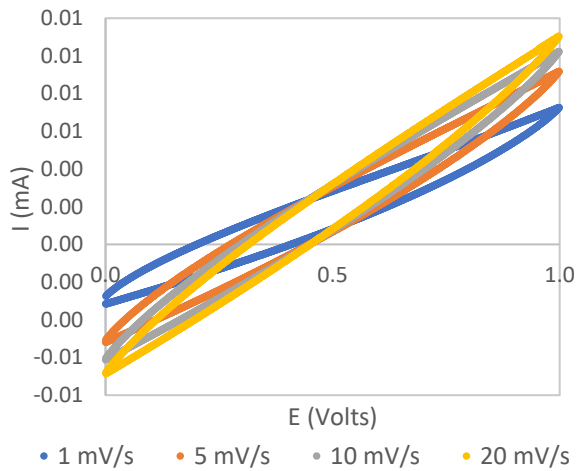


Figure 81. Cyclic voltammograms performed at 1 mV/s, 5 mV/s, 10 mV/s and 20 mV/s scan rates for a voltage limit of 1 volt for the $\text{NaC}_6:\text{C}_8(0.6)$ mixture.

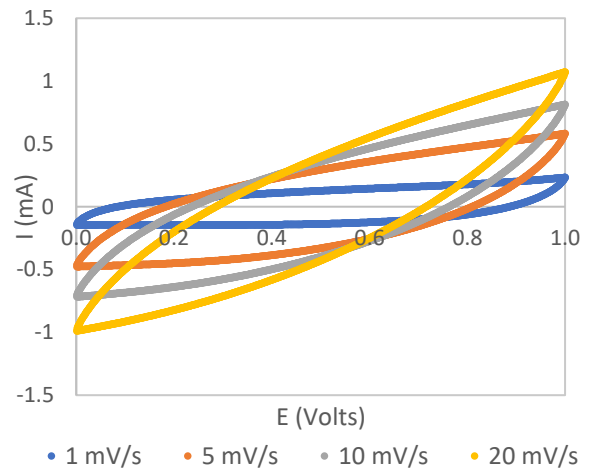


Figure 82. Cyclic voltammograms performed at 1 mV/s, 5 mV/s, 10 mV/s and 20 mV/s scan rates for a voltage limit of 1 volt for the $\text{NaC}_6:\text{C}_8(0.6) + 10\% \text{H}_2\text{O}$ mixture.

iv) $\text{NaC}_6:\text{C}_8(0.7)$

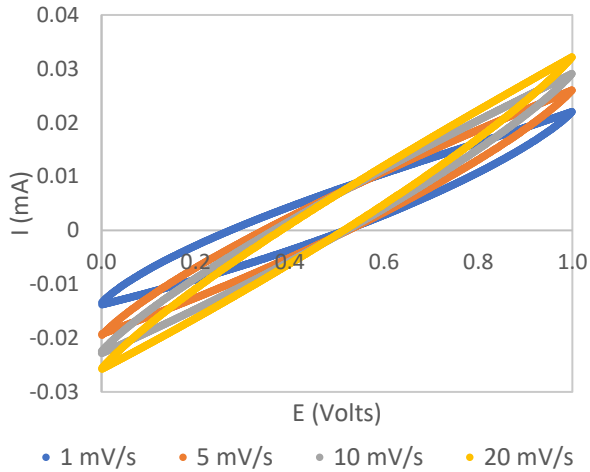


Figure 83. Cyclic voltammograms performed at 1 mV/s, 5 mV/s, 10 mV/s and 20 mV/s scan rates for a voltage limit of 1 volt for the $\text{NaC}_6:\text{C}_8(0.7)$ mixture.

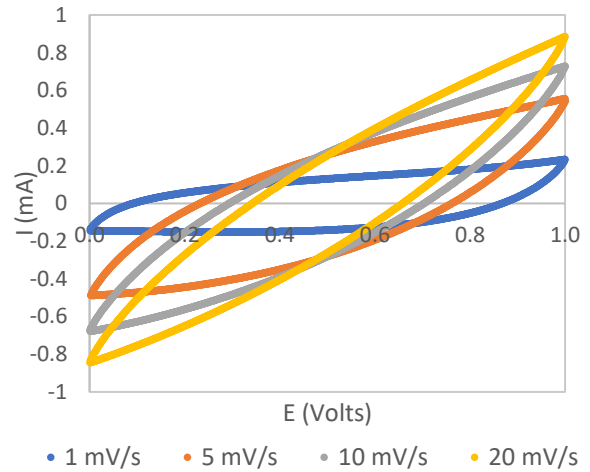


Figure 84. Cyclic voltammograms performed at 1 mV/s, 5 mV/s, 10 mV/s and 20 mV/s scan rates for a voltage limit of 1 volt for the $\text{NaC}_6:\text{C}_8(0.7) + 10\% \text{H}_2\text{O}$ mixture.

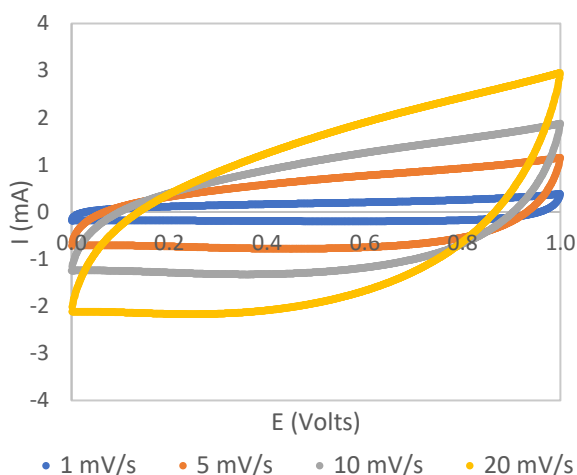


Figure 85. Cyclic voltammograms performed at 1 mV/s, 5 mV/s, 10 mV/s and 20 mV/s scan rates for a voltage limit of 1 volt for the $\text{NaC}_6:\text{C}_8(0.7) + 20\% \text{H}_2\text{O}$ mixture.

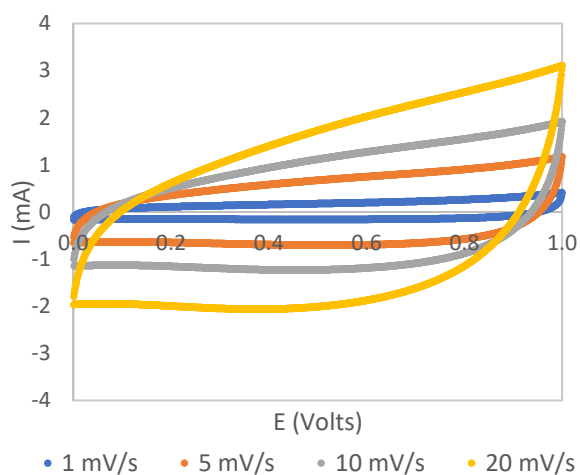


Figure 86. Cyclic voltammograms performed at 1 mV/s, 5 mV/s, 10 mV/s and 20 mV/s scan rates for a voltage limit of 1 volt for the $\text{NaC}_6:\text{C}_8(0.7) + 30\% \text{H}_2\text{O}$ mixture.

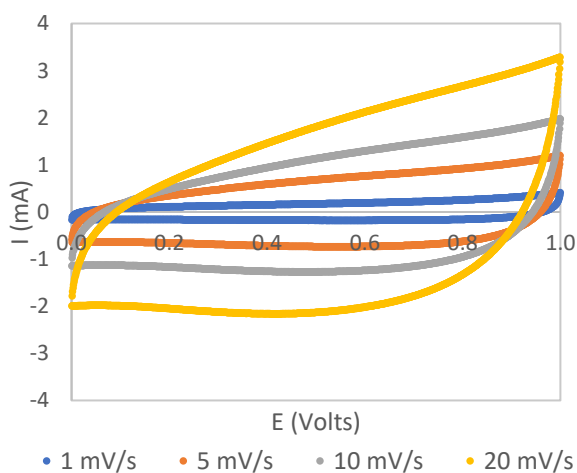


Figure 87. Cyclic voltammograms performed at 1 mV/s, 5 mV/s, 10 mV/s and 20 mV/s scan rates for a voltage limit of 1 volt for the $\text{NaC}_6:\text{C}_8(0.7) + 40\% \text{H}_2\text{O}$ mixture.

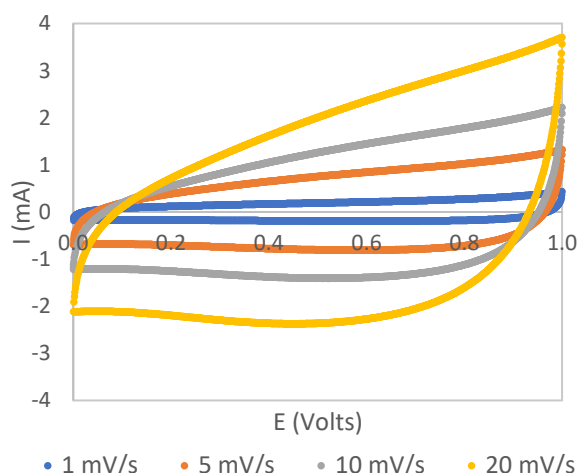


Figure 88. Cyclic voltammograms performed at 1 mV/s, 5 mV/s, 10 mV/s and 20 mV/s scan rates for a voltage limit of 1 volt for the $\text{NaC}_6:\text{C}_8(0.7) + 50\% \text{H}_2\text{O}$ mixture.

v) $\text{NaC}_6:\text{C}_9(0.7)$

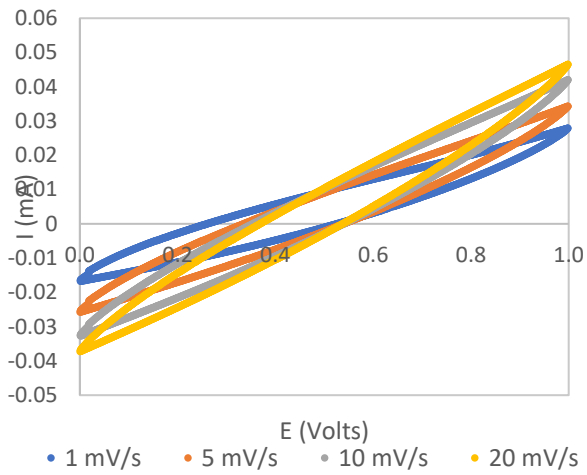


Figure 89. Cyclic voltammograms performed at 1 mV/s, 5 mV/s, 10 mV/s and 20 mV/s scan rates for a voltage limit of 1 volt for the $\text{NaC}_6:\text{C}_9(0.7)$ mixture.

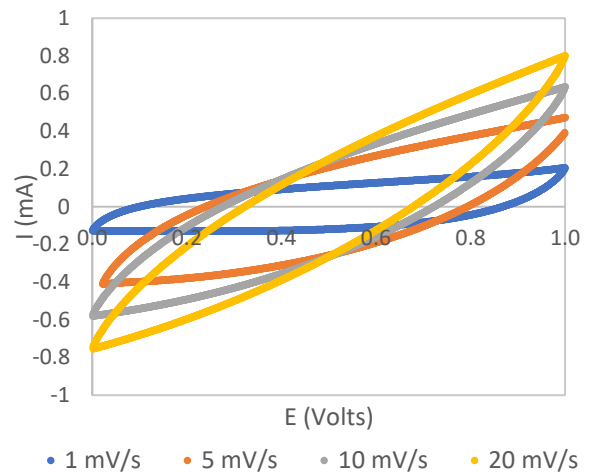


Figure 90. Cyclic voltammograms performed at 1 mV/s, 5 mV/s, 10 mV/s and 20 mV/s scan rates for a voltage limit of 1 volt for the $\text{NaC}_6:\text{C}_9(0.7) + 10\% \text{H}_2\text{O}$ mixture.

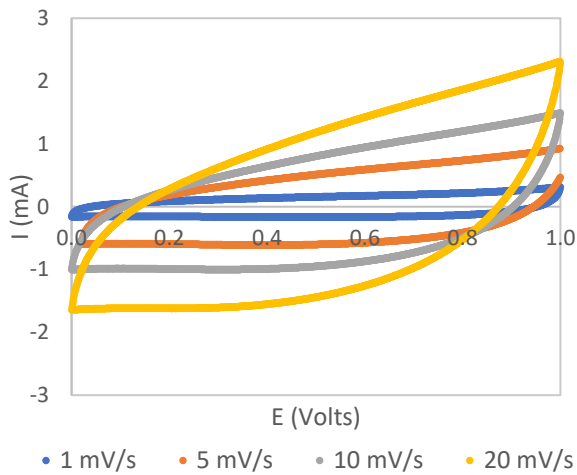


Figure 91. Cyclic voltammograms performed at 1 mV/s, 5 mV/s, 10 mV/s and 20 mV/s scan rates for a voltage limit of 1 volt for the $\text{NaC}_6:\text{C}_9(0.7) + 20\% \text{H}_2\text{O}$ mixture.

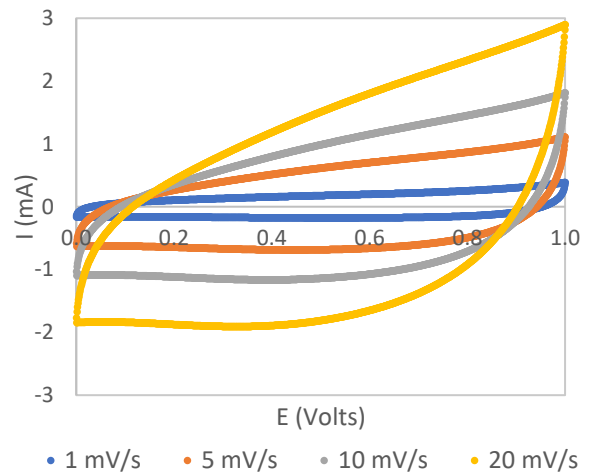


Figure 92. Cyclic voltammograms performed at 1 mV/s, 5 mV/s, 10 mV/s and 20 mV/s scan rates for a voltage limit of 1 volt for the $\text{NaC}_6:\text{C}_9(0.7) + 30\% \text{H}_2\text{O}$ mixture.

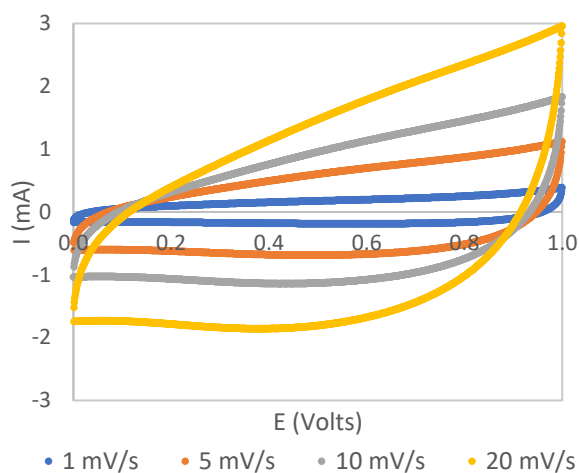


Figure 93. Cyclic voltammograms performed at 1 mV/s, 5 mV/s, 10 mV/s and 20 mV/s scan rates for a voltage limit of 1 volt for the $\text{NaC}_6\text{:C}_9(0.7)$ + 40% H_2O mixture.

vi) $\text{NaC}_6\text{:C}_{10}(0.7)$

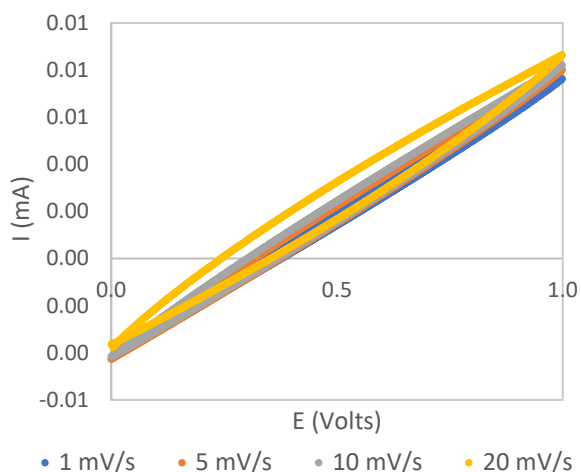


Figure 94. Cyclic voltammograms performed at 1 mV/s, 5 mV/s, 10 mV/s and 20 mV/s scan rates for a voltage limit of 1 volt for the $\text{NaC}_6\text{:C}_{10}(0.7)$ mixture.

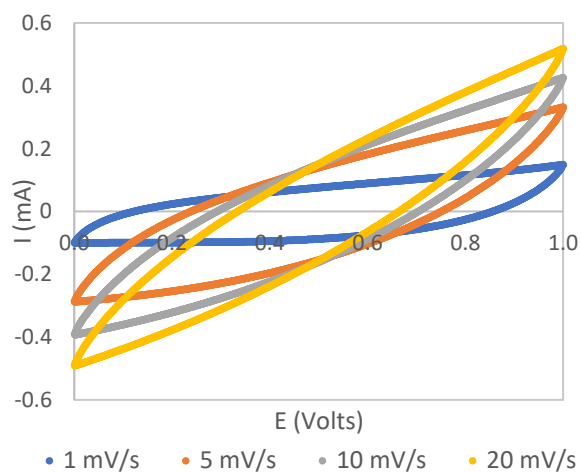


Figure 95. Cyclic voltammograms performed at 1 mV/s, 5 mV/s, 10 mV/s and 20 mV/s scan rates for a voltage limit of 1 volt for the $\text{NaC}_6\text{:C}_{10}(0.7)$ + 10% H_2O mixture.

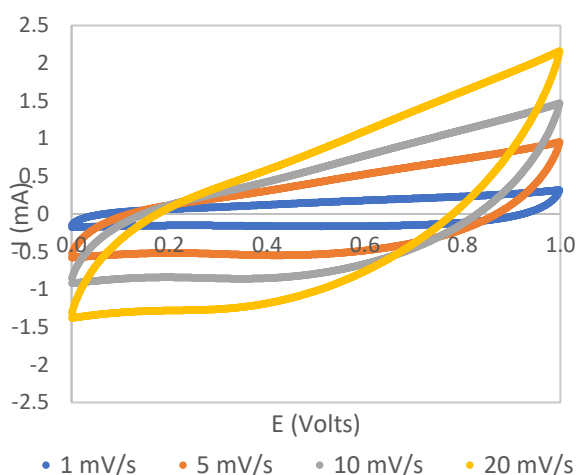


Figure 96. Cyclic voltammograms performed at 1 mV/s, 5 mV/s, 10 mV/s and 20 mV/s scan rates for a voltage limit of 1 volt for the $\text{NaC}_6:\text{C}_{10}(0.7) + 20\% \text{H}_2\text{O}$ mixture.

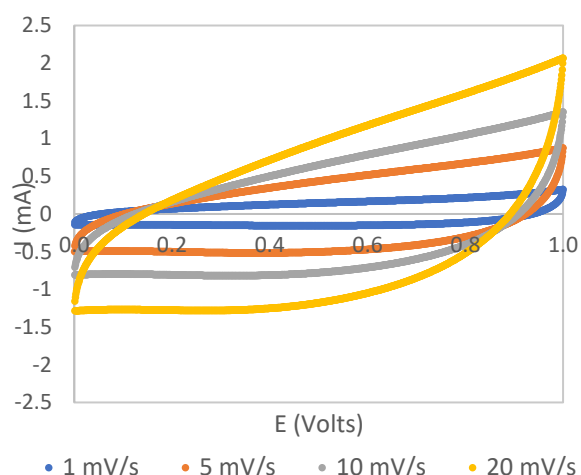


Figure 97. Cyclic voltammograms performed at 1 mV/s, 5 mV/s, 10 mV/s and 20 mV/s scan rates for a voltage limit of 1 volt for the $\text{NaC}_6:\text{C}_{10}(0.7) + 30\% \text{H}_2\text{O}$ mixture.

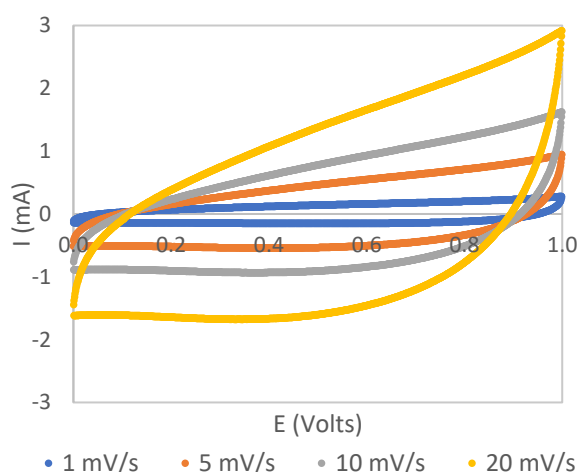


Figure 98. Cyclic voltammograms performed at 1 mV/s, 5 mV/s, 10 mV/s and 20 mV/s scan rates for a voltage limit of 1 volt for the $\text{NaC}_6:\text{C}_{10}(0.7) + 40\% \text{H}_2\text{O}$ mixture.

The CV curves presented from **Figure 70** to **Figure 98** allow to make a first qualitative evaluation on the electrolyte performance. Firstly, it is possible to state that redox behaviour was not clearly observed in the performed cyclic voltammetry, once that the characteristic peaks from faradaic phenomena were not evident in all voltammograms. The voltammogram shape dependence on the scan rate was observed, as with the increasing of the scan rate, the shape of the voltammogram deviates from the quasi-rectangular shape. For lower scan rates, a plateau region is observed indicating that the ions move at an almost constant rate (producing a constant current) with the increment of the voltage, this indicates that the ions insertion in the pores and accumulation in the electrode surface occurs with low ohmic resistance [38,39]. As the scan rate increases, the plateau region reduces and a current dependence on the voltage is observed (inclination of the voltammogram). This suggests

that the ions time scale to reach the electrode surface (related to the resistance) and pores is higher than the voltage scan rate.

Inside each eutectic-water system, the water content influence was clearly seen, as the higher the water content the more pronounced is the quasi-rectangular shape. Moreover, for all eutectic-water systems the 20 wt% in water is the composition at which the quasi-rectangular shape is firstly detected (replacing the “leaf-like” shape obtained until then). This effect of the water content on the voltammograms shape is an indication that the presence of water lowers the electrolyte resistance (by improving the ionic mobility) and allows the ions to have a faster response to the applied voltage, and therefore establish in the electrode pores and surface faster.

In order to analyse the acid chain length effect on cyclic voltammetry, the voltammograms recorded at a potential scan rate of 5 mV/s regarding NaC₆:C₆(0.7), NaC₆:C₈(0.7), NaC₆:C₉(0.7), and NaC₆:C₁₀(0.7) with 40 wt% H₂O were plotted in **Figure 99**.

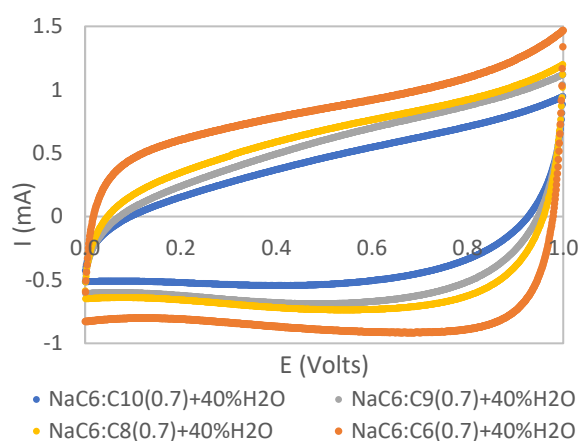


Figure 99. Cyclic Voltammetry curves plotted at 5 mV/s potential scan rate for NaC₆:C₆(0.7), NaC₆:C₈(0.7), NaC₆:C₉(0.7), NaC₆:C₁₀(0.7) with 40 wt% H₂O.

From the previous figure it is possible to observe that lower acid chain leads to a voltammogram that as more rectangular shape. This can be related to the fact that smaller molecules have greater mobility and as a consequence, their time scale to establish at the electrode surface to form the EDL is smaller. Moreover, smaller ions can introduce easily in the microporosity (less resistance).

For the mixtures presenting a quasi-rectangular shape voltammogram (starting at 20 wt% H₂O), the capacitance was determined for each scan rate (1 mV/s; 5 mV/s; 10 mV/s and 20 mV/s) using equation (22), then the electrode specific capacitance was determined through equation (13). The obtained values are plotted by group from **Figure 100** to **Figure 104**.

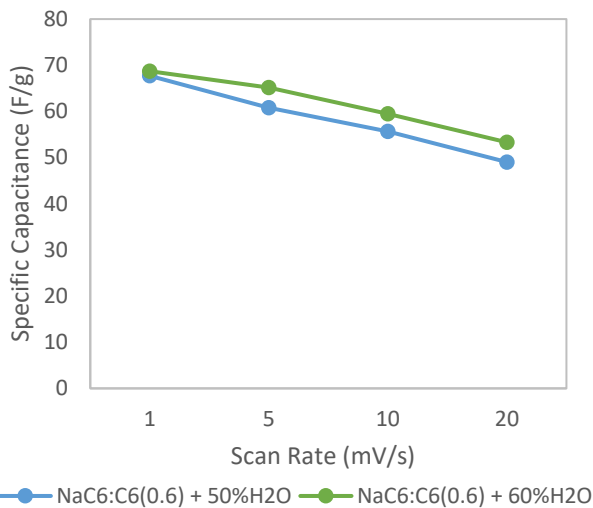


Figure 100. Electrode Specific Capacitance as function of the CV scan rate for the $\text{NaC}_6:\text{C}_6(0.6)$ -water mixtures (50 wt% H_2O and 60 wt% H_2O).

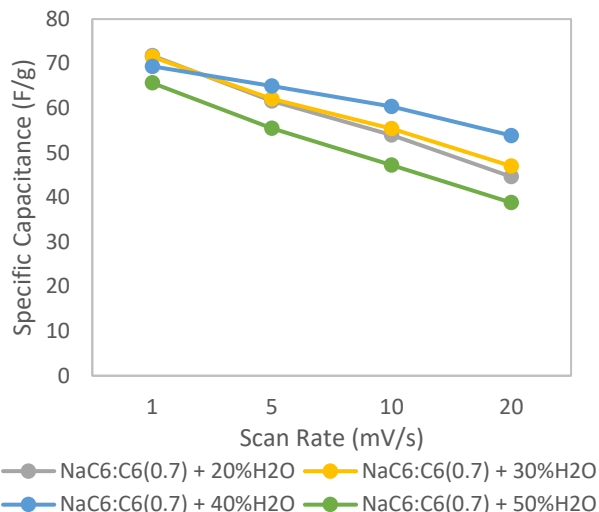


Figure 101. Electrode Specific Capacitance as function of the CV scan rate for the $\text{NaC}_6:\text{C}_6(0.7)$ -water mixtures (20 wt% H_2O , 30 wt% H_2O , 40 wt% H_2O and 50 wt% H_2O).

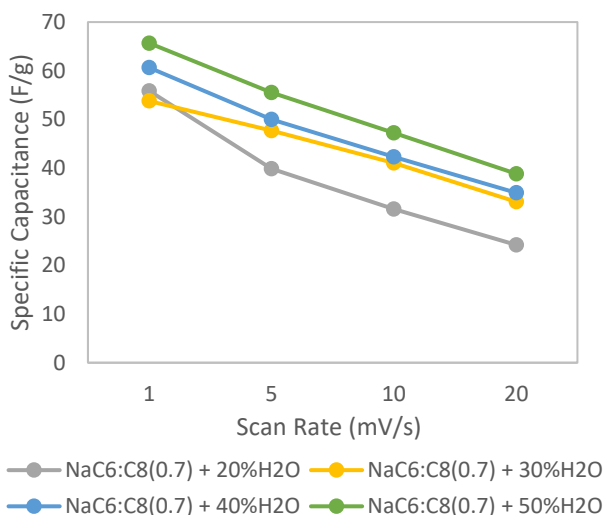


Figure 102. Electrode Specific Capacitance as function of the CV scan rate for the $\text{NaC}_6:\text{C}_8(0.7)$ -water mixtures (20 wt% H_2O , 30 wt% H_2O , 40 wt% H_2O and 50 wt% H_2O).

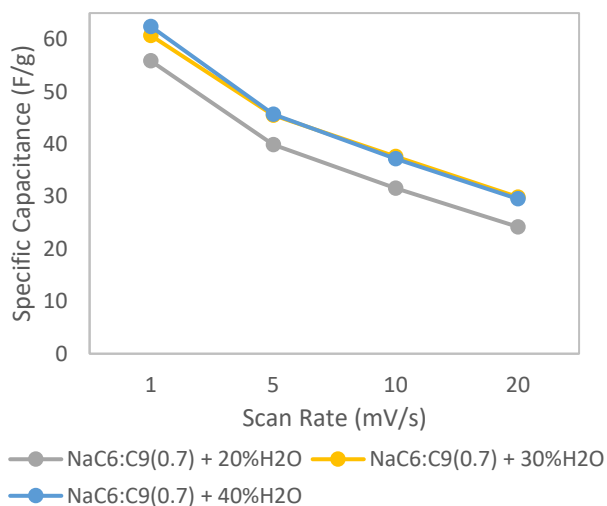


Figure 103. Electrode Specific Capacitance as function of the CV scan rate for the $\text{NaC}_6:\text{C}_9(0.7)$ -water mixtures (20 wt% H_2O , 30 wt% H_2O and 40 wt% H_2O).

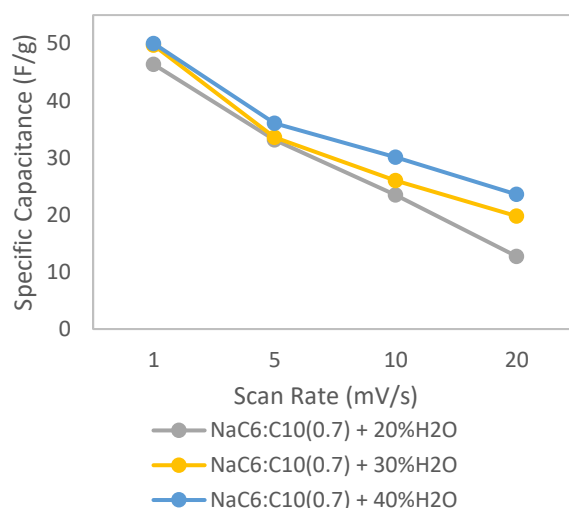


Figure 104. Electrode Specific Capacitance as function of the CV scan rate for the $\text{NaC}_6:\text{C}_{10}(0.7)$ -water mixtures (20 wt% H_2O , 30 wt% H_2O and 40 wt% H_2O).

From the above presented figures, is observed that for all mixtures the specific capacitance decreases with the potential scan rate, which is a typical behaviour observed for EDLC often reported on literature [38,39]. This capacitance drop with the voltage scan rate is consequence of the resistance enhancement with the scan rate as was previously discussed through the analysis of the voltammograms shape. The estimated specific capacitance decreases with the acid chain, once larger anions have their insertion in the micropores as well as their establishment at the electrode surface more limited.

In order to test the electrochemical stability of the electrolyte, cyclic voltammetry was performed for different voltage limits (1V, 1.2V, 1.4V, 1.6V, 1.8V and 2V) with a scan rate of 1 mV/s. The obtained voltammograms for the $\text{NaC}_6:\text{C}_6(0.6) + 10\%\text{H}_2\text{O}$ mixture are presented in **Figure 105**.

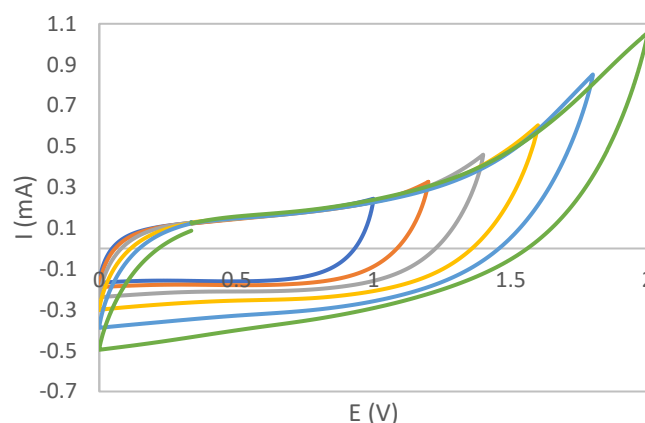


Figure 105. Cyclic Voltammogram for 1 mV scan rate and 1V, 1.2V, 1.4V, 1.6V, 1.8 V and 2V maximum potential of $\text{NaC}_6:\text{C}_6(0.6) + 10\%\text{H}_2\text{O}$.

As it can be observed in the previous figure, the voltammograms do not present peaks related to faradaic processes, and therefore, the electrolyte did not present signs of degradation even for the highest tested electrochemical window (2 volts). Thus, it is possible to say that, although water is present, the mixture can

withstand voltages higher than 1 Volt. On the other hand, with the increment of potential the voltammograms deviate from the quasi-rectangular shape. This behaviour represents a poor response from the electrolyte ions to insert in the electrode porosity and form the double layer as the applied voltage increases.

4.3.2. Galvanostatic Charge-Discharge

After performing CV and based on the results, some samples were selected for further testing (Galvanostatic charge/discharge, GCD), namely those with higher water content, which as discussed in the previous subsection, were those demonstrating better performance (quasi-rectangular shape voltammograms). The operational conditions to perform GCD method were based in the results of CV, namely the applied current in GCD corresponded, approximately, to the current obtained in CV at the plateau zone (current supported by the system). The following table summarizes the samples selected to perform GCD and the respective operational conditions. All GCD test were performed at room temperature.

Table 16. GCD operational conditions for each sample.

Mixture	wt% H ₂ O	Potential limit (V)	Applied current (mA)
NaC₆:C₆(0.6)	50	1	1
	60	1	1
NaC₆:C₆(0.7)	30	1	1
	40	1	1
	50	1	1
NaC₆:C₈(0.7)	20	1	1
	30	1	1
	40	1	1
	50	1	1
NaC₆:C₉(0.7)	20	1	0.5
	30	1	1
	40	1	1
NaC₆:C₁₀(0.7)	20	1	0.5
	30	1	1
	40	1	1

The capacitance calculated from galvanostatic method as function of the number of cycles is presented in **Figure 106** to **Figure 119**, as well as the charge/discharge efficiency and the capacitance of retention (Initial capacitance/Capacitance at cycle n).

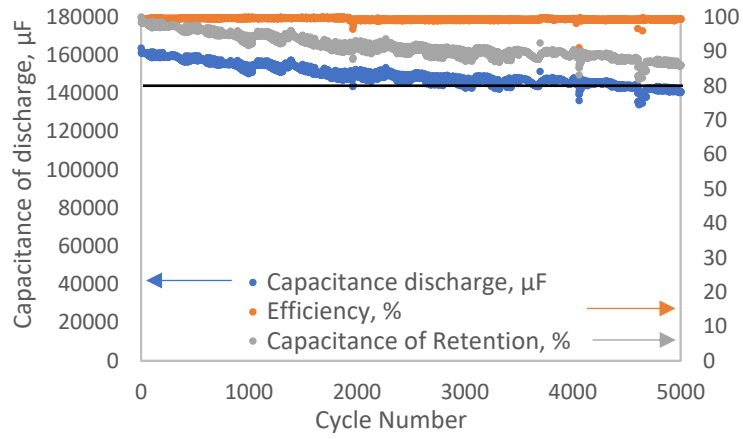


Figure 106. Capacitance, Capacitance of retention, and efficiency as function of cycle number for $\text{NaC}_6:\text{C}_6(0.6) + 50\%\text{H}_2\text{O}$ mixture.

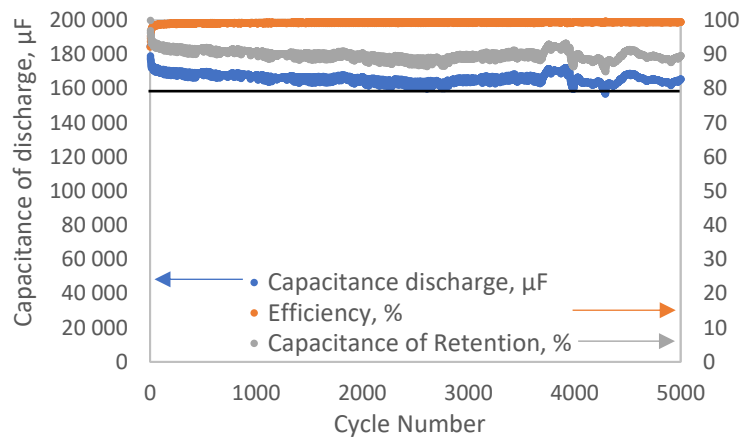


Figure 107. Capacitance, Capacitance of retention, and efficiency as function of cycle number for $\text{NaC}_6:\text{C}_6(0.6) + 60\%\text{H}_2\text{O}$ mixture.

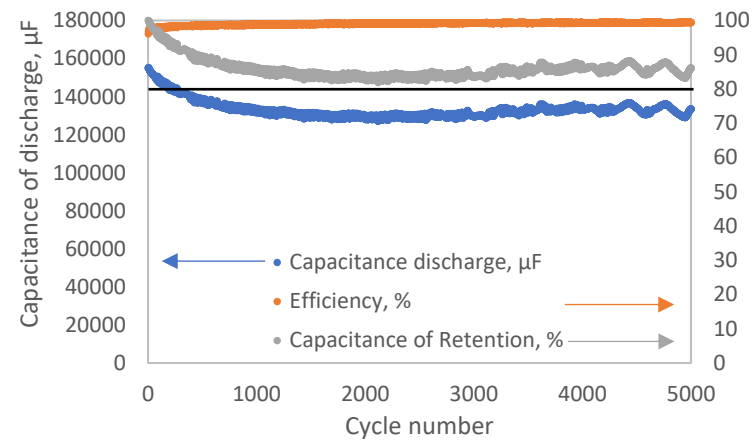


Figure 108. Capacitance, Capacitance of retention, and efficiency as function of cycle number for $\text{NaC}_6:\text{C}_6(0.7) + 30\%\text{H}_2\text{O}$ mixture.

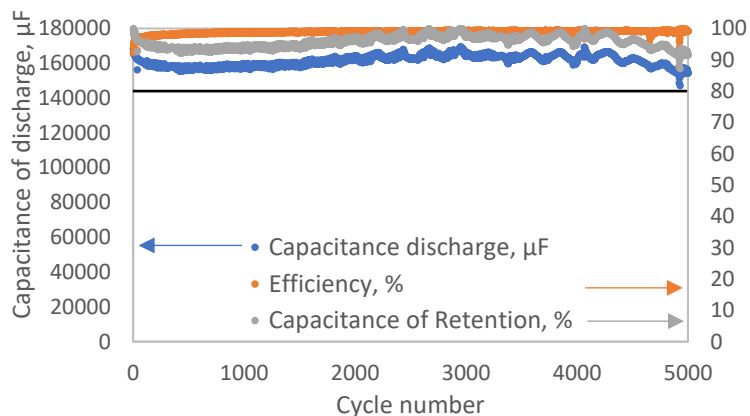


Figure 109. Capacitance, Capacitance of retention, and efficiency as function of cycle number for $\text{NaC}_6:\text{C}_8(0.7)$ + 40% H_2O mixture.

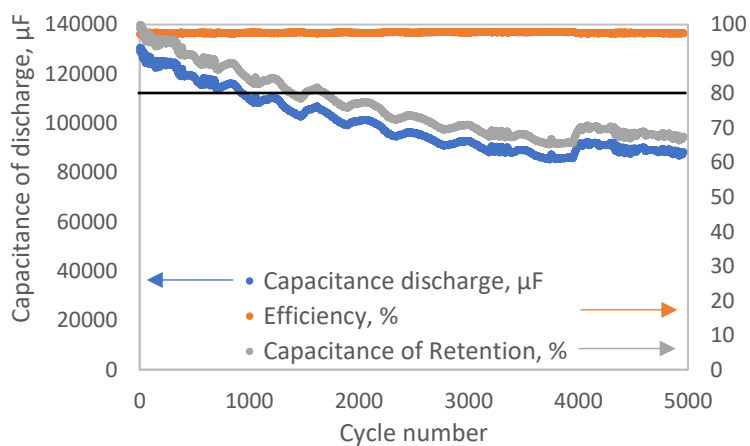


Figure 110. Capacitance, Capacitance of retention, and efficiency as function of cycle number for $\text{NaC}_6:\text{C}_8(0.7)$ + 50% H_2O mixture.

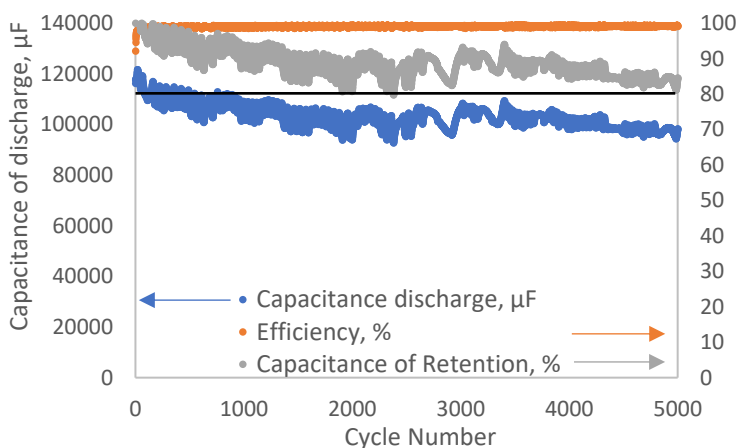


Figure 111. Capacitance, Capacitance of retention, and efficiency as function of cycle number for $\text{NaC}_6:\text{C}_8(0.7)$ + 20% H_2O mixture.

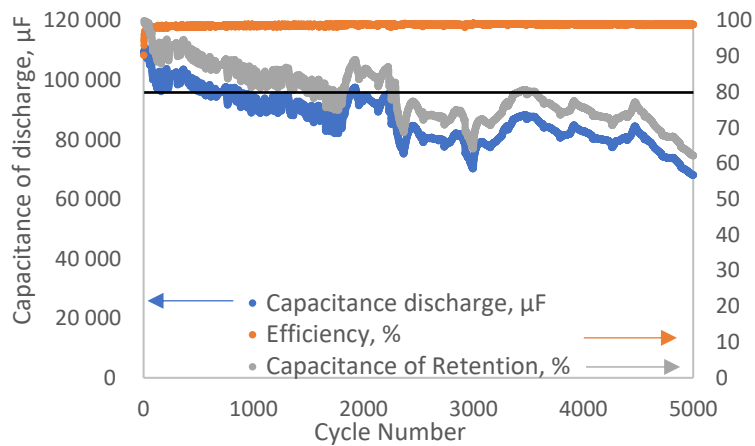


Figure 112. Capacitance, Capacitance of retention, and efficiency as function of cycle number for $\text{NaC}_6:\text{C}_8(0.7)$ + 30% H_2O mixture.

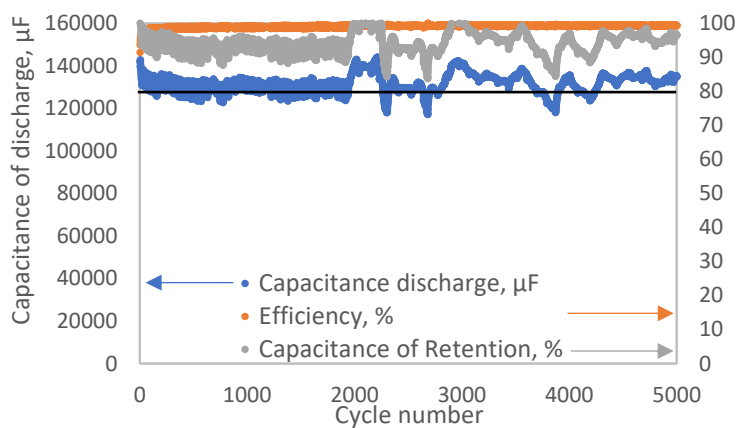


Figure 113. Capacitance, Capacitance of retention, and efficiency as function of cycle number for $\text{NaC}_6:\text{C}_8(0.7)$ + 50% H_2O mixture.

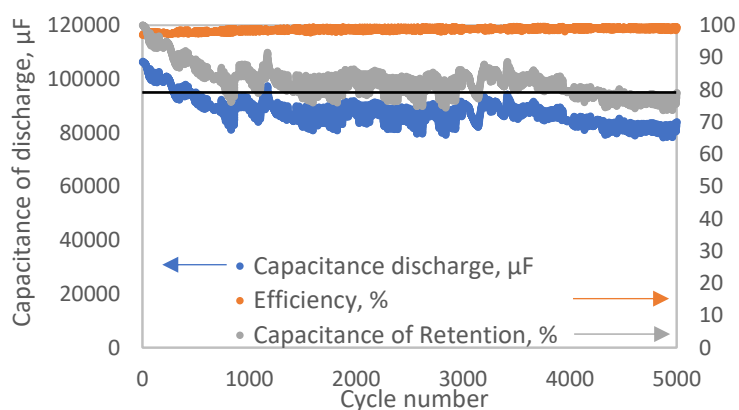


Figure 114. Capacitance, Capacitance of retention, and efficiency as function of cycle number for $\text{NaC}_6:\text{C}_9(0.7)$ + 20% H_2O mixture.

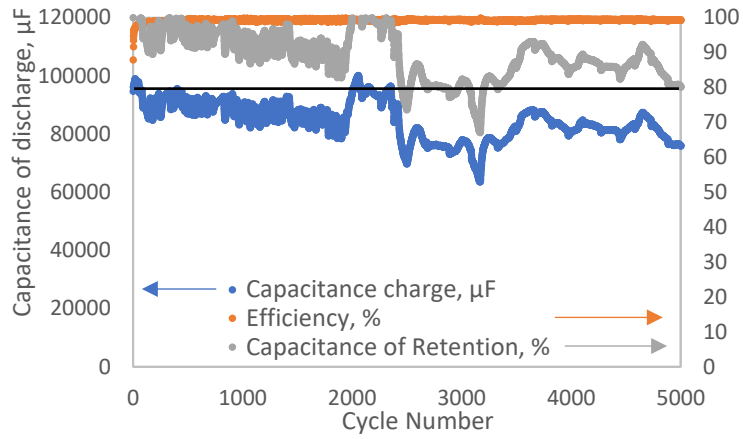


Figure 115. Capacitance, Capacitance of retention, and efficiency as function of cycle number for $\text{NaC}_6:\text{C}_9(0.7)$ + 30% H_2O mixture.

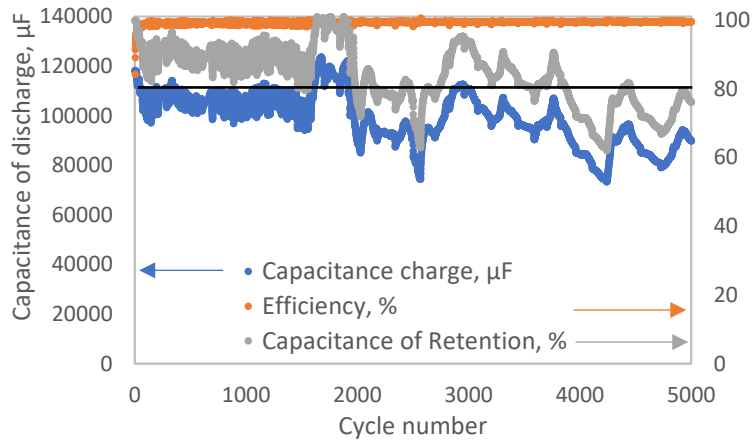


Figure 116. Capacitance, Capacitance of retention, and efficiency as function of cycle number for $\text{NaC}_6:\text{C}_9(0.7)$ + 40% H_2O mixture.

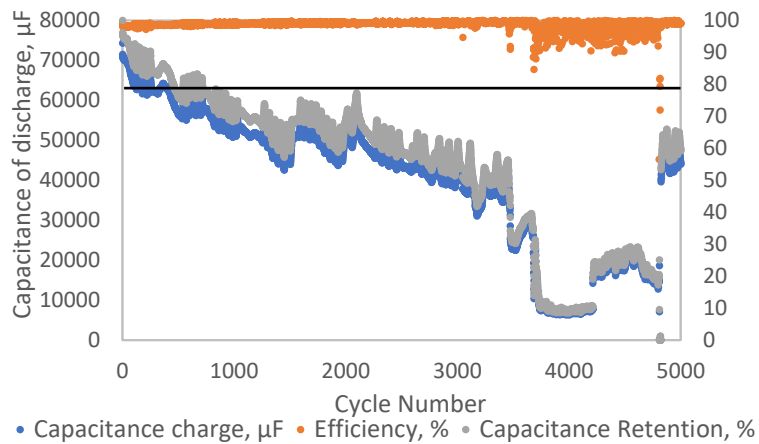


Figure 117. Capacitance, Capacitance of retention, and efficiency as function of cycle number for $\text{NaC}_6:\text{C}_{10}(0.7)$ + 20% H_2O mixture.

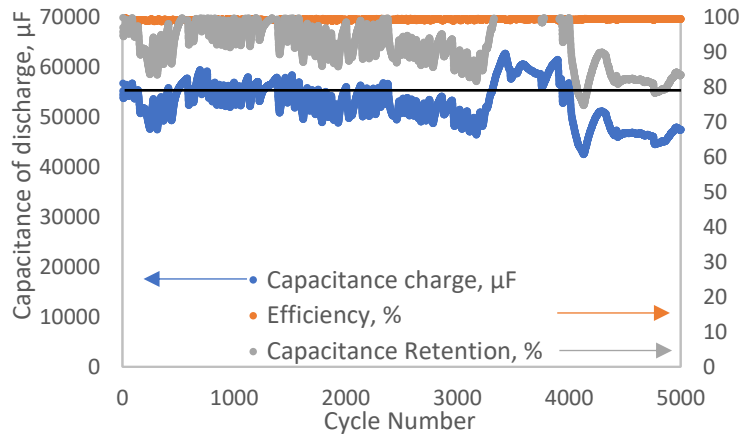


Figure 118. Capacitance, Capacitance of retention, and efficiency as function of cycle number for $\text{NaC}_6:\text{C}_{10}(0.7) + 30\% \text{H}_2\text{O}$ mixture.

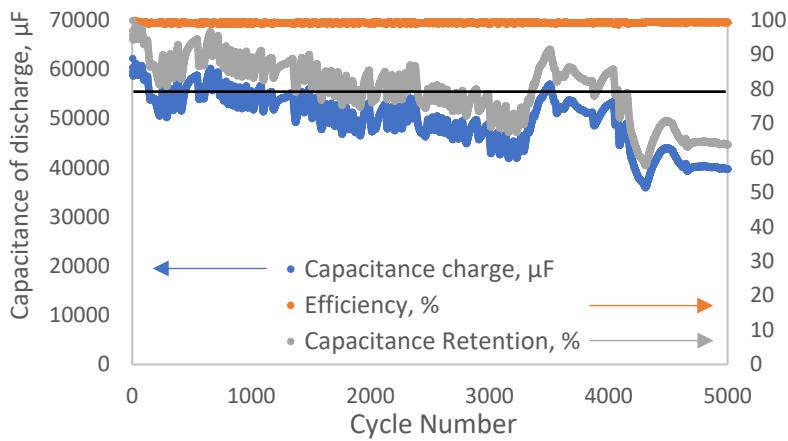


Figure 119. Capacitance, Capacitance of retention, and efficiency as function of cycle number for $\text{NaC}_6:\text{C}_{10}(0.7) + 40\% \text{H}_2\text{O}$ mixture.

In all tests the efficiency of charge and discharge was maintained closed to 100%. For the sample $\text{NaC}_6:\text{C}_8(0.7) + 40\% \text{H}_2\text{O}$ results are absent because after performing two independent tests, it was not possible to reach more than 1000 cycles. To evaluate the life cycle of each mixture the capacitance loss between the initial capacitance and the capacitance at the 5000 cycle was quantified ($\frac{C_i - C_{5000}}{C_i} \times 100$) and is presented in **Table 17**, as well as the capacitance retained after 5000 cycles.

Table 17. Specific Capacitance at the beginning of cycling and at the 5000th cycle, % of capacitance loss and % of retained capacitance.

Mixture	wt% H ₂ O	C _{initial} (F/g)	C ₅₀₀₀ (F/g)	$\frac{\Delta C}{C_i}$	% Retained Capacitance (C _i /C ₅₀₀₀)
NaC ₆ :C ₆ (0.6)	50	64.6	56.3	12.8	87
	60	71.6	66.2	7.5	92
NaC ₆ :C ₆ (0.7)	30	62.1	53.4	14.0	86
	40	67.2	61.8	8.0	92
	50	52	35.4	31.9	68
NaC ₆ :C ₈ (0.7)	20	47.1	39.3	16.6	83
	30	44	27.3	38.0	62
	40	-	-	-	-
	50	56.8	54	4.9	95
NaC ₆ :C ₉ (0.7)	20	42.5	33.6	20.9	79
	30	38.5	30.4	21.0	79
	40	47.3	36	23.9	76
NaC ₆ :C ₁₀ (0.7)	20	28.6	17.6	38.5	62
	30	22.8	19.1	16.2	84
	40	24.9	15.9	36.1	64

Often in literature, a value of 80% retained capacitance is given as a reference to evaluate the life cycle. Therefore, the greater the number of cycles with a capacitance retention higher than 80%, the better the cycling stability. From the above presented table, it is seen that a substantial number of electrolytes fulfil this parameter after 5000 cycles. Only four samples have much lower capacitance retention than 80%, namely NaC₆:C₁₀(0.7) with 20% and 40% of water, NaC₆:C₈(0.7) +30%H₂O and NaC₆:C₆(0.7) +50%H₂O. Moreover, the life cycle, here evaluated by the specific capacitance decay, does not seem to be related to the water content or the acid chain, but to a more complex phenomenon.

The potential versus time GCD curves evolution with the number of cycles are presented in **Figure 120** for NaC₆:C₆(0.6) +50%H₂O as an illustrative example.

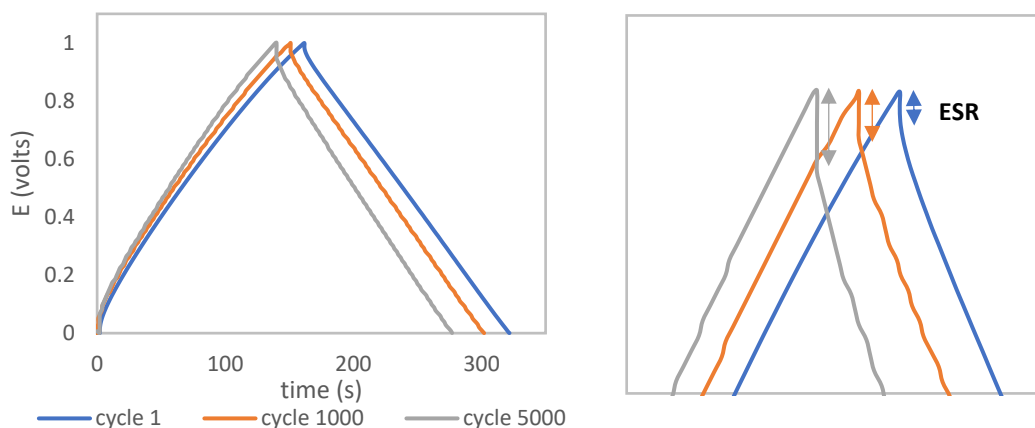


Figure 120. Galvanostatic charge-discharge cycles for the $\text{NaC}_6:\text{C}_6(0.6) + 50\% \text{H}_2\text{O}$. Right: ESR increasing with the number of cycles.

A typical symmetrical triangle shape characteristic of EDLC supercapacitor is obtained for the GCD potential versus times curves. Additionally, the internal resistance (ESR) increases with the number of cycles as expected, which can be related, for example, to the irreversible adsorption of species in the microporosity overtime, reflecting in a decrease of the capacitance as observed in **Figure 106** to **Figure 119**.

In order to have a better comparison of the results the initial specific capacitance and the specific capacitance at, approximately, cycle 5000 are presented in **Figure 121** and **Figure 122**, respectively.

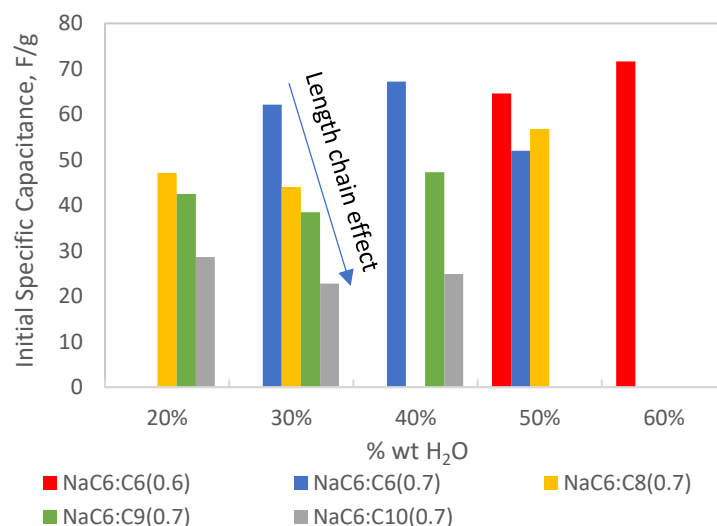


Figure 121. Initial specific capacitance per electrode as a function of massic water content.

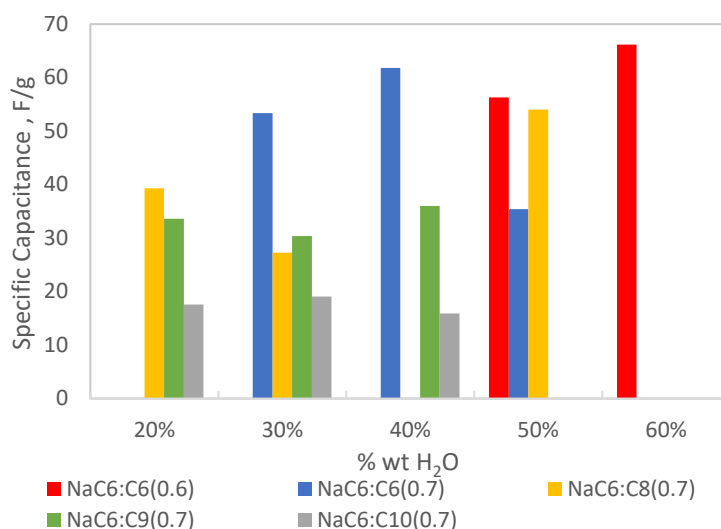


Figure 122. Specific capacitance per electrode after approximately 5000 cycles as a function of massic water content.

From the previous figures, it can be seen that the acid chain length has an important effect in the obtained specific capacitance. The highest capacitance (71.6 F/g) is obtained for the mixture containing the acid with the smallest alkyl chain and with the highest water content, NaC₆:C₆(0.6) + 60% H₂O. The conjugate bases of the carboxyl acids (hexanoate, octanoate, nonanoate and decanoate) are the anion in the studied mixtures, making them the negative charge carriers. Since the capacitance greatly decreases with the increment of the anions size (as already observed above from the CV results), as observed in **Figure 121** and **Figure 122**, this may reflect the difficulty of these species to insert in the microporosity of the carbon electrodes (and even to establish at the surface) as their sizes increases. The decrease of the specific capacitance with the increase of the alkyl chain using microporous carbon electrodes, has also been reported on literature for electrolytes containing tetralkylammonium cations [59]. Additionally, for mixtures containing the same acid (i.e. NaC₆:C₆(0.6) and NaC₆:C₆(0.7)) and with similar molar water composition, for example NaC₆:C₆(0.6) + 50 wt% H₂O (87.4 molar% H₂O) and NaC₆:C₆(0.7) + 50 wt% H₂O (87.2 molar% H₂O), the capacitance is higher for the mixture with higher salt content NaC₆:C₆(0.6), which has more quantity of sodium cations that have smaller size, and therefore can insert in the porosity and form the EDL more easily.

Although the highest specific capacitance obtained, 71.6 F/g, is lower than the ones obtained for other eutectic systems, namely the Choline Chloride: Urea (96 F/g at 0.2 A/g in three dimensional graphene [30]), this is a promising value that can be enhanced through the optimization of the electrode used (for example, testing these systems in mesoporous carbon).

4.3.3. Potentiostatic Electrochemical Impedance Spectroscopy

Potentiostatic Electrochemical Impedance Spectroscopy was performed for the same mixtures used in GCD, before ("fresh" cell) and after cycling (100 charge/discharging cycles at the same conditions of GCD). The obtained Nyquist plots are presented from **Figure 129** to **Figure 144** (in Supporting Information), for all mixtures a spectrum shape characteristic of EDLC was observed. Three main regions can be highlighted: A semi-circle at

high frequencies, a 45° line at middle frequencies and a straighter line at lower frequencies. In **Figure 123** the three main impedances values extracted for each mixture, R_A , R_B , and R_C are identified.

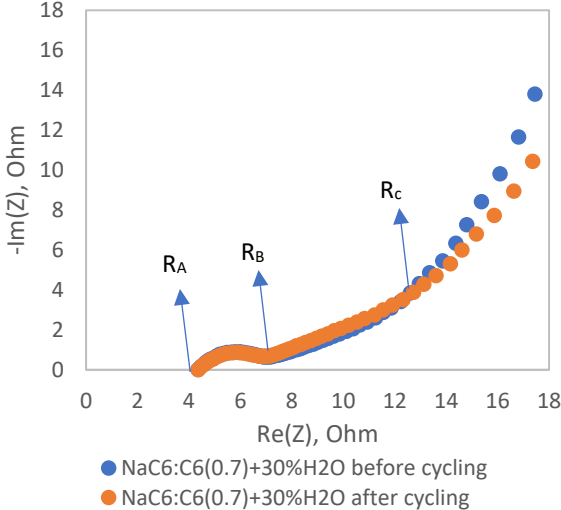


Figure 123. Nyquist plot for NaC6:C6(0.7) + 30% H2O with identification of the different zone limits.

Moreover, in all cases, for the low frequency zone, there is a straighter shape before cycling than after cycling (**Figure 129** to **Figure 144** in Supporting Information), which reflects the decrease of the capacitive behaviour with the usage as expected, being in accordance with the GCD results in which it is observed a decrease of the capacitance with the number of performed cycles.

The values of R_A are associated with the internal resistance (ESR) of the cell, which is greatly influenced by the electrolyte resistance. The determined values for each mixture are presented in **Figure 124**.

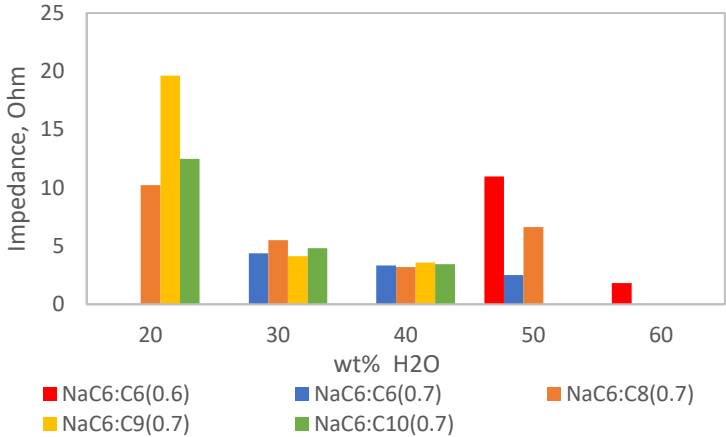


Figure 124. R_A values before cycling displayed by water content.

As it can be seen from the previous figure, the R_A values present higher values for 20% water content, decreasing until 40%. This reflects the higher resistance of the electrolytes with lower water content, which are associated with higher viscosity and lower conductivity. However, the NaC6:C6(0.6) and NaC6:C8(0.7) at 50% H2O

the electrolyte resistance increases, which was not expected. Despite this, it is important to point that these compositions are “limit” compositions, in a sense that the NaC₆:C₆(0.6) + 50% H₂O is the composition after the gel formation, and the NaC₆:C₈(0.7) + 50% H₂O is the composition close to the limit of miscibility of the water/eutectic. The NaC₆:C₆(0.6) + 60% H₂O is the mixture that has the lowest internal resistance (ESR), 1.83 Ω, this value is close to the ESR of organic electrolytes, for 1M TEABF₄ in acetonitrile in activated carbon electrodes is approximately 1 Ω [2].

The decrease of the ESR values with water content for eutectic-based electrolytes was also observed for the Choline Chloride: Urea system [30]. Moreover, the cells using Choline Chloride: Urea systems present an internal resistance of approximately 10 Ω for a 5 wt% of water content which is equivalent to the 20 wt% of water for the here studied systems.

The semi-circle values (R_B-R_A) are associated with polarization resistance of the electrodes and electrolyte components. In **Figure 125** the values corresponding to the semi-circle for each mixture are presented as a function of the water composition.

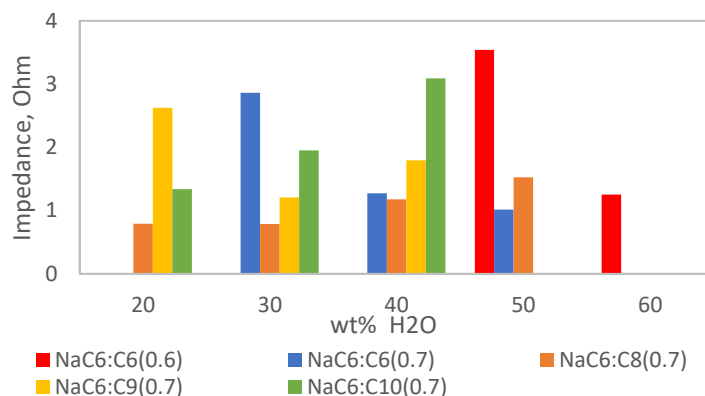


Figure 125. R_B-R_A values before cycling displayed as a function of water content.

Smaller ions, such as Na⁺, H⁺ have high charge density and are less polarizable, adsorbing perfectly to the interface. In the other hand, the carboxylic acid anions, have a delocalized charge, lower charge density and, therefore, are more polarizable. Taking this into account, the organization of the double layer by interface polarization is anarchic and the R_B-R_A values do not seem to have a clear evolution with the acid chain or the water content. Additionally, the very irregular surface of the carbon on which weakly polarizable long-chain species are adsorbed, creates an inhomogeneity of the surface polarization according to the entanglement of the chain. It is therefore not possible to find a direct correlation between the nature of the eutectic mixture, the water content, with the polarization resistance. The R_c values delimit the Warburg region which is related to the ion's diffusion in the microporosity of the electrodes. The determined R_c values for each mixture are presented in **Figure 126**.

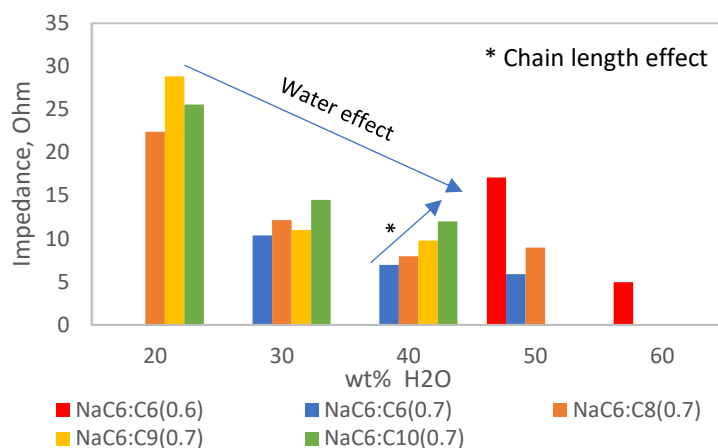


Figure 126. R_c values before cycling displayed by water content.

As can be seen in the previous figure, the values of R_c generally increase with the acid alkyl chain and decrease with water content, for a water composition ranging between 20% and 40%. These results are in accordance with the previous results from CV in which more resistive voltammograms (deviating from the quasi-rectangular shape) were obtained for mixtures containing longer chains, and with the GCD results showing lower capacitance for higher alkyl chains. All these findings are a reflex of a more difficult diffusion of the anions in the microporosity. In this case, an increase for the NaC₆:C₆(0.6) and NaC₆:C₈(0.7) at 50% H₂O is also observed. The NaC₆:C₆(0.6) + 60% H₂O has the lowest resistance associated to the diffusion of the ions in the microporosity.

The specific capacitances obtained through PEIS analysis before and after cycling is present in **Figure 127** and **Figure 128**.

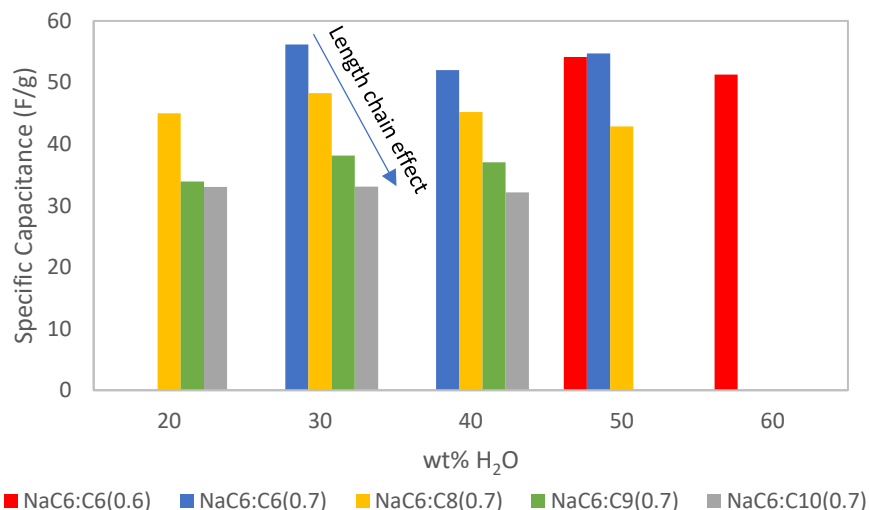


Figure 127. Electrode Specific Capacitance obtained through Potentiostatic Electrochemical Impedance Spectroscopy (PEIS) before cycling.

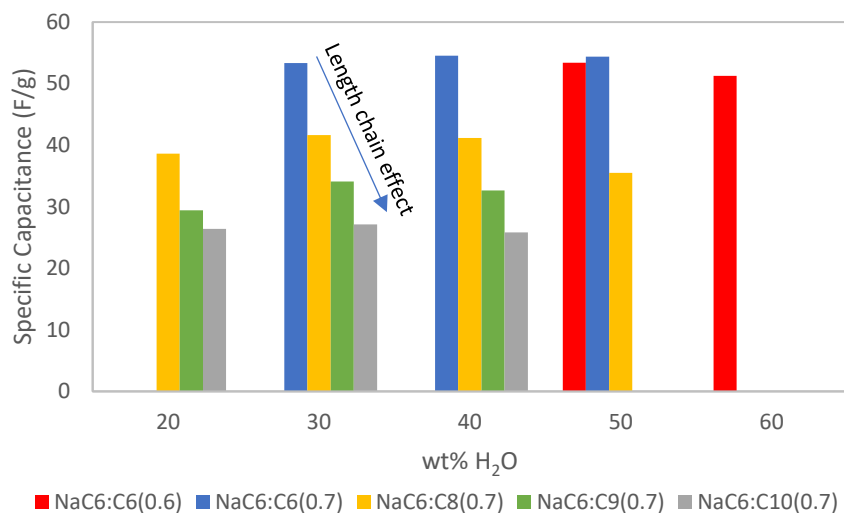


Figure 128. Electrode Specific Capacitance obtained through Potentiostatic Electrochemical Impedance Spectroscopy (PEIS) after cycling.

Analogous to the specific capacitance results from CV and GCD, here it also detected that the alkyl chain length is the parameter that mostly influences the capacitance obtained.

5. Conclusions

Mixing water with eutectic mixtures of sodium hexanoate with fatty acids (hexanoic, octanoic, nonanoic, decanoic) leads to a complex variety of physical states for different concentrations of each compound. Those physical states include clear homogeneous liquid phase, two phases, three phases and, even, turbid gel mixtures. These observations are clear evidence of the variety of interactions established between the different compounds in solution. On one hand, this limits the operational temperature range of these mixtures as electrolytes. On the other hand, it allows the preparation of stable gel media without the need to use an additional supporting matrix, making these mixtures potential candidates for quasi-solid electrolytes, which are advantageous to prevent the electrolyte leakage.

In the conductivity study, it was concluded that three parameters highly influence the results: the water content, the acid chain length, and the amount of salt in the mixture. Generally, it was observed that the conductivity increased with the water content and decreased with the acid chain length, reflecting the higher mobility of the species triggered by the presence of water and the intrinsic higher capability of diffusion of smaller species. Moreover, it was observed that for mixtures with the same acid chain length and containing similar molar water composition, the conductivity was higher for those with higher amount of salt. Overall, $\text{NaC}_6\text{:C}_6(0.6) + 60\%\text{H}_2\text{O}$ presented the highest conductivity, 22.3 mS/cm at 20 °C. The viscosity results showed that the water addition decreases the viscosity of the mixtures resulting in higher mobility of the species, in accordance with the conductivity observations. The pH measurements allowed to conclude that the deprotonated form of the acids is predominant for all mixtures. Additionally, as the pH was approximately constant with the water content for all mixtures, the number of free protons in solution was not considerably altered, meaning that the amount of free protons does not significantly affect the conductivity rise with the water content.

Using EDLC type supercapacitor cells of microporous activated carbon the electrochemical performance of these mixtures was studied through Cyclic Voltammetry (CV), Galvanostatic Charge-Discharge (GCD) and Potentiostatic Electrochemical Impedance Spectroscopy (PEIS).

In CV, the water content influence was clearly seen, as the higher the water content the more pronounced is the quasi-rectangular shape, indicating that the presence of water lowers the electrolyte resistance allowing the ions to have a faster response to the applied voltage, and therefore establish in the electrode pores and surface faster. Comparing voltammograms of mixtures with same water content but different acid chain lengths, a more rectangular shape voltammogram was observed for lower acid chain, which is associated with their higher mobility and ability to form the Electrical Double Layer (EDL) and adsorb in the electrode microporosity.

GCD tests, allowed to test the life cycle of the cells using the studied mixtures as electrolytes, as well as the electrode specific capacitance. About half of the tested mixtures presented a capacitance retention higher than 80% after 5000 charge-discharge cycle, although a clear evolution of the life-cycling with the water content or the acid chain was not found. The specific capacitance obtained showed a clear decrease with the increase of

the acid chain, which was in accordance with the CV results, proving that large anions have more difficulty in forming the EDL and adsorbing at the electrode microporosity. The highest specific capacitance was obtained for the $\text{NaC}_6:\text{C}_6(0.6) + 60\%\text{H}_2\text{O}$ mixture, 71.6 F/g at 0.2 A/g.

In PEIS experiments a spectrum shape characteristic of EDLC was observed for all mixtures: a semi-circle at high frequencies, a 45° line at middle frequencies and a straighter line at lower frequencies. The equivalent series resistance (ESR) presented higher values for a smaller water content, which reflects the higher resistance of the electrolytes with lower water content, which are associated with higher viscosity and lower conductivity. The $\text{NaC}_6:\text{C}_6(0.6) + 60\%\text{H}_2\text{O}$ electrolyte presented the lowest resistance, 1.83 Ω . The resistance related to the ions diffusion in the microporosity of the electrodes, generally showed to decrease with the water content and increased with acid chain length, in agreement with the CV and GCD results. Once more, the $\text{NaC}_6:\text{C}_6(0.6) + 60\%\text{H}_2\text{O}$ presented the best result, having the lowest resistance associated to the ions diffusion in the microporosity.

To conclude, this study showed that aqueous solutions of eutectic mixtures of sodium hexanoate and long alkyl chain fatty acids have a promising future as electrolytes, being the $\text{NaC}_6:\text{C}_6(0.6) + 60\%\text{H}_2\text{O}$ the electrolyte with most promising results. However, further optimization of the performance of these mixtures can still be done, namely studying these mixtures in different electrode materials, for example mesoporous carbon.

6. Future work

Considering the complex nature of the proposed mixtures, further tests can be done in the future in order to deeply understand the organization and diffusion process of the electrolyte species, for example using X-ray scattering, to understand the liquid mixture structure.

Once it was proved that the gel mixtures present promising ionic conductivity, their physical properties (for example rheological behaviour) should be further explored. The electrochemical performance of these gel mixtures is a subject of major interest since solid and quasi-solid electrolytes are foreseen to play a key role to prevent electrolyte's leakage.

Considering that the three main parameters that have a high influence in the studied properties, water content, acid chain length and amount of salt, deeply influence the species diffusion, the determination of the diffusion coefficients using Diffusion Ordered ^1H NMR Spectroscopy, is of great interest.

Additionally, the promising electrochemical performance of the aqueous electrolytic solutions with eutectic systems of sodium hexanoate with fatty acids showed in this study, are encouraging results to further design and test these electrolytes. Possibilities of further electrochemical studies are the study electrochemical stability window, the temperature effect, and the design and test of different electrode materials (for example mesoporous carbon).

7. Bibliography

- [1] International Energy Agency, Global Energy Review: CO2 Emissions in 2021 Global emissions rebound sharply to highest ever level, Iea. (2022) 1–14. <https://iea.blob.core.windows.net/assets/c3086240-732b-4f6a-89d7-db01be018f5e/GlobalEnergyReviewCO2Emissionsin2021.pdf>.
- [2] C. Zhong, Y. Deng, W. Hu, D. Sun, X. Han, J. Qiao, J. Zhang, Electrolytes for electrochemical supercapacitors, 2016. <https://doi.org/10.1201/b21497-6>.
- [3] M. Anouti, E. Couadou, L. Timperman, H. Galiano, Protic ionic liquid as electrolyte for high-densities electrochemical double layer capacitors with activated carbon electrode material, *Electrochim. Acta.* 64 (2012) 110–117. <https://doi.org/10.1016/J.ELECTACTA.2011.12.120>.
- [4] S. Kulandaivalu, Y. Sulaiman, Recent Advances in Layer-by-Layer Assembled Conducting Polymer Based Composites for Supercapacitors, (n.d.). <https://doi.org/10.3390/en12112107>.
- [5] M. Horn, J. MacLeod, M. Liu, J. Webb, N. Motta, Supercapacitors: A new source of power for electric cars?, *Econ. Anal. Policy.* 61 (2019) 93–103. <https://doi.org/10.1016/j.eap.2018.08.003>.
- [6] R. Dubey, V. Guruviah, Review of carbon-based electrode materials for supercapacitor energy storage, *Ionics (Kiel).* 25 (2019) 1419–1445. <https://doi.org/10.1007/s11581-019-02874-0>.
- [7] G. Navarro, J. Torres, M. Blanco, N. Jorge, M. Santos-herran, M. Lafoz, Present and Future of Supercapacitor Technology Applied to Powertrains , Renewable Generation and Grid Connection Applications, (2021).
- [8] S. Hamlen, *Advanced materials. An Introduction to Modern Materials Science*, Springer, 2017. <https://doi.org/10.1201/b10862-5>.
- [9] M.E. Sahin, F. Blaabjerg, A. Sangwongwanich, A Comprehensive Review on Supercapacitor Applications and Developments, *Compr. Rev. Supercapacitor Appl. Dev. Energies.* (2022) 15. <https://doi.org/10.3390/en15030674>.
- [10] S.T. Senthilkumar, K. Vijaya Sankar, J.S. Melo, A. Gedanken, R. Kalai Selvan, Carbon-Based Hybrid Composites as Advanced Electrodes for Supercapacitors, 2015. <https://doi.org/10.1002/9781118998977.ch9>.
- [11] A. Alizadeh, W.L. Hsu, M. Wang, H. Daiguji, Electroosmotic flow: From microfluidics to nanofluidics, *Electrophoresis.* 42 (2021) 834–868. <https://doi.org/10.1002/elps.202000313>.
- [12] H. Tao, C. Lian, H. Liu, Multiscale modeling of electrolytes in porous electrode: From equilibrium structure to non-equilibrium transport, *Green Energy Environ.* 5 (2020) 303–321. <https://doi.org/10.1016/j.gee.2020.06.020>.
- [13] S.U.M.K. John O’M. Bockris, *Surface Electrochemistry: A Molecular Level Approach, Volume 1*, Springer Science & Business Media, 1993.

- [14] V.S. BAGOTSKY, A.M. SKUNDIN, Y.M. VOLFKOVICH, *Electrochemical Power Sources: Batteries, Fuel Cells and Supercapacitors*, John Wiley & Sons, 2015.
- [15] T.K. Nguyen, S. Aberoumand, D.V. Dao, *Advances in Si and SiC Materials for High-Performance Supercapacitors toward Integrated Energy Storage Systems*, *Small*. 17 (2021). <https://doi.org/10.1002/sml.202101775>.
- [16] H. He, Y. Liu, P.R. Shearing, G. He, D.J.L. Brett, *Mesoporous Carbon for Supercapacitors*, (2022) 147–163. https://doi.org/10.1007/978-3-030-99302-3_7.
- [17] E. Buehler, P. Verma, F. Application, P. Data, (12) Patent Application Publication (10) Pub. No.: US 2017/0092439 A1, 2017.
- [18] A. Muzaffar, M.B. Ahamed, K. Deshmukh, J. Thirumalai, A review on recent advances in hybrid supercapacitors: Design, fabrication and applications, *Renew. Sustain. Energy Rev.* 101 (2019) 123–145. <https://doi.org/10.1016/j.rser.2018.10.026>.
- [19] E. Goikolea, R. Mysyk, *Nanotechnology in Electrochemical Capacitors*, *Emerg. Nanotechnologies Recharg. Energy Storage Syst.* (2017) 131–169. <https://doi.org/10.1016/B978-0-323-42977-1.00004-2>.
- [20] Y. Shao, M.F. El-Kady, J. Sun, Y. Li, Q. Zhang, M. Zhu, H. Wang, B. Dunn, R.B. Kaner, Design and Mechanisms of Asymmetric Supercapacitors, *Chem. Rev.* 118 (2018) 9233–9280. <https://doi.org/10.1021/acs.chemrev.8b00252>.
- [21] C. Zhong, Y. Deng, W. Hu, J. Qiao, L. Zhang, J. Zhang, A review of electrolyte materials and compositions for electrochemical supercapacitors, *Chem. Soc. Rev.* 44 (2015) 7484–7539. <https://doi.org/10.1039/c5cs00303b>.
- [22] T.S. Bhat, P.S. Patil, R.B. Rakhi, Recent trends in electrolytes for supercapacitors, *J. Energy Storage*. 50 (2022) 104222. <https://doi.org/10.1016/j.est.2022.104222>.
- [23] L. Timperman, A. Vigeant, M. Anouti, Eutectic mixture of Protic Ionic Liquids as an Electrolyte for Activated Carbon-Based Supercapacitors, *Electrochim. Acta*. 155 (2015) 164–173. <https://doi.org/10.1016/J.ELECTACTA.2014.12.130>.
- [24] X. Zang, C. Shen, M. Sanghadasa, L. Lin, High-Voltage Supercapacitors Based on Aqueous Electrolytes, *ChemElectroChem*. 6 (2019) 976–988. <https://doi.org/10.1002/celec.201801225>.
- [25] L. Yu, G.Z. Chen, Ionic liquid-based electrolytes for supercapacitor and supercapattery, *Front. Chem.* 7 (2019) 1–15. <https://doi.org/10.3389/fchem.2019.00272>.
- [26] Y. Wang, W. Chen, Q. Zhao, G. Jin, Z. Xue, Y. Wang, T. Mu, Ionicity of deep eutectic solvents by Walden plot and pulsed field gradient nuclear magnetic resonance (PFG-NMR), *Phys. Chem. Chem. Phys.* 22 (2020) 25760. <https://doi.org/10.1039/d0cp01431a>.

- [27] A. Dutta, J. Mahanta, T. Banerjee, Supercapacitors in the Light of Solid Waste and Energy Management: A Review, *Adv. Sustain. Syst.* 4 (2020) 1–32. <https://doi.org/10.1002/adsu.202000182>.
- [28] R. Chen, F. Wu, H. Liang, L. Li, B. Xu, Novel Binary Room-Temperature Complex Electrolytes Based on LiTFSI and Organic Compounds with Acylamino Group, *J. Electrochem. Soc.* 152 (2005) A1979. <https://doi.org/10.1149/1.2007167>.
- [29] F. Pettersson, J. Keskinen, T. Remonen, L. Von Hertzen, E. Jansson, K. Tappura, Y. Zhang, C.E. Wilén, R. Österbacka, Printed environmentally friendly supercapacitors with ionic liquid electrolytes on paper, *J. Power Sources.* 271 (2014) 298–304. <https://doi.org/10.1016/j.jpowsour.2014.08.020>.
- [30] S. Azmi, M.F. Koudahi, E. Frackowiak, Reline deep eutectic solvent as a green electrolyte for electrochemical energy storage applications†, *Energy Environ. Sci.* 15 (2022) 1156–1171. <https://doi.org/10.1039/d1ee02920g>.
- [31] N. Ozdemir, H. Zengin, A. Yavuz, Electropolymerization of pyrrole from a deep eutectic solvent for supercapacitor applications, *Mater. Chem. Phys.* 256 (2020) 123645. <https://doi.org/10.1016/j.matchemphys.2020.123645>.
- [32] H. Liang, R. Shi, Y. Zhou, W. Jiang, Q. Kang, H. Zhang, K. Liu, J. Lian, Y. Bu, Ferroelectric benzimidazole additive-induced interfacial water confinement for stable 2.2 V supercapacitor electrolytes exposed to air, *Chem. Commun.* 58 (2022) 9536–9539. <https://doi.org/10.1039/d2cc03732g>.
- [33] W. Zaidi, A. Boisset, J. Jacquemin, L. Timperman, M. Anouti, Deep eutectic solvents based on N-methylacetamide and a lithium salt as electrolytes at elevated temperature for activated carbon-based supercapacitors, *J. Phys. Chem. C.* 118 (2014) 4033–4042. <https://doi.org/10.1021/jp412552v>.
- [34] S. Phadke, S. Amara, M. Anouti, Gas Evolution in Activated-Carbon-Based Supercapacitors with Protic Deep Eutectic Solvent as Electrolyte, *ChemPhysChem.* 18 (2017) 2364–2373. <https://doi.org/10.1002/cphc.201700621>.
- [35] L.H. Xu, D. Wu, M. Zhong, G.B. Wang, X.Y. Chen, Z.J. Zhang, The construction of a new deep eutectic solvents system based on choline chloride and butanediol: The influence of the hydroxyl position of butanediol on the structure of deep eutectic solvent and supercapacitor performance, *J. Power Sources.* 490 (2021). <https://doi.org/10.1016/j.jpowsour.2020.229365>.
- [36] S. Zhang, N. Pan, Supercapacitors performance evaluation, *Adv. Energy Mater.* 5 (2015) 1–19. <https://doi.org/10.1002/aenm.201401401>.
- [37] J. Yu, N. Fu, J. Zhao, R. Liu, F. Li, Y. Du, Z. Yang, High Specific Capacitance Electrode Material for Supercapacitors Based on Resin-Derived Nitrogen-Doped Porous Carbons, *ACS Omega.* 4 (2019) 15904–15911. <https://doi.org/10.1021/acsomega.9b01916>.
- [38] E.M.A. Dannoun, S.B. Aziz, M.A. Brza, M.M. Nofal, A.S.F.M. Asnawi, Y.M. Yusof, S. Al-Zangana, M.H.

- Hamsan, M.F.Z. Kadir, H.J. Woo, The Study of Plasticized Solid Polymer Blend Electrolytes Based on Natural Polymers and Their Application for Energy Storage EDLC Devices, *Polymers (Basel)*. 12 (2020) 2531. <https://doi.org/10.3390/polym12112531>.
- [39] C.W. Liew, S. Ramesh, A.K. Arof, Enhanced capacitance of EDLCs (electrical double layer capacitors) based on ionic liquid-added polymer electrolytes, *Energy*. 109 (2016) 546–556. <https://doi.org/10.1016/j.energy.2016.05.019>.
- [40] C.P. Tien, W.J. Liang, P.L. Kuo, H.S. Teng, Electric double layer capacitors with gelled polymer electrolytes based on poly(ethylene oxide) cured with poly(propylene oxide) diamines, *Electrochim. Acta*. 53 (2008) 4505–4511. <https://doi.org/10.1016/J.ELECTACTA.2008.01.021>.
- [41] F. Markoulidis, A. Dawe, · Constantina Lekakou, Electrochemical double-layer capacitors with lithium-ion electrolyte and electrode coatings with PEDOT:PSS binder, *J. Appl. Electrochem*. 51 (2021) 373–385. <https://doi.org/10.1007/s10800-020-01497-y>.
- [42] L.E. Helseth, Comparison of methods for finding the capacitance of a supercapacitor, *J. Energy Storage*. 35 (2021) 102304. <https://doi.org/10.1016/J.EST.2021.102304>.
- [43] M.A. Saleem, M.A. Saleem, Carbon nanomaterial-based interconnects , integrated capacitors and supercapacitors, 2017.
- [44] H.S. Magar, R.Y.A. Hassan, A. Mulchandani, Electrochemical impedance spectroscopy (Eis): Principles, construction, and biosensing applications, *Sensors*. 21 (2021). <https://doi.org/10.3390/s21196578>.
- [45] X.Z. Sun, B. Huang, X. Zhang, D.C. Zhang, H.T. Zhang, Y.W. Ma, Experimental investigation of electrochemical impedance spectroscopy of electrical double layer capacitor, *Wuli Huaxue Xuebao/ Acta Phys. - Chim. Sin.* 30 (2014) 2071–2076. <https://doi.org/10.3866/PKU.WHXB201408292>.
- [46] B.A. Mei, O. Munteshari, J. Lau, B. Dunn, L. Pilon, Physical Interpretations of Nyquist Plots for EDLC Electrodes and Devices, *J. Phys. Chem. C*. 122 (2018) 194–206. <https://doi.org/10.1021/acs.jpcc.7b10582>.
- [47] S. Amara, W. Zaidi, L. Timperman, G. Nikiforidis, M. Anouti, Amide-based deep eutectic solvents containing LiFSI and NaFSI salts as superionic electrolytes for supercapacitor applications, *J. Chem. Phys.* 154 (2021). <https://doi.org/10.1063/5.0048392>.
- [48] B. Soares, F. Cunha, I. Silva, C. Florindo, L.C. Branco, I.M. Marrucho, Sodium Hexanoate and Dodecanoate Salt-Based Eutectic Solvents: Density, Viscosity, and Kamlet–Taft Parameters, *J. Chem. Eng. Data*. 66 (2021) 2793–2802. <https://doi.org/10.1021/ACS.JCED.1C00188>.
- [49] L.J. dos Santos, L.A. Espinoza-Velasquez, J.A.P. Coutinho, S. Monteiro, Theoretically consistent calculation of viscous activation parameters through the Eyring equation and their interpretation, *Fluid Phase Equilib.* 522 (2020) 112774. <https://doi.org/10.1016/j.fluid.2020.112774>.

- [50] G. Nikiforidis, M. El Yagoubi, M. Anouti, Polarizable cesium cations for energy storage from electrolyte characterization to-EDLC application, *Electrochim. Acta.* 402 (2022) 139529. <https://doi.org/10.1016/j.electacta.2021.139529>.
- [51] J. Chidiac, L. Timperman, M. Anouti, Small dissymmetry, yet large effects on the transport properties of electrolytes based on imide salts: Consequences on performance in Li-ion batteries, *J. Energy Chem.* 65 (2021) 352–366. <https://doi.org/10.1016/j.jechem.2021.05.054>.
- [52] R.S. Patil, V.R. Shaikh, P.D. Patil, A.U. Borse, K.J. Patil, The viscosity B and D coefficient (Jones–Dole equation) studies in aqueous solutions of alkyltrimethylammonium bromides at 298.15 K, *J. Mol. Liq.* 200 (2014) 416–424. <https://doi.org/10.1016/J.MOLLIQ.2014.11.003>.
- [53] H. Abbasov, A new model for the relative viscosity of aqueous electrolyte solutions, *Chem. Phys. Lett.* 800 (2022) 6267–6272. <https://doi.org/10.1016/j.cplett.2022.139670>.
- [54] M.M. Lencka, A. Anderko, S.J. Sanders, R.D. Young, Modeling viscosity of multicomponent electrolyte solutions, *Int. J. Thermophys.* 19 (1998) 367–378. <https://doi.org/10.1023/A:1022501108317>.
- [55] M. Anouti, P.Y. Sizaret, C. Ghimbeu, H. Galiano, D. Lemordant, Physicochemical characterization of vesicles systems formed in mixtures of protic ionic liquids and water, *Colloids Surfaces A Physicochem. Eng. Asp.* 395 (2012) 190–198. <https://doi.org/10.1016/j.colsurfa.2011.12.030>.
- [56] S.K. Mann, S.P. Brown, D.R. MacFarlane, Structure Effects on the Ionicity of Protic Ionic Liquids, *ChemPhysChem.* 21 (2020) 1444–1454. <https://doi.org/10.1002/cphc.202000242>.
- [57] S.T.K. Riddick, J.A., W.B. Bunger, *Techniques of Chemistry*, 4th ed., 1985.
- [58] J.A. Dean, *Handbook of Organic Chemistry*, NY: McGraw-Hill Book Co., New York, 1987.
- [59] H. Tamai, M. Kunihiro, M. Morita, H. Yasuda, Mesoporous activated carbon as electrode for electric double layer capacitor, *J. Mater. Sci.* 40 (2005) 3703–3707. <https://doi.org/10.1007/s10853-005-2838-2>.

8. Supporting Information

8.1. Sodium hexanoate preparation

Under constant stirring and under a bath a water at ambient temperature, a solution of 0.5 M of NaOH is prepared using methanol as a solvent. The hexanoic acid is mixed with methanol in the least quantity of methanol possible until a clear homogeneous solution is obtained. The NaOH solution is placed in a separatory funnel and slowly added to the hexanoic acid solution while the pH is monitored through pH strips. When pH 7 is reached the addition is interrupted. After the methanol is removed from the resulting solution using a rotary evaporator. After this the salt is placed in an oven at 40 °C for three days to be further dried.

8.2. Concentration of salt

The salt concentration, C (mol/L), for each eutectic-water mixture was determined by the following equation:

$$C = \frac{n_{salt}}{\frac{m_{solution}}{\rho_{solution}}} \quad [44]$$

Where n_{salt} are the moles of salt in solution, $m_{solution}$ is the total mass of the eutectic-water solution and the $\rho_{solution}$ is the average of the measured densities at the respective range of temperatures.

8.3. Conductivity

Table 18. Conductivity of each mixture at 20 °C.

wt% H2O	NaC ₆ :C ₆ (0.6)	NaC ₆ :C ₆ (0.7)	NaC ₆ :C ₈ (0.6)	NaC ₆ :C ₈ (0.7)	NaC ₆ :C ₉ (0.7)	NaC ₆ :C ₁₀ (0.7)
0	1.13E-03	3.08E-04	3.08E-04	4.41E-04	4.48E-04	3.61E-03
10	0.30	0.26	0.13	0.10	0.08	0.05
20	3.03	2.51	-	1.23	1.12	0.95
30	-	6.525	-	4.132	3.590	2.41
40	16.87	11.537	5.242	7.567	7.142	5.91
50	19.77	12.935	2.726	10.852	-	-
60	22.30	-	1.378	-	-	-

8.4. Viscosity

Table 19. Viscosity data for the NaC₆:C₆(0.6) with water mixtures.

NaC ₆ :C ₆ (0.6)									
0% H ₂ O		10% H ₂ O		20% H ₂ O		50% H ₂ O		60% H ₂ O	
T (°C)	η (mPa.s)	T (°C)	η (mPa.s)	T (°C)	η (mPa.s)	T (°C)	η (mPa.s)	T (°C)	η (mPa.s)
49.99	153.40	10.01	341.42	10.01	121.36	13.98	17.02	15.98	9.83
51.99	136.60	11.98	296.41	11.98	107.30	15.98	14.59	17.98	8.97
53.99	123.50	13.98	258.72	13.98	95.48	17.98	13.15	19.98	8.37
56.00	112.10	15.98	226.02	15.98	85.23	19.98	12.12	21.98	7.76
58.00	101.50	17.98	198.55	17.98	76.05	21.98	11.22	23.99	7.22
60.00	92.05	19.98	175.54	19.98	68.23	23.98	10.41	25.99	6.72
		21.99	155.23	21.98	61.40	25.99	9.68	27.99	6.28
		23.99	137.87	23.98	55.45	27.99	9.01	29.99	5.87
		25.99	122.65	25.99	50.24	29.99	8.41	31.99	5.50
		27.99	109.41	27.99	45.69	31.99	7.85	33.99	5.16
		29.99	98.71	29.99	41.53	33.99	7.36	35.99	4.85
		31.99	88.02	31.99	37.85	35.99	6.90	37.99	4.56
		33.99	79.22	33.99	34.58	37.99	6.48	39.99	4.29
		35.99	71.77	35.99	31.69	39.99	6.09	41.99	4.05
		37.99	64.91	37.99	29.18	41.99	5.73	43.99	3.82
		39.99	58.91	39.99	26.76	43.99	5.40	45.99	3.61
		41.99	53.49	41.99	24.73	45.99	5.10	47.99	3.42
		43.99	48.88	43.99	22.83	47.99	4.82	49.99	3.21
		45.99	44.66	45.99	21.14	49.99	4.55		
		47.99	40.94	47.99	19.59				
		49.99	37.53	49.99	18.13				

Table 20. Viscosity data for the NaC₆:C₆(0.7) with water mixtures.

NaC ₆ :C ₆ (0.7)											
0%H ₂ O		10%H ₂ O		20%H ₂ O		30%H ₂ O		40%H ₂ O		50%H ₂ O	
T (°C)	η (mPa.s)	T (°C)	η (mPa.s)	T (°C)	η (mPa.s)	T (°C)	η (mPa.s)	T (°C)	η (mPa.s)	T (°C)	η (mPa.s)
10.02	305.49	10.01	122.01	10.01	57.94	10.02	34.93	10.01	16.97	19.99	10.89
11.98	266.53	11.98	107.97	11.98	51.90	11.98	31.89	11.98	15.97	21.99	10.06
13.99	233.86	13.98	95.98	13.98	47.01	13.98	29.10	13.98	15.01	23.99	9.30
15.99	206.23	15.98	85.57	15.98	42.62	15.98	26.62	15.98	14.10	25.99	8.62
17.99	181.75	17.98	76.60	17.98	38.66	17.98	24.48	17.98	13.26	27.99	8.02
19.99	161.40	19.98	68.65	19.98	35.21	19.99	22.48	19.98	12.46	29.99	7.48
21.99	143.70	21.98	61.76	21.99	32.29	21.99	20.70	21.98	11.71	31.99	6.97
23.99	128.16	23.98	55.77	23.99	29.52	23.99	19.11	23.98	11.01	34.00	6.51
25.99	114.82	25.98	50.48	25.99	27.10	25.99	17.64	25.98	10.34	35.99	6.09
27.99	102.92	27.99	45.74	27.99	24.90	27.99	16.41	27.99	9.72	38.00	5.70
29.99	92.58	29.99	41.68	29.99	23.00	29.99	15.29	29.99	9.14	40.00	5.35
31.99	83.57	31.99	38.09	31.99	21.20	31.99	14.22	31.99	8.59	42.00	5.04
33.99	75.80	33.99	34.83	33.99	19.63	33.99	13.26	33.99	8.07	44.00	4.74
35.99	68.69	35.99	31.94	35.99	18.11	35.99	12.37	35.99	7.58	46.00	4.47
37.99	62.50	37.99	29.21	37.99	16.92	37.99	11.55	37.99	7.13	48.00	4.22
40.00	56.90	39.99	26.94	39.99	15.78	39.99	10.80	39.99	6.70	50.00	3.98
42.00	50.69	41.99	24.81	41.99	14.71	41.99	10.10	41.99	6.30		
44.00	46.46	43.99	22.99	43.99	13.74	43.99	9.45	43.99	5.92		
46.00	42.61	45.99	21.30	45.99	12.83	45.99	8.87	45.99	5.56		
48.00	40.03	47.99	19.73	47.99	11.99	48.00	8.33	47.99	5.23		
50.00	37.57	49.99	18.29	49.99	11.22	50.00	7.83	49.99	4.91		

Table 21. Viscosity data for the $\text{NaC}_6\text{:C}_8(0.6)$ with water mixtures.

$\text{NaC}_6\text{:C}_8(0.6)$			
0%H_2O		10%H_2O	
T (°C)	η (mPa.s)	T (°C)	η (mPa.s)
25.98	544.34	10.01	556.48
27.99	477.87	11.98	482.28
29.99	419.63	13.98	419.09
31.99	371.21	15.98	366.53
33.99	330.32	17.98	320.68
35.99	293.58	19.98	281.75
37.99	261.86	21.98	248.32
39.99	233.44	23.99	219.74
41.99	208.55	25.99	196.18
43.99	186.96	27.99	174.65
45.99	168.47	29.99	155.79
47.99	152.07	31.99	139.02
49.99	138.05	33.99	124.91
		35.99	112.37
		37.99	101.57
		39.99	91.744
		42.00	83.061
		43.99	75.7
		46.00	68.828
		48.00	62.824
		50.00	57.68

Table 22. Viscosity data for the NaC₆:C₈(0.7) with water mixtures.

NaC ₆ :C ₈ (0.7)											
0%H ₂ O		10%H ₂ O		20%H ₂ O		30%H ₂ O		40%H ₂ O		50%H ₂ O	
T (°C)	η (mPa.s)	T (°C)	η (mPa.s)	T (°C)	η (mPa.s)	T (°C)	η (mPa.s)	T (°C)	η (mPa.s)	T (°C)	η (mPa.s)
10.02	295.28	10.01	172.26	10.02	100.48	10.02	61.69	10.02	53.10	11.98	39.32
11.98	259.42	11.98	152.76	11.99	89.86	11.99	57.13	11.99	48.88	13.97	35.82
13.98	227.92	13.98	135.79	13.98	80.76	13.98	52.86	13.98	45.41	15.98	32.36
15.98	201.38	15.98	120.61	15.98	72.96	15.98	48.89	15.98	42.17	17.98	29.79
17.98	177.87	17.98	108.02	17.98	65.91	17.98	45.23	17.98	39.16	19.98	28.08
19.99	158.65	19.98	96.54	19.98	59.64	19.98	41.83	19.98	36.37	21.98	26.59
21.99	141.4	21.98	86.60	21.98	54.23	21.98	38.69	21.98	33.77	23.98	25.25
23.99	126.32	23.98	77.95	23.98	49.42	23.98	35.79	23.98	31.36	25.98	23.99
25.99	114.02	25.98	70.34	25.98	45.05	25.98	33.10	25.98	29.13	27.98	22.78
27.99	102.12	27.98	63.65	27.99	41.20	27.99	30.61	27.99	27.04	29.98	21.66
29.99	91.95	29.98	57.73	29.99	37.78	29.99	28.31	29.99	25.11	31.98	20.63
31.99	83.29	31.98	53.26	31.99	34.65	31.99	26.19	31.99	23.32	33.99	19.61
33.99	75.445	33.99	48.44	33.99	31.86	33.99	24.22	33.99	21.66	35.98	18.53
35.99	68.723	35.99	44.23	35.99	29.36	35.99	22.40	35.99	20.11	37.99	17.52
37.99	62.678	37.99	40.53	37.99	27.04	37.99	20.72	37.99	18.68	39.99	16.72
39.99	57.239	39.99	37.13	39.99	25.02	39.99	19.17	39.99	17.35	41.99	16.15
42	52.361	41.99	34.17	41.99	23.15	41.99	17.73	41.99	16.11	43.99	15.38
44	48.252	43.99	31.43	43.99	21.47	43.99	16.40	43.99	14.96	45.99	14.81
46	44.231	45.99	29.01	45.99	19.92	45.99	15.17	45.99	13.89	47.99	14.27
48	40.763	47.99	26.79	47.99	18.51	47.99	14.03	47.99	12.90	49.99	13.88
50	37.668	49.99	24.81	49.99	17.05	49.99	12.98	49.99	11.98		

Table 23. Viscosity data for the NaC₆:C₉(0.7) with water mixtures.

NaC ₆ :C ₉ (0.7)									
0%H ₂ O		10%H ₂ O		20%H ₂ O		30%H ₂ O		40%H ₂ O	
T (°C)	η (mPa.s)	T (°C)	η (mPa.s)	T (°C)	η (mPa.s)	T (°C)	η (mPa.s)	T (°C)	η (mPa.s)
10.01	310.57	10.01	203.15	10.01	130.88	10.01	87.822	10.01	82.578
11.98	270.96	11.97	179.6	11.97	117.37	11.97	79.654	11.98	75.994
13.98	237.85	13.98	159.34	13.97	105.3	13.97	72.037	13.98	70.042
15.98	210.23	15.98	141.68	15.98	94.712	15.97	65.394	15.98	64.836
17.98	187.22	17.98	126.42	17.98	85.317	17.98	59.546	17.98	59.938
19.98	166.18	19.98	113.07	19.98	77.086	19.98	54.43	19.98	55.383
21.98	148.24	21.98	101.57	21.98	69.936	21.98	49.642	21.98	51.333
23.99	132.56	23.98	91.267	23.98	63.526	23.98	45.393	23.98	47.568
25.99	119.23	25.98	82.295	25.98	58.081	25.98	41.641	25.98	44.059
27.99	107.21	27.98	74.604	27.98	52.785	27.98	38.293	27.98	40.873
29.99	96.329	29.98	67.438	29.98	48.208	29.98	35.144	29.98	37.939
31.99	87.223	31.99	61.443	31.98	44.197	31.98	32.365	31.99	35.287
33.99	79.035	33.99	55.862	33.99	40.581	33.99	29.893	33.99	32.712
35.99	71.911	35.99	50.607	35.99	37.301	35.99	27.623	35.99	30.354
37.99	65.521	37.99	46.285	37.99	34.303	37.99	25.542	37.99	28.2
39.99	60.104	39.99	42.389	39.99	31.689	39.99	23.643	39.99	26.232
42.00	54.989	41.99	38.955	41.99	29.253	41.99	21.927	41.99	24.373
43.99	50.466	43.99	35.789	43.99	27.081	43.99	20.357	43.99	22.623
46.00	46.324	45.99	33.003	45.99	25.074	45.99	18.942	45.99	21.044
48.00	42.677	47.99	30.493	47.99	23.259	47.99	17.392	47.99	19.557
50.00	39.449	49.99	28.209	49.99	21.576	49.99	16.325	49.99	18.061

Table 24. Viscosity data for the NaC₆:C₁₀(0.7) with water mixtures.

NaC ₆ :C ₁₀ (0.7)									
0%H ₂ O		10%H ₂ O		20%H ₂ O		30%H ₂ O		40%H ₂ O	
T (°C)	η (mPa.s)	T (°C)	η (mPa.s)	T (°C)	η (mPa.s)	T (°C)	η (mPa.s)	T (°C)	η (mPa.s)
29.98	105.11	21.98	116.98	15.98	118.67	15.98	97.94	13.99	92.136
31.99	94.977	23.98	104.74	17.98	107.01	17.98	89.878	15.98	85.083
33.99	86.066	25.98	94.491	19.98	96.799	19.98	81.163	17.98	78.376
35.99	77.894	27.99	85.442	21.98	87.557	21.98	73.964	19.98	72.467
37.99	70.955	29.99	77.458	23.98	79.548	23.98	67.581	21.98	67.042
39.99	64.676	31.99	70.338	25.99	72.251	25.98	61.956	23.98	62.201
41.99	59.105	33.99	64.04	27.99	65.828	27.98	56.653	25.98	57.655
		35.99	58.464	29.99	59.978	29.98	51.953	27.98	53.536
		37.99	53.513	31.99	55.018	31.98	47.662	29.98	49.659
		39.99	49.081	33.99	50.392	33.99	43.849	31.99	46.106
		41.99	44.987	35.99	46.226	35.99	40.36	33.99	42.816
		43.99	41.334	37.99	42.512	37.99	37.251	35.99	39.75
		45.99	38.096	39.99	39.137	39.99	34.418	37.99	36.937
		47.99	35.123	41.99	36.076	41.99	31.844	39.99	34.324
		49.99	32.46	43.99	33.344	43.99	29.468	41.99	31.933
				45.99	30.842	45.99	27.312	43.99	29.707
				47.99	28.572	47.99	25.338	45.99	27.678
				49.99	26.49	49.99	23.525	47.99	25.729
								49.99	23.956

8.4.1. Eyring's Theory

Table 25. Fitting parameters from Eyring's theory for each mixture and respective enthalpy and entropy of activation.

Mixture	wt% H ₂ O	Slope (K), $\frac{\Delta H^\ddagger}{R}$	Interception, b	R ²	ΔH^\ddagger (kJ mol ⁻¹)	ΔS^\ddagger (J mol ⁻¹ K ⁻¹)
NaC₆:C₆(0.6)	0	5.44	-18.72	0.999	45.23	50.23
	10	5.04	-18.91	0.999	41.87	56.00
	20	4.32	-17.43	0.999	35.96	46.35
	50	3.14	-15.13	0.995	26.13	32.23
	60	3.03	-19.73	0.995	25.20	71.59
NaC₆:C₆(0.7)	0	4.84	-18.31	0.999	40.21	47.07
	10	4.32	-17.41	0.999	35.93	43.50
	20	3.73	-16.05	0.999	30.99	34.85
	30	3.40	-15.39	0.999	28.28	31.34
	40	2.84	-14.07	0.999	23.59	21.91
	50	3.17	-15.34	0.999	26.33	33.80
NaC₆:C₈(0.7)	0	4.70	-17.86	1.00	39.08	41.93
	10	4.42	-17.39	1.00	36.72	42.47
	20	4.02	-16.53	1.00	33.44	38.22
	30	3.57	-15.36	1.00	29.67	30.61
	40	3.39	-14.89	1.00	28.20	28.39
	50	2.45	-11.89	0.99	20.33	4.91
NaC₆:C₉(0.7)	0	4.70	-17.82	0.999	39.07	40.92
	10	4.51	-17.56	0.999	37.51	43.59
	20	4.11	-16.58	0.999	34.17	38.40
	30	3.84	-16.01	1.000	31.92	35.83
	40	3.45	-19.27	0.999	28.68	64.73
NaC₆:C₁₀(0.7)	0	4.58	-17.38	1.000	38.12	36.77
	10	4.35	-16.89	1.000	36.14	37.72
	20	4.11	-16.38	1.000	34.21	36.52
	30	3.92	-15.90	0.999	32.63	34.88
	40	3.46	-19.03	1.000	28.76	62.64

8.4.2. Jones-Dole-Kaminsky

Table 26. Fitting parameters of the Jones-Dole-Kaminsky model for the NaC₆:C₆: water mixtures.

T (°C)	A'	B	D	R ²
22	0.070	-15.91	16.54	0.9962
24	0.049	-15.33	15.91	0.9980
26	0.033	-14.84	15.36	0.9990
28	0.015	-14.33	14.82	0.9996
30	0.001	-13.93	14.37	0.9998
32	-0.011	-13.45	13.86	0.9995
34	-0.021	-13.09	13.44	0.9990
36	-0.032	-12.57	12.92	0.9981
38	-0.037	-12.42	12.66	0.9974
40	-0.042	-12.12	12.36	0.9965
42	-0.046	-11.89	12.00	0.9956
44	-0.049	-11.64	11.69	0.9947
46	-0.053	-11.36	11.36	0.9937
48	-0.056	-11.12	11.06	0.9927
50	-0.059	-10.89	10.80	0.9917

Table 27. Fitting parameters of the Jones-Dole-Kaminsky model for the NaC₆:C₈: water mixtures.

T (°C)	A'	B	D	R ²
18	0.985	2.56	18.92	0.9854
20	0.987	5.32	16.31	0.9872
22	0.988	7.73	14.03	0.9882
24	0.989	9.95	11.88	0.9886
26	0.989	12.02	9.83	0.9889
28	0.989	13.70	8.07	0.9887
30	0.988	15.13	6.49	0.9880
32	0.987	16.53	4.94	0.9868
34	0.985	17.60	3.64	0.9853
36	0.984	18.15	2.70	0.9838
38	0.982	18.72	1.74	0.9821
40	0.978	19.40	0.80	0.9783
42	0.972	20.48	-0.44	0.9719
44	0.193	20.84	-1.18	0.9665
46	0.209	21.56	-2.12	0.9581
48	0.226	22.21	-3.00	0.9477
50	0.244	23.66	-4.41	0.9350

Table 28. Fitting parameters of the Jones-Dole-Kaminsky model for the NaC₆:C₉: water mixtures.

T(°C)	A'	B	D	R ²
10	0.170	7.89	34.98	0.9769
12	0.163	12.83	29.66	0.9764
14	0.160	17.40	24.65	0.9748
16	0.157	21.99	19.76	0.9733
18	0.152	25.76	15.50	0.9724
20	0.145	28.65	11.95	0.9722
22	0.143	30.98	8.94	0.9704
24	0.140	32.87	6.26	0.9692
26	0.136	33.53	4.59	0.968
28	0.130	35.29	2.10	0.9681
30	0.127	36.09	0.36	0.9668
32	0.124	36.62	-1.08	0.9657
34	0.114	36.45	-1.98	0.9658
36	0.113	36.20	-2.80	0.9658
38	0.109	36.00	-3.60	0.9656
40	0.106	35.45	-4.04	0.965
42	0.101	34.73	-4.42	0.9652
44	0.096	33.66	-4.46	0.9656
46	0.092	32.87	-4.67	0.9662
48	0.092	31.46	-4.48	0.9626
50	0.083	30.01	-4.11	0.967

Table 29. Fitting parameters of the Jones-Dole-Kaminsky model for the NaC₆:C₁₀: water mixtures.

T(°C)	A'	B	D	R ²
16	-0.046	94.793	-21.72	0.9983
18	-0.076	107.59	-34.71	0.9949
20	-0.081	116.9	-45.01	0.9934
22	-0.093	125.56	-54.42	0.9904
24	-0.100	132.13	-61.94	0.9876
26	-0.109	137.14	-68.09	0.984
28	-0.111	140.65	-72.94	0.9817
30	-0.115	142.84	-76.63	0.9788
32	-0.115	143.64	-79.05	0.9769
34	-0.117	143.96	-81.00	0.9744
36	-0.117	143.4	-82.16	0.972
38	-0.118	142.34	-82.81	0.9696
40	-0.119	141.19	-83.27	0.9669
42	-0.118	138.99	-82.88	0.9647
44	-0.117	136.67	-82.30	0.9627
46	-0.116	134.35	-81.63	0.9608
48	-0.115	131.38	-80.41	0.9583
50	-0.114	128.79	-79.39	0.956

Table 30. Hydrodynamic radius as function of temperature determined through Jones-Dole-Kaminsky model and Einstein's viscosity theory.

T (°C)	Hydrodynamic Radius (nm)			
	NaC ₆ :C ₆ (0.7)	NaC ₆ :C ₈ (0.7)	NaC ₆ :C ₉ (0.7)	NaC ₆ :C ₁₀ (0.7)
10	-	-	1.08	-
12	-	-	1.27	-
14	-	-	1.40	-
16	-	0.46	1.52	2.47
18	-	0.74	1.60	2.57
20	-	0.94	1.66	2.65
22	1.4	1.07	1.70	2.71
24	1.3	1.16	1.73	2.76
26	1.3	1.24	1.75	2.79
28	1.3	1.30	1.78	2.81
30	1.3	1.34	1.79	2.83
32	1.3	1.38	1.80	2.83
34	1.3	1.41	1.79	2.84
36	1.3	1.42	1.79	2.83
38	1.3	1.44	1.79	2.83
40	1.2	1.45	1.78	2.82
42	1.2	1.48	1.77	2.80
44	1.2	1.49	1.75	2.79
46	1.2	1.51	1.73	2.77
48	1.2	1.52	1.71	2.75
50	1.2	1.55	1.68	2.73

8.5. Density

Table 31. Density data for the NaC₆:C₆(0.6) with water mixtures.

NaC ₆ :C ₆ (0.6)									
0%H ₂ O		10%H ₂ O		20%H ₂ O		50%H ₂ O		60%H ₂ O	
T(°C)	ρ (g/cm ³)	T(°C)	ρ (g/cm ³)	T(°C)	ρ (g/cm ³)	T(°C)	ρ (g/cm ³)	T(°C)	ρ (g/cm ³)
29.98	1.00328	10.01	1.0313	10.01	1.03457	10.01	1.03247	15.98	1.02466
31.98	1.00026	11.98	1.02976	11.98	1.03308	11.98	1.0313	17.98	1.02364
33.99	0.99726	13.98	1.02818	13.98	1.03154	13.98	1.03012	19.98	1.02257
35.99	0.99447	15.98	1.0266	15.98	1.02999	15.98	1.02892	21.98	1.02148
37.99	0.992	17.98	1.02502	17.98	1.02844	17.98	1.0277	23.99	1.02036
39.99	0.98987	19.98	1.02343	19.98	1.02689	19.98	1.02646	25.99	1.01922
41.99	0.98801	21.99	1.02184	21.98	1.02534	21.98	1.02521	27.99	1.01806
43.99	0.98651	23.99	1.02024	23.98	1.02378	23.98	1.02394	29.99	1.0169
45.99	0.98502	25.99	1.01864	25.99	1.02222	25.99	1.02266	31.99	1.01571
47.99	0.98348	27.99	1.01705	27.99	1.02066	27.99	1.02136	33.99	1.01452
49.99	0.98198	29.99	1.01545	29.99	1.01911	29.99	1.02006	35.99	1.0133
51.99	0.98026	31.99	1.01385	31.99	1.01755	31.99	1.01875	37.99	1.01207
53.99	0.97828	33.99	1.01225	33.99	1.01598	33.99	1.01742	39.99	1.01083
56.00	0.97808	35.99	1.01066	35.99	1.01442	35.99	1.01609	41.99	1.00957
58.00	0.97629	37.99	1.00906	37.99	1.01285	37.99	1.01475	43.99	1.0083
60.00	0.97453	39.99	1.00746	39.99	1.01129	39.99	1.01339	45.99	1.00702
		41.99	1.00587	41.99	1.00972	41.99	1.01201	47.99	1.00572
		43.99	1.00427	43.99	1.00815	43.99	1.01064	49.99	1.00441
		45.99	1.00267	45.99	1.00657	45.99	1.00923		
		47.99	1.00107	47.99	1.005	47.99	1.00781		
		49.99	0.99947	49.99	1.00342	49.99	1.00641		

Table 32. Density data for the NaC₆:C₆(0.7) with water mixtures.

NaC ₆ :C ₆ (0.7)											
0%H ₂ O		10%H ₂ O		20%H ₂ O		30%H ₂ O		40%H ₂ O		50%H ₂ O	
T(°C)	ρ (g/cm ³)	T(°C)	ρ (g/cm ³)	T(°C)	ρ (g/cm ³)	T(°C)	ρ (g/cm ³)	T(°C)	ρ (g/cm ³)	T(°C)	ρ (g/cm ³)
10.02	1.00526	10.01	1.01327	10.01	1.01746	10.02	1.01847	19.98	1.01159	19.99	1.01244
11.98	1.00363	11.98	1.01117	11.98	1.01597	11.98	1.01738	24.98	1.00834	21.99	1.01127
13.99	1.00198	13.98	1.01009	13.98	1.01443	13.98	1.01609	29.98	1.00488	23.99	1.01003
15.99	1.00032	15.98	1.00849	15.98	1.01289	15.98	1.01478	34.99	1.00135	25.99	1.00873
17.99	0.99866	17.98	1.00688	17.98	1.01134	17.98	1.01336	39.99	0.99768	27.99	1.00738
19.99	0.99701	19.98	1.00527	19.98	1.00978	19.99	1.01189	44.99	0.99387	29.99	1.00599
21.99	0.99535	21.98	1.00366	21.99	1.00821	21.99	1.01049	49.99	0.98966	31.99	1.00457
23.99	0.99369	23.98	1.00205	23.99	1.00664	23.99	1.0090	54.99	0.98577	34.00	1.00319
25.99	0.99203	25.98	1.00044	25.99	1.00507	25.99	1.00749	59.99	0.98162	35.99	1.00177
27.99	0.99037	27.99	0.99882	27.99	1.00349	27.99	1.00599			38.00	1.00032
29.99	0.98872	29.99	0.99721	29.99	1.00192	29.99	1.00450			40.00	0.99875
31.99	0.98706	31.99	0.9956	31.99	1.00034	31.99	1.00300			42.00	0.99453
33.99	0.98541	33.99	0.99399	33.99	0.99874	33.99	1.00147			44.00	0.99230
35.99	0.98376	35.99	0.99238	35.99	0.99711	35.99	0.9999			46.00	0.99193
37.99	0.98211	37.99	0.99077	37.99	0.9955	37.99	0.99829			48.00	0.99013
40.00	0.98046	39.99	0.98916	39.99	0.99393	39.99	0.99665			50.00	0.98834
42.00	0.9788	41.99	0.98755	41.99	0.99233	41.99	0.9949				
44.00	0.97713	43.99	0.98593	43.99	0.99071	43.99	0.99328				
46.00	0.97546	45.99	0.98432	45.99	0.98909	45.99	0.99162				
48.00	0.97377	47.99	0.9827	47.99	0.98745	48.00	0.98994				
50.00	0.97207	49.99	0.98108	49.99	0.98581	50.00	0.98821				

Table 33. Density data for the NaC₆:C₈(0.6) with water mixtures.

NaC ₆ :C ₈ (0.6)			
0%H ₂ O		10%H ₂ O	
T(°C)	ρ (g/cm ³)	T(°C)	ρ (g/cm ³)
10	1.00067	10	1.00662
12	0.99911	12	1.00561
14	0.99753	14	1.00405
16	0.99594	16	1.00249
18	0.99435	18	1.00092
20	0.99277	20	0.99936
22	0.99118	22	0.99779
24	0.98956	24	0.99621
26	0.98797	26	0.99464
28	0.98639	28	0.99306
30	0.98482	30	0.99148
32	0.98325	32	0.98991
34	0.98169	34	0.98833
36	0.98012	36	0.98675
38	0.97855	38	0.98518
40	0.97698	40	0.98360
42	0.97542	42	0.98202
44	0.97385	44	0.98044
46	0.97228	46	0.97886
48	0.97071	48	0.97728
50	0.96913	50	0.97570

Table 34. Density data for the NaC₆:C₈(0.7) with water mixtures.

NaC ₆ :C ₈ (0.7)											
0%H ₂ O		10%H ₂ O		20%H ₂ O		30%H ₂ O		40%H ₂ O		50%H ₂ O	
T (°C)	ρ (g/cm ³)	T (°C)	ρ (g/cm ³)	T (°C)	ρ (g/cm ³)	T (°C)	ρ (g/cm ³)	T (°C)	ρ (g/cm ³)	T (°C)	ρ (g/cm ³)
10.02	0.97986	10.01	0.9896	10.02	1.00028	19.98	0.99639	19.97	1.00011	11.98	1.00746
11.98	0.97835	11.98	0.98809	11.99	0.99888	24.98	0.99287	24.98	0.99684	13.97	1.00635
13.98	0.97680	13.98	0.98655	13.98	0.99744	29.98	0.98925	29.98	0.99344	15.98	1.00522
15.98	0.97525	15.98	0.98499	15.98	0.99597	34.98	0.98558	34.98	0.98998	17.98	1.00407
17.98	0.97370	17.98	0.98344	17.98	0.99448	39.98	0.98177	39.98	0.98647	19.98	1.00289
19.99	0.97215	19.98	0.98189	19.98	0.99298	44.98	0.97794	44.98	0.98287	21.98	1.00171
21.99	0.97059	21.98	0.98034	21.98	0.99146	49.98	0.97412	49.98	0.97913	23.98	1.00050
23.99	0.96903	23.98	0.97879	23.98	0.98995			54.98	0.97520	25.98	0.99927
25.99	0.96747	25.98	0.97723	25.98	0.98843			59.98	0.97130	27.98	0.99803
27.99	0.96591	27.98	0.97567	27.99	0.98690					29.98	0.99678
29.99	0.96435	29.98	0.97412	29.99	0.98538					31.98	0.99552
31.99	0.96279	31.98	0.97257	31.99	0.98385					33.99	0.99425
33.99	0.96122	33.99	0.97101	33.99	0.98232					35.98	0.99296
35.99	0.95966	35.99	0.96946	35.99	0.98079					37.99	0.99166
37.99	0.95809	37.99	0.96791	37.99	0.97925					39.99	0.99035
39.99	0.95653	39.99	0.96636	39.99	0.97772					41.99	0.98902
42	0.95496	41.99	0.9648	41.99	0.97618					43.99	0.98769
44	0.95340	43.99	0.96325	43.99	0.97464					45.99	0.98636
46	0.95183	45.99	0.96169	45.99	0.97309					47.99	0.98501
48	0.95027	47.99	0.96013	47.99	0.97154					49.99	0.98366
50	0.94871	49.99	0.95857	49.99	0.96997						

Table 35. Density data for the NaC₆:C₉(0.7) with water mixtures.

NaC ₆ :C ₉ (0.7)									
0%H ₂ O		10%H ₂ O		20%H ₂ O		30%H ₂ O		40%H ₂ O	
T (°C)	ρ (g/cm ³)	T (°C)	ρ (g/cm ³)	T (°C)	ρ (g/cm ³)	T (°C)	ρ (g/cm ³)	T (°C)	ρ (g/cm ³)
25.99	0.95784	10.01	0.98581	10.01	0.99279	10.01	0.99616	10.01	1.00146
27.99	0.95633	11.97	0.98432	11.97	0.99144	11.97	0.99491	11.98	1.00024
29.99	0.95482	13.98	0.98279	13.97	0.99	13.97	0.99356	13.98	0.99897
31.99	0.95331	15.98	0.98125	15.98	0.98853	15.97	0.99219	15.98	0.9977
33.99	0.95179	17.98	0.97972	17.98	0.98705	17.98	0.99079	17.98	0.99641
35.99	0.95026	19.98	0.97819	19.98	0.98556	19.98	0.98938	19.98	0.9951
37.99	0.94874	21.98	0.97666	21.98	0.98407	21.98	0.98796	21.98	0.9938
39.99	0.94722	23.98	0.97512	23.98	0.98257	23.98	0.98653	23.98	0.99246
42.00	0.9457	25.98	0.97359	25.98	0.98107	25.98	0.98508	25.98	0.99111
43.99	0.94419	27.98	0.97205	27.98	0.97956	27.98	0.98362	27.98	0.98975
46.00	0.94268	29.98	0.97051	29.98	0.97806	29.98	0.98215	29.98	0.98835
48.00	0.94117	31.99	0.96897	31.98	0.97656	31.98	0.98067	31.99	0.98692
50.00	0.93965	33.99	0.96744	33.99	0.97505	33.99	0.97918	33.99	0.98548
		35.99	0.9659	35.99	0.97354	35.99	0.97767	35.99	0.98406
		37.99	0.96436	37.99	0.97203	37.99	0.97613	37.99	0.98262
		39.99	0.96283	39.99	0.97052	39.99	0.97454	39.99	0.98112
		41.99	0.96129	41.99	0.96901	41.99	0.97302	41.99	0.97954
		43.99	0.95976	43.99	0.9675	43.99	0.97147	43.99	0.97788
		45.99	0.95822	45.99	0.96598	45.99	0.96987	45.99	0.97621
		47.99	0.95668	47.99	0.96447	47.99	0.96824	47.99	0.97452
		49.99	0.95513	49.99	0.96295	49.99	0.96661	49.99	0.97313

Table 36. Density data for the NaC₆:C₁₀(0.7) with water mixtures.

NaC ₆ :C ₁₀ (0.7)									
0%H ₂ O		10%H ₂ O		20%H ₂ O		30%H ₂ O		40%H ₂ O	
T (°C)	ρ (g/cm ³)	T (°C)	ρ (g/cm ³)	T (°C)	ρ (g/cm ³)	T (°C)	ρ (g/cm ³)	T (°C)	ρ (g/cm ³)
10.02	0.96927	21.98	0.96458	15.98	0.97667	15.98	0.98743	13.99	0.99038
11.98	0.97464	23.98	0.96306	17.98	0.97519	17.98	0.98603	15.98	0.98934
13.98	0.97832	25.98	0.96155	19.98	0.97371	19.98	0.98463	17.98	0.98821
15.98	0.98132	27.99	0.96003	21.98	0.97223	21.98	0.98323	19.98	0.98705
17.98	0.98404	29.99	0.95853	23.98	0.97074	23.98	0.98182	21.98	0.98585
19.98	0.98659	31.99	0.95702	25.99	0.96926	25.98	0.98041	23.98	0.98463
21.98	0.98877	33.99	0.95551	27.99	0.96778	27.98	0.97899	25.98	0.98339
23.98	0.98636	35.99	0.954	29.99	0.96629	29.98	0.97757	27.98	0.98211
25.98	0.97553	37.99	0.95249	31.99	0.96481	31.98	0.97615	29.98	0.98087
27.98	0.96387	39.99	0.95098	33.99	0.96333	33.99	0.97472	31.99	0.97959
29.98	0.95114	41.99	0.94947	35.99	0.96184	35.99	0.97329	33.99	0.97827
31.99	0.94600	43.99	0.94796	37.99	0.96036	37.99	0.97185	35.99	0.97691
33.99	0.94450	45.99	0.94645	39.99	0.95887	39.99	0.97041	37.99	0.97553
35.99	0.94300	47.99	0.94494	41.99	0.95738	41.99	0.96896	39.99	0.97411
37.99	0.94149	49.99	0.94342	43.99	0.95589	43.99	0.96750	41.99	0.97264
39.99	0.93999			45.99	0.9544	45.99	0.96602	43.99	0.97113
41.99	0.93848			47.99	0.95291	47.99	0.96454	45.99	0.96956
43.99	0.93697			49.99	0.95141	49.99	0.96303	47.99	0.96791
45.99	0.93546							49.99	0.96618
47.99	0.93396								
49.99	0.93245								

Table 37. Fitting parameters from ρ vs T for NaC₆:C₆(0.6) with water mixtures.

H ₂ O%	NaC ₆ :C ₆ (0.6)				
	0%	10%	20%	50%	60%
a (g cm ⁻³ °C ⁻¹)	-7.04E-04	-7.97E-04	-7.80E-04	-6.53E-04	-5.97E-04
b (g cm ⁻³)	1.02	1.04	1.04	1.04	1.03
R ²	0.976	1.000	1.000	0.999	0.999

Table 38. Fitting parameters from ρ vs T for NaC₆:C₆(0.7) with water mixtures.

H ₂ O%	NaC ₆ :C ₆ (0.7)				
	0%	10%	20%	30%	40%
a (g cm ⁻³ °C ⁻¹)	-8.29E-04	-8.05E-04	-7.92E-04	-7.62E-04	-7.51E-04
b (g cm ⁻³)	1.01	1.02	1.03	1.03	1.03
R ²	1.000	1.000	1.000	0.998	0.998

Table 39. Fitting parameters from p vs T for $\text{NaC}_6:\text{C}_8(0.6)$ with water mixtures.

	$\text{NaC}_6:\text{C}_8(0.6)$	
$\text{H}_2\text{O}\%$	0%	10%
a ($\text{g cm}^{-3}\text{ }^\circ\text{C}^{-1}$)	-7.89E-04	-7.83E-04
b (g cm^{-3})	1.01E+00	1.01E+00
R^2	1.000	1.000

Table 40. Fitting parameters from p vs T for $\text{NaC}_6:\text{C}_8(0.7)$ with water mixtures.

	$\text{NaC}_6:\text{C}_8(0.7)$					
$\text{H}_2\text{O}\%$	0%	10%	20%	30%	40%	50%
a ($\text{g cm}^{-3}\text{ }^\circ\text{C}^{-1}$)	-7.80E-04	-7.76E-04	-7.60E-04	-7.44E-04	-7.20E-04	-6.28E-04
b (g cm^{-3})	0.99	1.00	1.01	1.01	1.01	1.02
R^2	1.000	1.000	1.000	1.000	0.999	0.999

Table 41. Fitting parameters from p vs T for $\text{NaC}_6:\text{C}_9(0.7)$ with water mixtures.

	$\text{NaC}_6:\text{C}_9(0.7)$				
$\text{H}_2\text{O}\%$	0%	10%	20%	30%	40%
a ($\text{g cm}^{-3}\text{ }^\circ\text{C}^{-1}$)	-7.58E-04	-7.67E-04	-7.49E-04	-7.40E-04	-7.08E-04
b (g cm^{-3})	0.98	0.99	1.00	1.00	1.01
R^2	1.000	1.000	1.000	0.999	0.998

Table 42. Fitting parameters from p vs T for $\text{NaC}_6:\text{C}_{10}(0.7)$ with water mixtures.

	$\text{NaC}_6:\text{C}_{10}(0.7)$				
$\text{H}_2\text{O}\%$	0%	10%	20%	30%	40%
a ($\text{g cm}^{-3}\text{ }^\circ\text{C}^{-1}$)	-7.53E-04	-7.55E-04	-7.42E-04	-7.16E-04	-6.66E-04
b (g cm^{-3})	0.97	0.98	0.99	1.00	1.00
R^2	1.000	1.000	1.000	1.000	0.997

8.6. Surface Tension

Table 43. Surface Tension in water results for the different studied eutectic systems.

NaC6:C6		NaC6:C8		NaC6:C9		NaC6:C10	
γ (mN/m)	C (mol/L)	γ (mN/m)	C (mol/L)	γ (mN/m)	C (mol/L)	γ (mN/m)	C (mol/L)
69.4	0.00E+00	69.2	0.00E+00	68.33	0.00E+00	69.7	0.00E+00
63.6	3.45E-03	58.1	1.05E-03	48.10	9.76E-04	33.7	9.65E-04
57.0	6.89E-03	51.0	1.54E-03	31.60	1.95E-03	32.7	1.93E-03
54.0	1.03E-02	44.5	3.08E-03	30.87	2.87E-03	31.3	2.88E-03
50.9	1.38E-02	35.2	6.16E-03	30.77	5.75E-03	30.9	5.75E-03
51.3	1.72E-02	31.8	9.24E-03	30.63	8.61E-03	30.4	8.63E-03
48.3	2.06E-02	30.9	1.23E-02	30.50	1.15E-02	30.1	1.15E-02
44.3	2.41E-02	30.8	1.54E-02	30.30	1.43E-02	29.9	1.44E-02
41.7	2.75E-02	30.7	1.85E-02	30.20	1.72E-02	29.7	1.72E-02
42.1	3.09E-02	30.3	2.15E-02	30.10	2.01E-02	29.4	2.01E-02
44.0	3.43E-02	30.2	2.46E-02	30.03	2.29E-02	29.3	2.30E-02
43.3	3.77E-02	30.2	2.76E-02	30.00	2.58E-02	29.1	2.58E-02
40.6	4.12E-02	30.1	3.07E-02	29.83	2.86E-02	29.0	2.87E-02
39.1	4.46E-02	30.0	3.37E-02	29.80	3.15E-02	28.9	3.15E-02
39.4	4.80E-02	30.0	3.68E-02	29.70	3.43E-02	28.6	3.44E-02
38.6	5.14E-02	30.0	3.98E-02	29.60	3.71E-02	28.5	3.72E-02
37.7	5.48E-02	30.0	4.29E-02	29.50	4.00E-02	28.4	4.00E-02
37.2	5.82E-02	29.9	4.59E-02	29.43	4.28E-02	28.3	4.29E-02
36.6	6.16E-02	29.9	4.90E-02	29.33	4.56E-02	28.3	4.57E-02
36.0	6.49E-02	29.8	5.20E-02	29.20	4.85E-02	28.1	4.86E-02
		29.6	5.50E-02	29.10	5.13E-02	27.7	5.14E-02
		29.7	5.81E-02				
		29.5	6.11E-02				

8.7. Walden Plot

Table 44. Molar conductivity for $\text{NaC}_6\text{:C}_6(0.6)$ with water mixtures.

T(°C)	$\text{NaC}_6\text{:C}_6(0.6)$				
	0% H_2O	10% H_2O	20% H_2O	50% H_2O	60% H_2O
10	-	11.8	102.3	-	-
12	-	13.7	118.2	-	-
14	-	15.5	123.8	486.1	-
16	-	18.2	138.2	512.6	526.6
18	-	21.0	152.0	549.7	548.7
20	-	23.1	168.2	606.2	597.1
22	-	27.5	183.5	646.6	640.3
24	-	30.6	197.4	684.0	681.0
26	-	33.6	210.3	735.7	735.1
28	-	37.7	227.2	757.0	778.4
30	-	41.1	247.7	806.0	809.6
32	-	47.8	263.5	850.2	854.1
34	-	52.1	280.3	890.6	896.5
36	-	59.0	303.1	940.4	946.9
38	-	61.9	323.0	985.7	992.8
40	-	69.1	337.6	1018.5	1027.4
42	-	74.9	359.1	1063.0	1093.3
44	-	80.3	378.4	1106.5	1114.3
46	-	87.3	410.5	1169.6	1177.1
48	-	94.6	422.4	1215.3	1222.6
50	0.2	100.3	440.1	1234.9	1244.4

Table 45. Molar conductivity for $\text{NaC}_6\text{:C}_6(0.7)$ with water mixtures.

T(°C)	$\text{NaC}_6\text{:C}_6(0.7)$					
	0% H_2O	10% H_2O	20% H_2O	30% H_2O	40% H_2O	50% H_2O
10		11.3	87.4	203.2		
12		13.6	99.8	220.2		
14		14.5	108.6	233.4		
16		16.8	116.3	256.0		
18	0.04	18.8	127.3	265.8		
20	0.04	20.3	136.3	287.9	419.5	401.1
22	0.04	23.7	153.3	308.2		431.2
24	0.05	26.0	165.0	327.7	486.3	460.5
26	0.05	28.4	175.5	355.2		499.6
28	0.06	31.3	189.5	366.7	563.9	543.1
30	0.07	34.7	200.7	390.7		567.2
32	0.08	38.2	220.2	414.4	664.7	601.0
34	0.08	41.5	235.1	437.7		635.5
36	0.10	44.5	255.5	468.3	743.0	674.5
38	0.11	48.5	264.8	493.9		711.2
40	0.12	53.1	283.6	510.7	835.0	739.9
42	0.14	57.6	298.3	536.5		793.9
44	0.16	60.7	315.4	562.3	921.7	822.8
46	0.18	66.2	334.7	604.4		858.7
48	0.22	71.0	354.9	619.6		898.7
50	0.24	74.5	368.6	640.0		919.1

Table 46. Molar conductivity for $\text{NaC}_6\text{:C}_8(0.6)$ with water mixtures.

T(°C)	$\text{NaC}_6\text{:C}_8(0.6)$	
	0% H_2O	10% H_2O
10		5.3
12		6.1
14		7.0
16		8.4
18		9.6
20		10.6
22		12.0
24		13.6
26	0.1	15.9
28	0.1	17.9
30	0.1	19.3
32	0.1	22.9
34	0.1	24.1
36	0.1	27.6
38	0.1	30.6
40	0.1	34.1
42	0.2	37.6
44	0.2	40.3
46	0.2	45.4
48	0.3	49.4
50	0.3	51.3

Table 47. Molar conductivity for NaC₆:C₈(0.7) with water mixtures.

T(°C)	NaC ₆ :C ₈ (0.7)					
	0%H ₂ O	10%H ₂ O	20%H ₂ O	30%H ₂ O	40%H ₂ O	50%H ₂ O
10	0.04	4.9	48.6			251.2
12	0.05	5.8	55.3			274.8
14	0.05	6.1	59.8			306.2
16	0.05	7.1	64.1			330.5
18	0.06	8.0	69.8			346.6
20	0.06	9.0	74.3	191.6	287.0	383.1
22	0.07	10.0	82.9			394.6
24	0.08	11.0	89.3	227.2	332.1	423.2
26	0.08	12.5	97.9			447.4
28	0.09	13.1	105.8	257.7	385.3	465.2
30	0.10	14.8	111.6			498.1
32	0.11	16.4	120.5	298.2	439.7	516.3
34	0.12	17.9	129.1			544.1
36	0.13	20.0	139.6	337.2	492.0	556.4
38	0.14	21.7	149.9			582.5
40	0.15	23.2	157.8	386.6	553.9	621.3
42	0.16	25.3	168.7			639.5
44	0.17	26.8	179.1	426.0	605.7	675.9
46	0.19	30.1	194.6			713.8
48	0.20	32.1	206.8			736.1
50	0.20	32.7	212.5			

Table 48. Molar conductivity for $\text{NaC}_6\text{:C}_9(0.7)$ with water mixtures.

$\text{NaC}_6\text{:C}_9(0.7)$					
T(°C)	0% H_2O	10% H_2O	20% H_2O	30% H_2O	40% H_2O
10		3.8	46.9	119.3	186.6
12		4.3	51.0	128.5	201.7
14		4.8	55.1	138.7	219.4
16		5.6	60.8	151.4	240.9
18		5.9	65.7	162.4	260.1
20		6.7	69.3	170.6	274.3
22		7.5	75.0	182.0	302.2
24		8.3	80.5	193.7	311.7
26		9.5	88.4	209.0	336.6
28		10.1	94.9	222.6	357.1
30		11.3	99.8	232.2	372.0
32	0.05	12.5	107.1	245.4	392.1
34	0.05	13.6	114.3	256.4	412.7
36	0.05	15.3	124.4	273.4	438.0
38	0.06	16.1	133.0	288.6	459.4
40	0.06	17.8	138.6	299.5	475.0
42	0.06	19.5	148.2	314.1	505.9
44	0.07	20.8	156.1	328.9	515.8
46	0.07	22.7	171.3	350.8	545.7
48	0.08	24.4	176.4	366.7	566.9
50	0.08	25.4	183.9	374.7	577.1

Table 49. Molar conductivity for $\text{NaC}_6\text{:C}_{10}(0.7)$ with water mixtures.

T(°C)	$\text{NaC}_6\text{:C}_{10}(0.7)$				
	0% H_2O	10% H_2O	20% H_2O	30% H_2O	40% H_2O
14					183.4
16			53.3	105.0	198.9
18			57.0	111.4	214.0
20			60.0	115.6	229.7
22		5.0	66.5	126.3	245.7
24		5.4	71.0	133.1	260.8
26		6.1	74.8	142.9	281.5
28		6.7	80.3	147.0	298.0
30	0.09	7.3	84.0	156.8	309.9
32	0.09	8.1	92.5	165.3	335.0
34	0.10	8.8	95.8	173.7	343.4
36	0.10	9.7	102.9	184.4	364.1
38	0.10	10.7	110.3	194.1	382.1
40	0.10	11.8	115.5	201.4	402.5
42	0.12	12.8	126.1	215.0	420.8
44		13.7	131.9	222.9	436.2
46		15.2	140.8	237.2	460.4
48		16.4	149.0	247.2	478.4
50		16.5	153.5	251.2	487.5

8.8. pH

Table 50. pH of each mixture.

Group	% H ₂ O	pH
NaC₆:C₆(0.6)	10	6.30
	20	6.08
	40	6.13
	50	5.97
	60	5.95
NaC₆:C₆(0.7)	10	6.21
	20	5.61
	30	5.63
	40	5.67
	50	5.73
NaC₆:C₈(0.6)	10	6.3
	20	6.04
	30	6.37
NaC₆:C₈(0.7)	10	6.47
	20	6.27
	30	6.24
	40	6.27
	50	5.75
NaC₆:C₉(0.7)	10	5.67
	20	5.62
	30	5.71
	40	5.77
NaC₆:C₁₀(0.7)	10	5.8
	20	6.4
	30	5.78
	40	5.81

8.9. Cyclic Voltammetry

Table 51. Specific Capacitance (F/g) obtained from CV for the different scan-rates 1 mV/s, 5 mV/s, 10 mV/s and 20 mV/s.

Mixture	Scan rate (mV/s)	1 mV/s	5 mV/s	10 mV/s	20 mV/s
	%H2O	Specific Capacitance (F/g)			
NaC ₆ :C ₆ (0.6)	50	67.71	60.80	55.64	49.03
	60	68.71	65.17	59.48	53.31
NaC ₆ :C ₆ (0.7)	30	71.52	62.12	55.45	47.03
	40	69.41	65.03	60.38	53.88
	50	76.71	70.76	65.30	58.40
NaC ₆ :C ₈ (0.7)	20	67.17	51.20	41.67	32.12
	30	53.79	47.70	41.07	33.07
	40	60.65	50.01	42.31	34.92
	50	65.68	55.52	47.25	38.83
NaC ₆ :C ₉ (0.7)	20	55.87	39.90	31.59	24.21
	30	60.73	45.53	37.65	29.90
	40	62.46	45.67	37.18	29.54
NaC ₆ :C ₁₀ (0.7)	20	46.36	33.15	23.50	12.72
	30	49.71	33.59	26.01	19.77
	40	50.04	36.07	30.12	23.57

8.10. Potentiostatic Electrochemical Impedance Spectroscopy

8.10.1. EIS Nyquist Plots

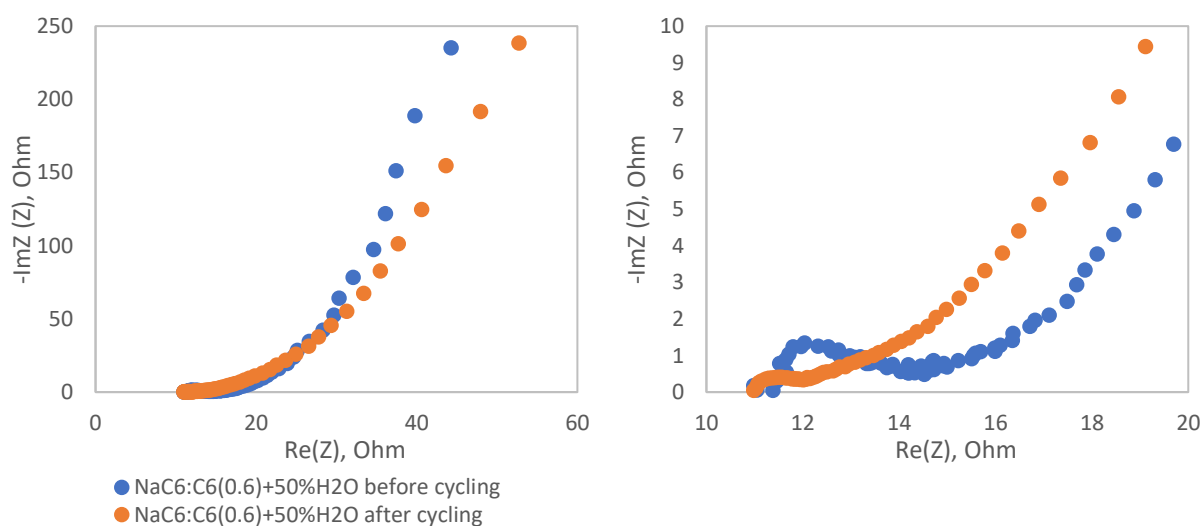


Figure 129. Nyquist plots of the NaC₆:C₆(0.6) + 50%H₂O electrolyte before and after cycling. Left: full scale; Right: Zoom for high frequencies.

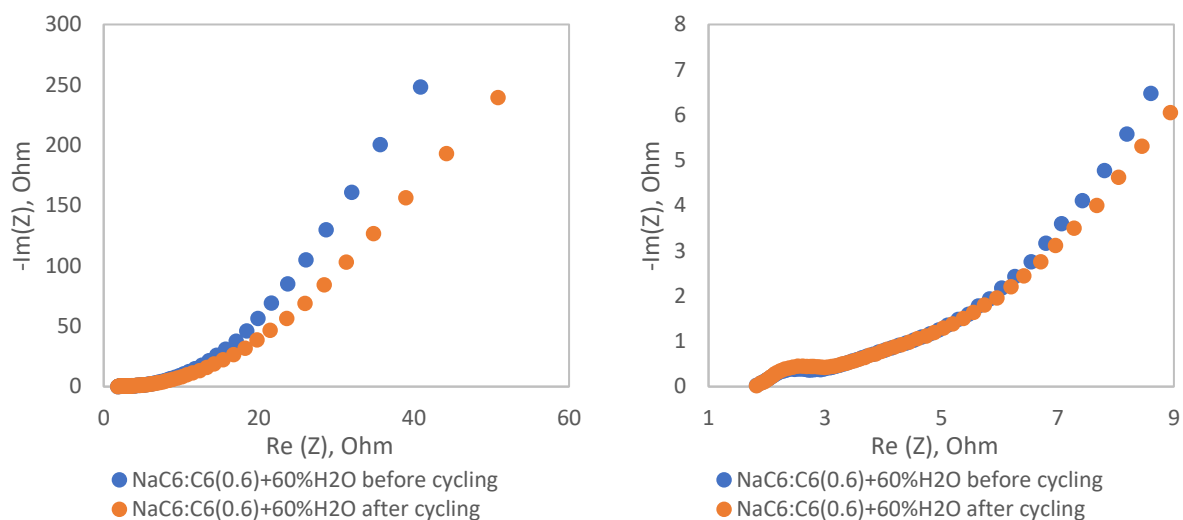


Figure 130. Nyquist plots of the $\text{NaC}_6:\text{C}_6(0.6) + 60\% \text{H}_2\text{O}$ electrolyte before and after cycling. Left: full scale; Right: Zoom for high frequencies.

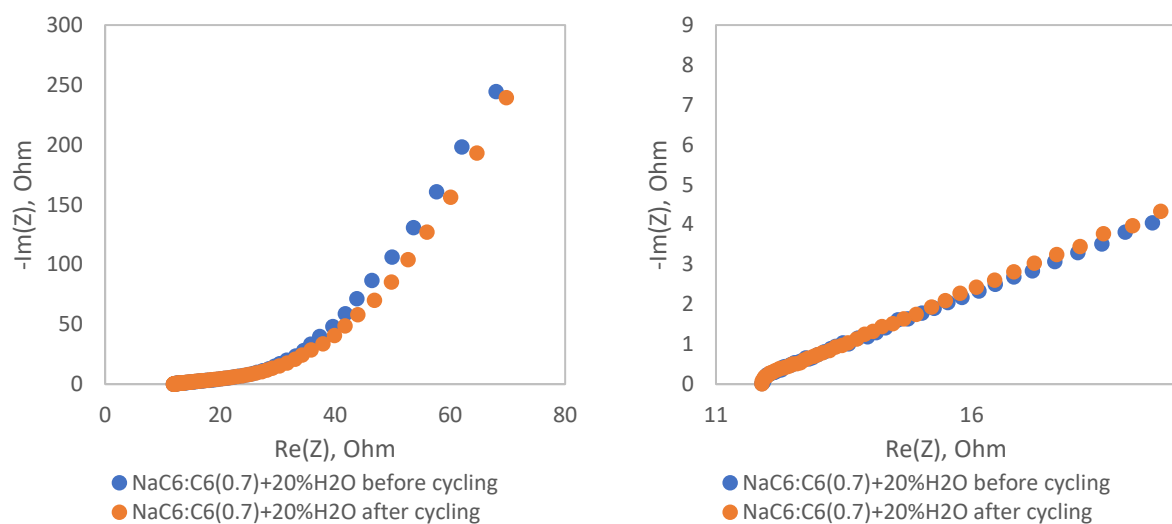


Figure 131. Nyquist plots of the $\text{NaC}_6:\text{C}_6(0.7) + 20\% \text{H}_2\text{O}$ electrolyte before and after cycling. Left: full scale; Right: Zoom for high frequencies.

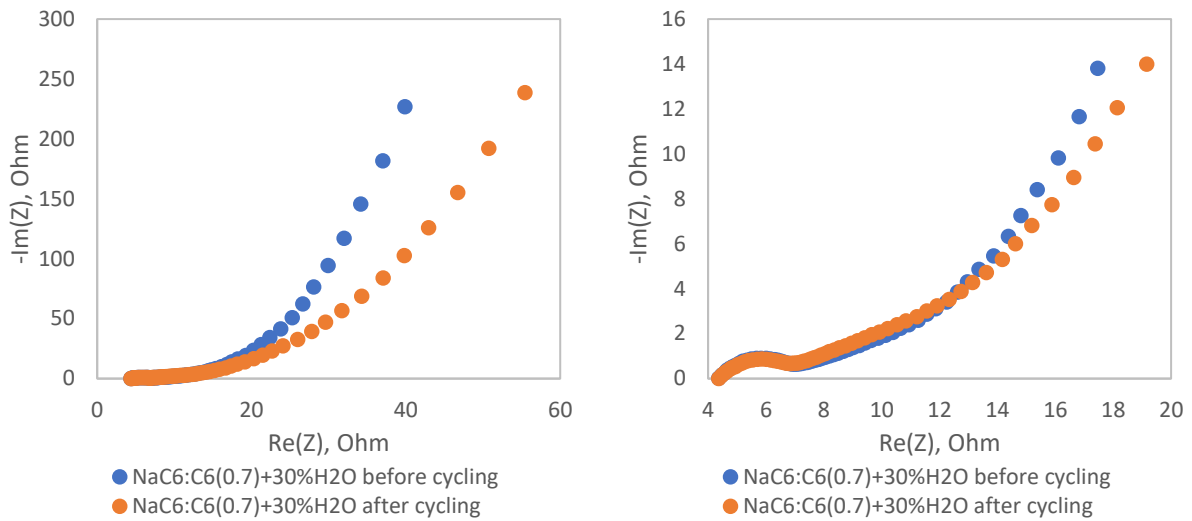


Figure 132. Nyquist plots of the $\text{NaC}_6:\text{C}_6(0.7) + 30\% \text{H}_2\text{O}$ electrolyte before and after cycling. Left: full scale; Right: Zoom for high frequencies.

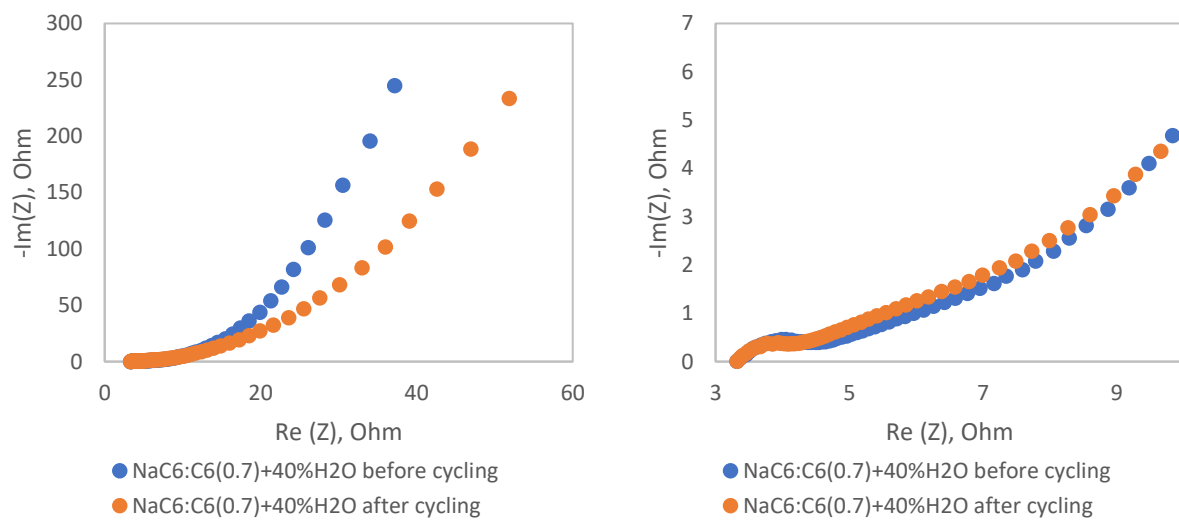


Figure 133. Nyquist plots of the $\text{NaC}_6:\text{C}_6(0.7) + 40\% \text{H}_2\text{O}$ electrolyte before and after cycling. Left: full scale; Right: Zoom for high frequencies.

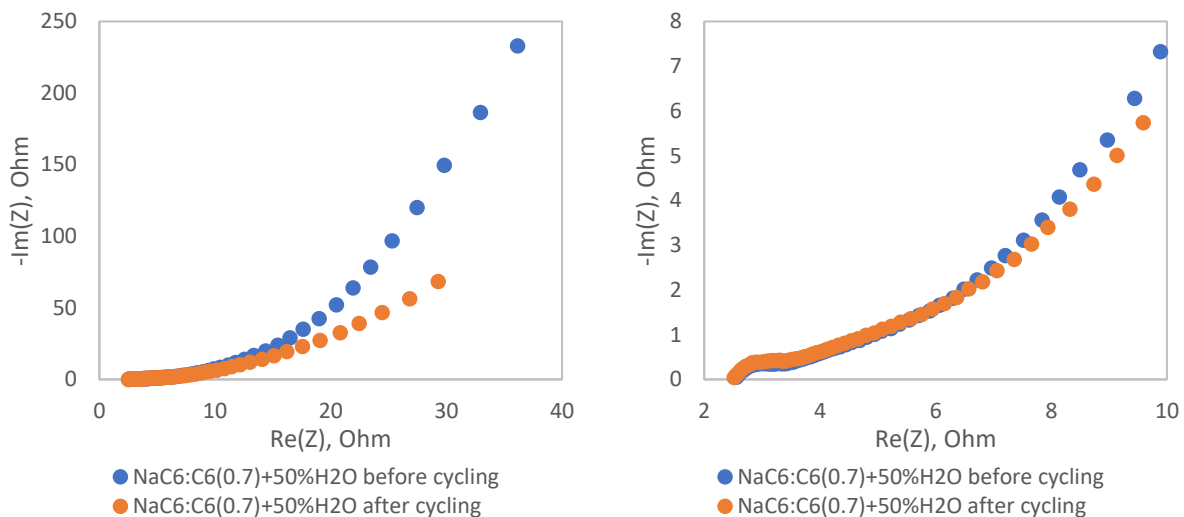


Figure 134. Nyquist plots of the $\text{NaC}_6:\text{C}_6(0.7) + 50\% \text{H}_2\text{O}$ electrolyte before and after cycling. Left: full scale; Right: Zoom for high frequencies.

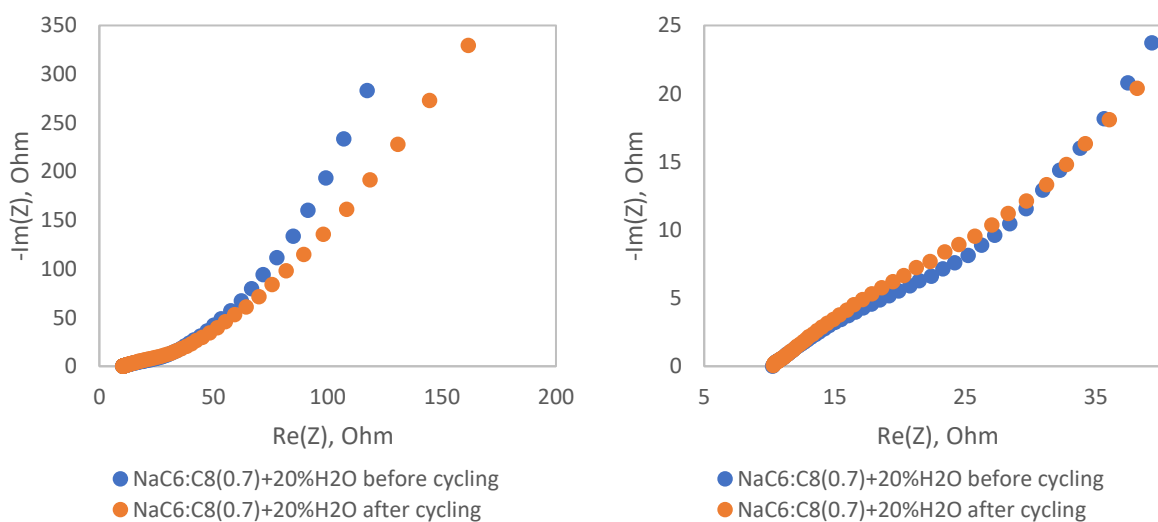


Figure 135. Nyquist plots of the $\text{NaC}_6:\text{C}_8(0.7) + 20\% \text{H}_2\text{O}$ electrolyte before and after cycling. Left: full scale; Right: Zoom for high frequencies.

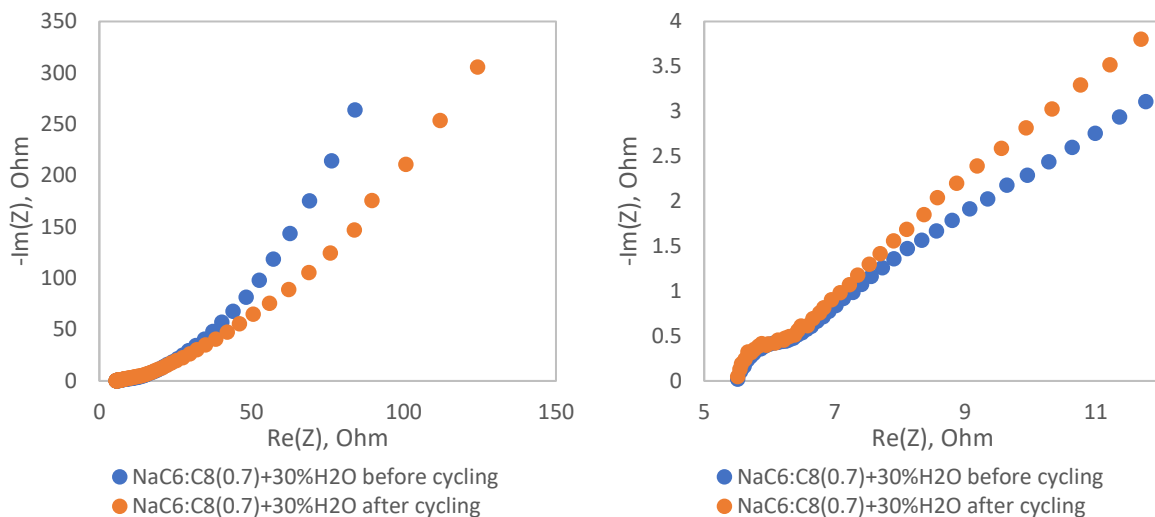


Figure 136. Nyquist plots of the $\text{NaC}_6:\text{C}_8(0.7) + 30\% \text{H}_2\text{O}$ electrolyte before and after cycling. Left: full scale; Right: Zoom for high frequencies.

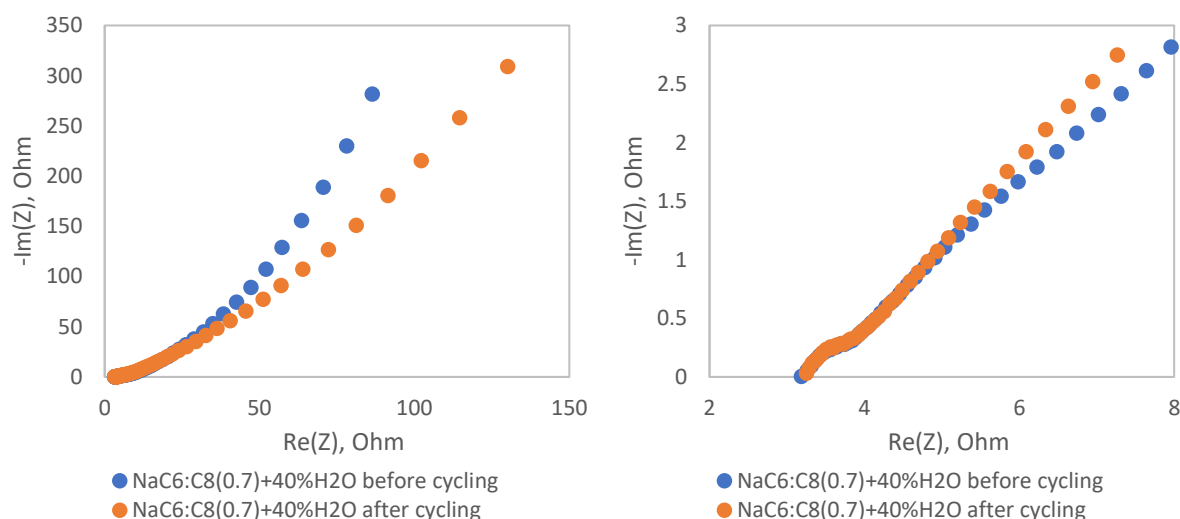


Figure 137. Nyquist plots of the $\text{NaC}_6:\text{C}_8(0.7) + 40\% \text{H}_2\text{O}$ electrolyte before and after cycling. Left: full scale; Right: Zoom for high frequencies.

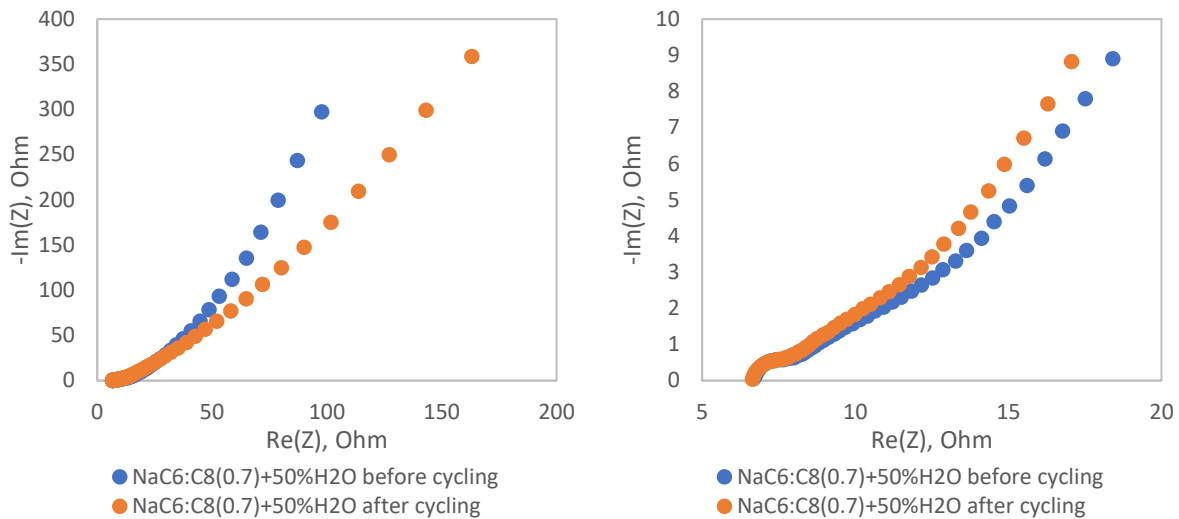


Figure 138. Nyquist plots of the $\text{NaC}_6:\text{C}_8(0.7) + 50\% \text{H}_2\text{O}$ electrolyte before and after cycling. Left: full scale; Right: Zoom for high frequencies.

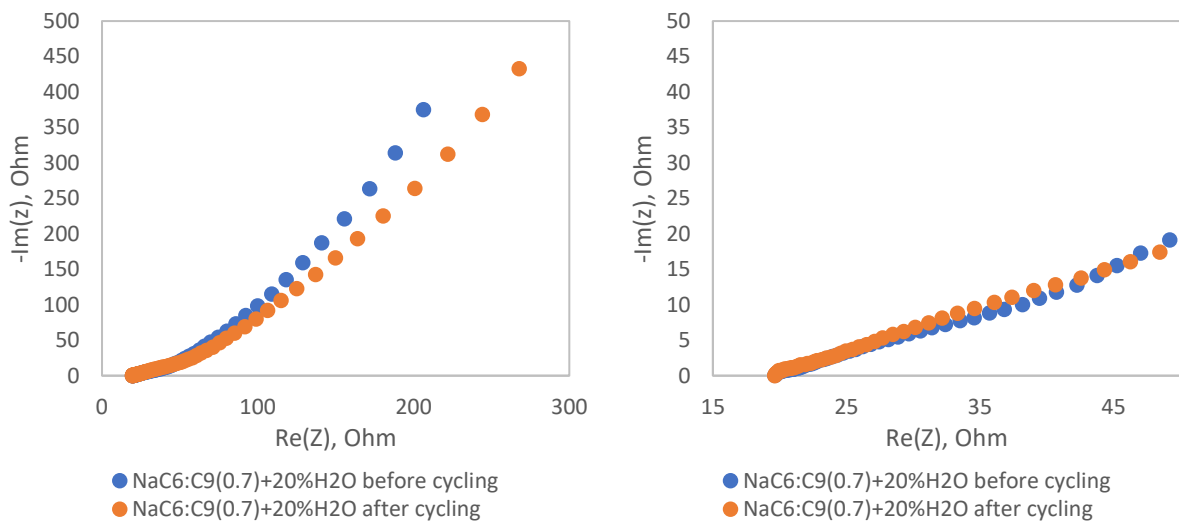


Figure 139. Nyquist plots of the $\text{NaC}_6:\text{C}_9(0.7) + 20\% \text{H}_2\text{O}$ electrolyte before and after cycling. Left: full scale; Right: Zoom for high frequencies.

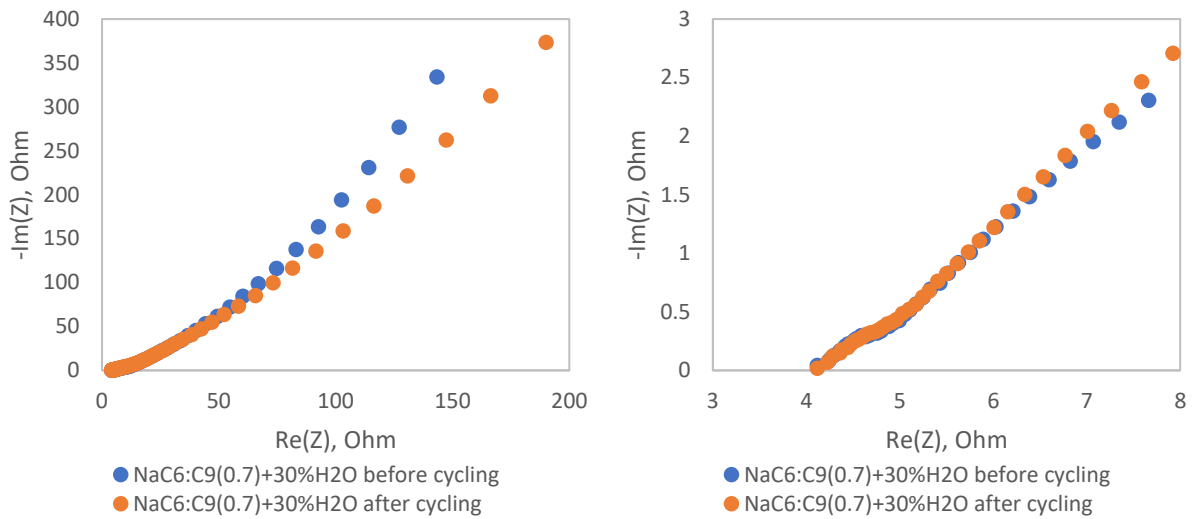


Figure 140. Nyquist plots of the $\text{NaC}_6:\text{C}_9(0.7) + 30\% \text{H}_2\text{O}$ electrolyte before and after cycling. Left: full scale; Right: Zoom for high frequencies.

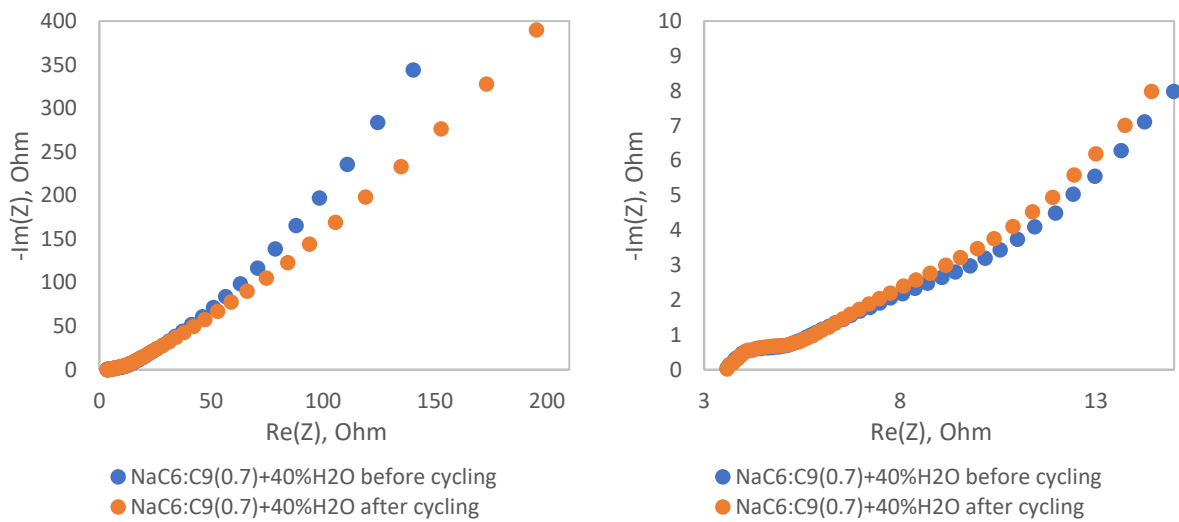


Figure 141. Nyquist plots of the $\text{NaC}_6:\text{C}_9(0.7) + 40\% \text{H}_2\text{O}$ electrolyte before and after cycling. Left: full scale; Right: Zoom for high frequencies.

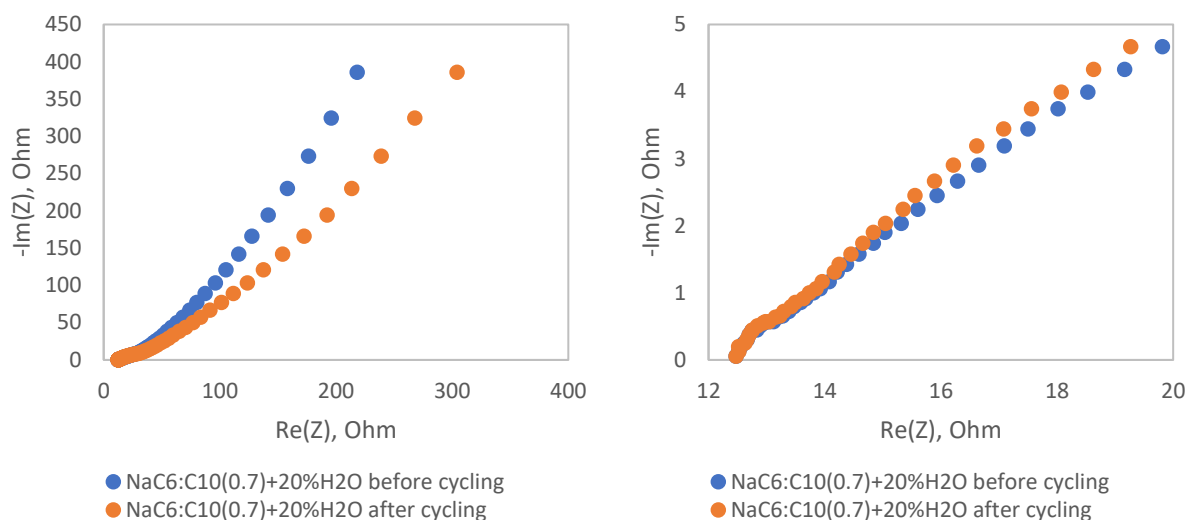


Figure 142. Nyquist plots of the $\text{NaC}_6:\text{C}_{10}(0.7) + 20\% \text{H}_2\text{O}$ electrolyte before and after cycling. Left: full scale; Right: Zoom for high frequencies.

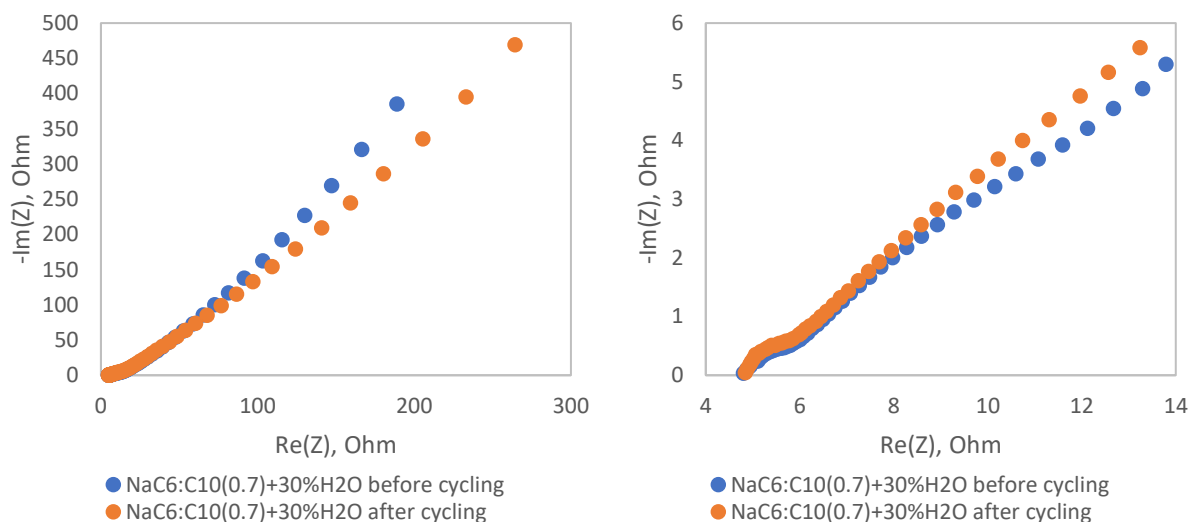


Figure 143. Nyquist plots of the $\text{NaC}_6:\text{C}_{10}(0.7) + 30\% \text{H}_2\text{O}$ electrolyte before and after cycling. Left: full scale; Right: Zoom for high frequencies.

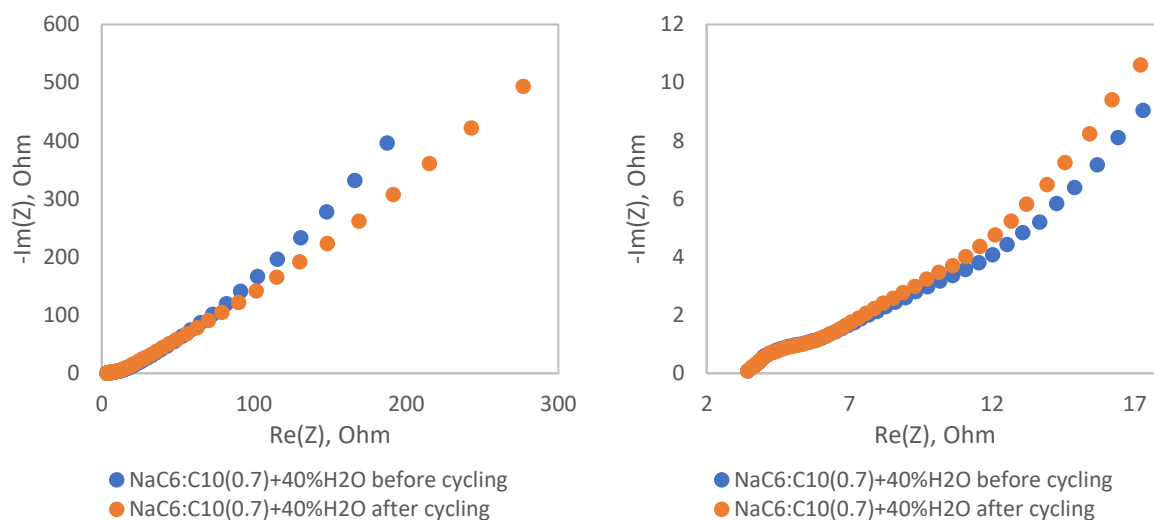


Figure 144. Nyquist plots of the NaC₆:C₁₀(0.7) + 40%H₂O electrolyte before and after cycling. Left: full scale; Right: Zoom for high frequencies.

8.10.2. Impedance Values: R_A, R_B, R_C

Table 52. R_A values before cycling.

R _A Before cycling					
%H ₂ O	NaC ₆ :C ₆ (0.6)	NaC ₆ :C ₆ (0.7)	NaC ₆ :C ₈ (0.7)	NaC ₆ :C ₉ (0.7)	NaC ₆ :C ₁₀ (0.7)
20	-	-	10.2	19.6	12.5
30	-	4.4	5.5	4.1	4.8
40	-	3.3	3.2	3.6	3.4
50	11.0	2.5	6.6	-	-
60	1.8	-	-	-	-

Table 53. R_B - R_A values before cycling.

R _B - R _A Before cycling					
%H ₂ O	NaC ₆ :C ₆ (0.6)	NaC ₆ :C ₆ (0.7)	NaC ₆ :C ₈ (0.7)	NaC ₆ :C ₉ (0.7)	NaC ₆ :C ₁₀ (0.7)
20	-	-	0.8	2.6	1.3
30	-	2.9	0.8	1.2	2.0
40	-	1.3	1.2	1.8	3.1
50	3.5	1.0	1.5	-	-
60	1.3	-	-	-	-

Table 54. *R_C values before cycling.*

R_C Before cycling					
%H₂O	NaC₆:C₆(0.6)	NaC₆:C₆(0.7)	NaC₆:C₈(0.7)	NaC₆:C₉(0.7)	NaC₆:C₁₀(0.7)
20	-	-	22.4	28.8	25.6
30	-	10.4	12.2	11.0	14.5
40	-	7.0	8.0	9.8	12.0
50	17.1	5.9	9.0	-	-
60	5.0	-	-	-	-

Table 55. *R_B - R_A values after cycling.*

R_B - R_A After cycling					
%H₂O	NaC₆:C₆(0.6)	NaC₆:C₆(0.7)	NaC₆:C₈(0.7)	NaC₆:C₉(0.7)	NaC₆:C₁₀(0.7)
20	-	-	0.9	2.3	1.3
30	-	2.8	0.9	1.4	1.8
40	-	1.0	1.1	2.1	3.0
50	1.2	1.1	1.6	-	-
60	1.3	-	-	-	-

Table 56. *R_C values after cycling.*

R_C After cycling					
%H₂O	NaC₆:C₆(0.6)	NaC₆:C₆(0.7)	NaC₆:C₈(0.7)	NaC₆:C₉(0.7)	NaC₆:C₁₀(0.7)
20	-	5.3	27.0	15.5	11.1
30	-	3.7	11.7	7.2	11.6
40	-	2.7	8.8	4.8	4.6
50	14.2	2.3	9.1	-	-
60	5.0	-	-	-	-

8.10.3. Electrode Specific Capacitance versus Frequency plots

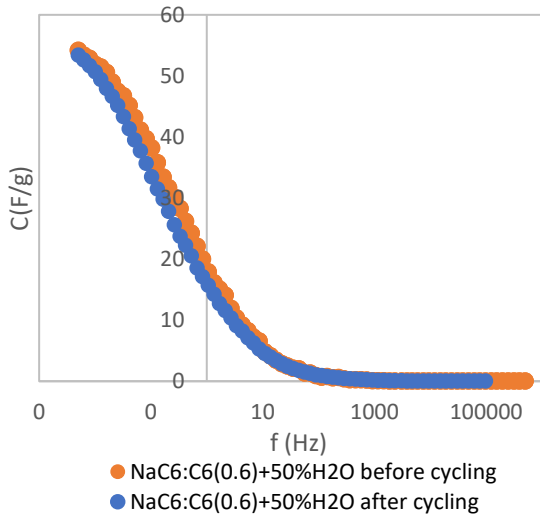


Figure 145. Specific Capacitance as function of frequency obtained from EIS for the $\text{NaC}_6:\text{C}_6(0.6) + 50\%\text{H}_2\text{O}$ mixture before and after cycling.

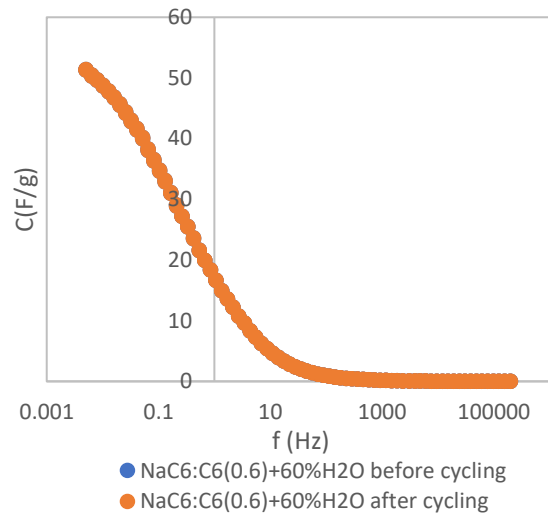


Figure 146. Specific Capacitance as function of frequency obtained from EIS for the $\text{NaC}_6:\text{C}_6(0.6) + 60\%\text{H}_2\text{O}$ mixture before and after cycling.

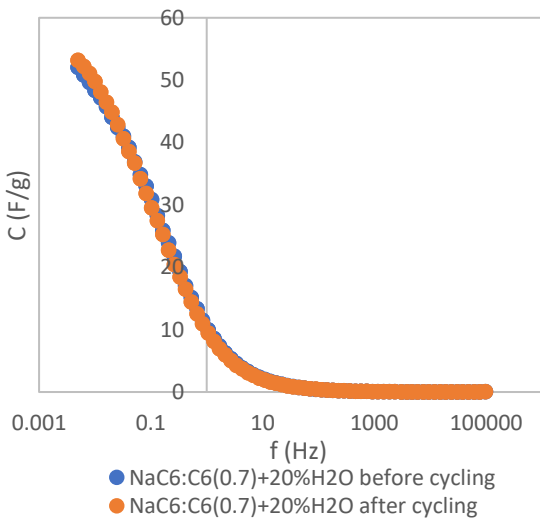


Figure 147. Specific Capacitance as function of frequency obtained from EIS for the $\text{NaC}_6:\text{C}_6(0.7) + 20\%\text{H}_2\text{O}$ mixture before and after cycling.

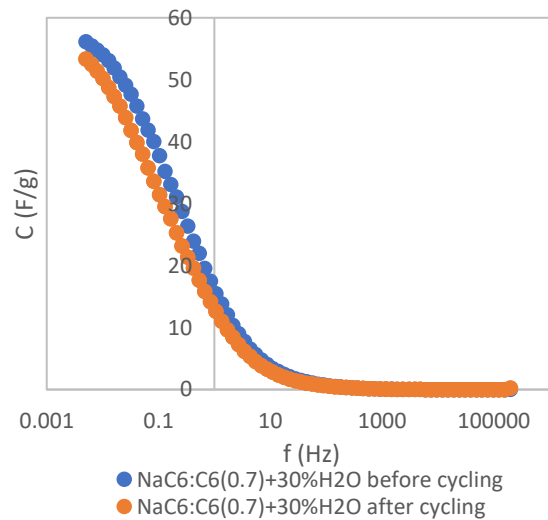


Figure 148. Specific Capacitance as function of frequency obtained from EIS for the $\text{NaC}_6:\text{C}_6(0.7) + 30\%\text{H}_2\text{O}$ mixture before and after cycling.

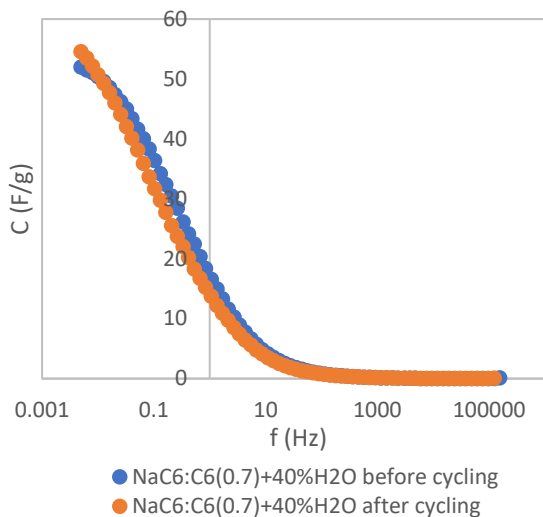


Figure 149. Specific Capacitance as function of frequency obtained from EIS for the NaC₆:C₆(0.7) + 40%H₂O mixture before and after cycling.

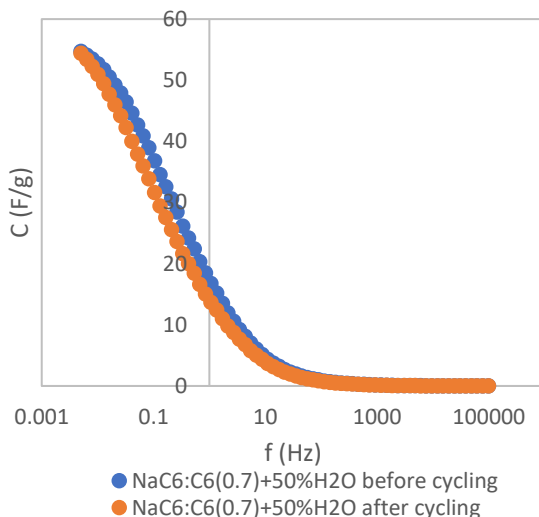


Figure 150. Specific Capacitance as function of frequency obtained from EIS for the NaC₆:C₆(0.7) + 50%H₂O mixture before and after cycling.

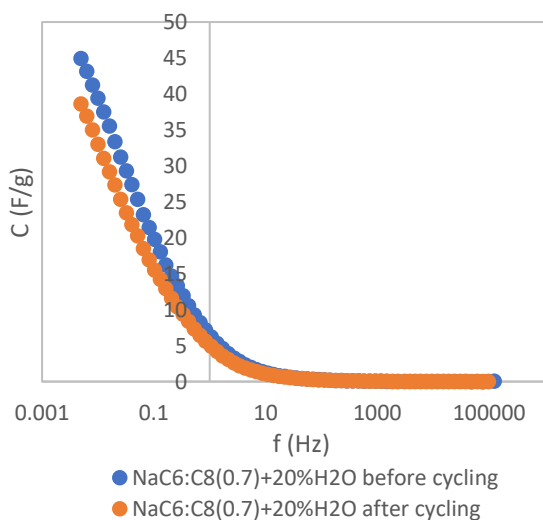


Figure 151. Specific Capacitance as function of frequency obtained from EIS for the NaC₆:C₈(0.7) + 20%H₂O mixture before and after cycling.

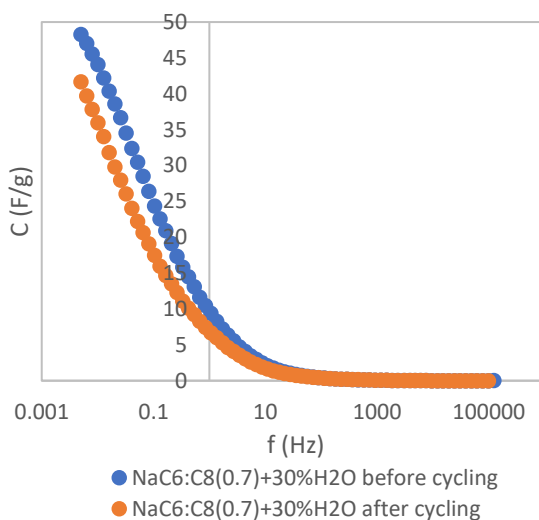


Figure 152. Specific Capacitance as function of frequency obtained from EIS for the NaC₆:C₈(0.7) + 30%H₂O mixture before and after cycling.

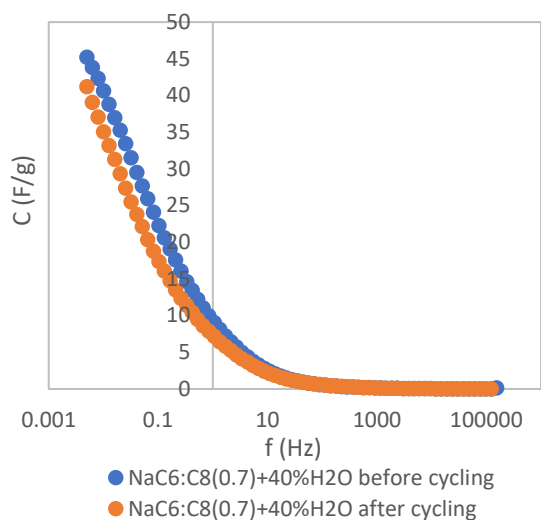


Figure 153. Specific Capacitance as function of frequency obtained from EIS for the $\text{NaC}_6\text{:C}_8(0.7) + 40\% \text{H}_2\text{O}$ mixture before and after cycling.

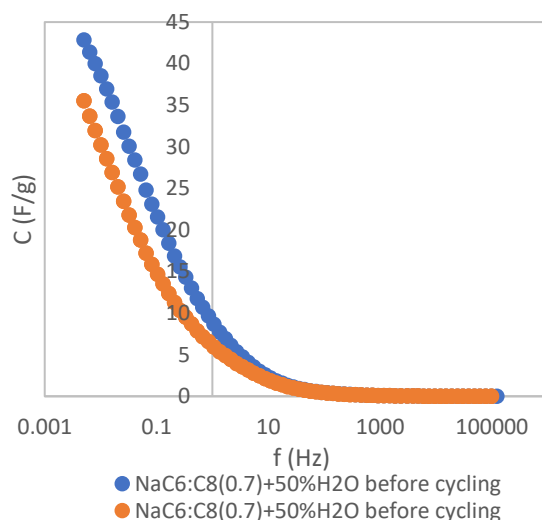


Figure 154. Specific Capacitance as function of frequency obtained from EIS for the $\text{NaC}_6\text{:C}_8(0.7) + 50\% \text{H}_2\text{O}$ mixture before and after cycling.

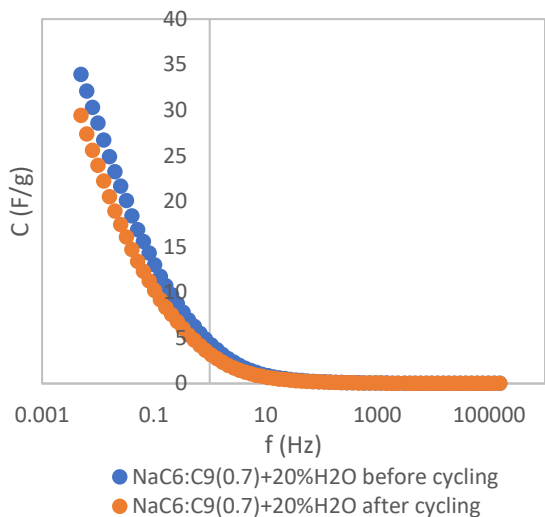


Figure 155. Specific Capacitance as function of frequency obtained from EIS for the $\text{NaC}_6\text{:C}_9(0.7)$ + $20\% \text{H}_2\text{O}$ mixture before and after cycling.

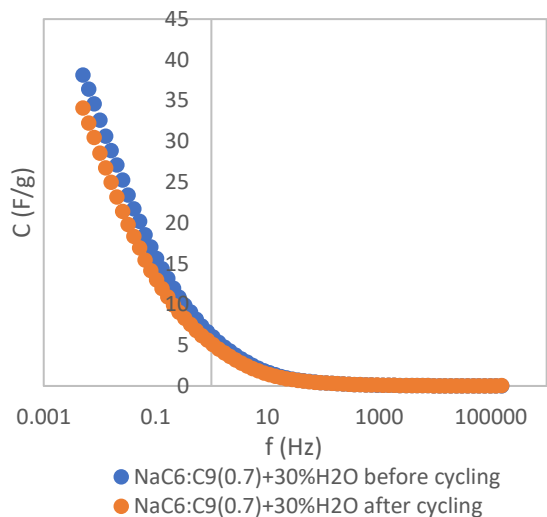


Figure 156. Specific Capacitance as function of frequency obtained from EIS for the $\text{NaC}_6\text{:C}_9(0.7)$ + $30\% \text{H}_2\text{O}$ mixture before and after cycling.

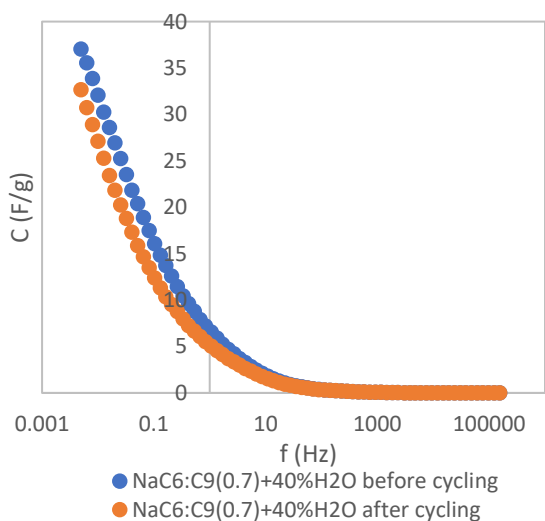


Figure 157. Specific Capacitance as function of frequency obtained from EIS for the $\text{NaC}_6\text{:C}_9(0.7)$ + $40\% \text{H}_2\text{O}$ mixture before and after cycling.

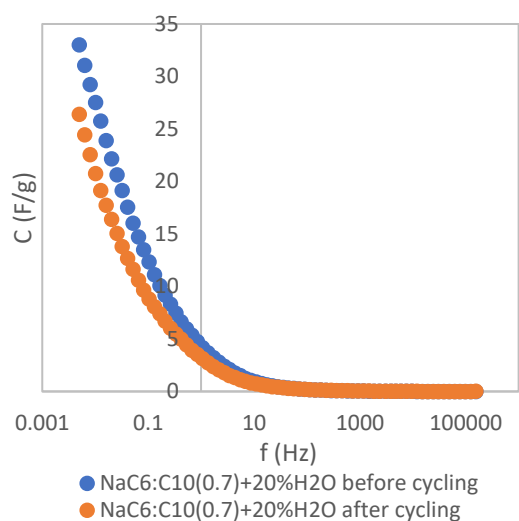


Figure 158. Specific Capacitance as function of frequency obtained from EIS for the $\text{NaC}_6\text{:C}_{10}(0.7)$ + $20\% \text{H}_2\text{O}$ mixture before and after cycling.

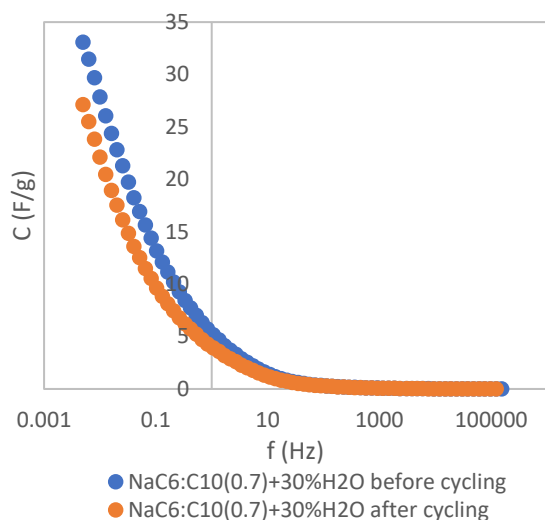


Figure 159. Specific Capacitance as function of frequency obtained from EIS for the $\text{NaC}_6\text{:C}_{10}(0.7) + 30\%\text{H}_2\text{O}$ mixture before and after cycling.

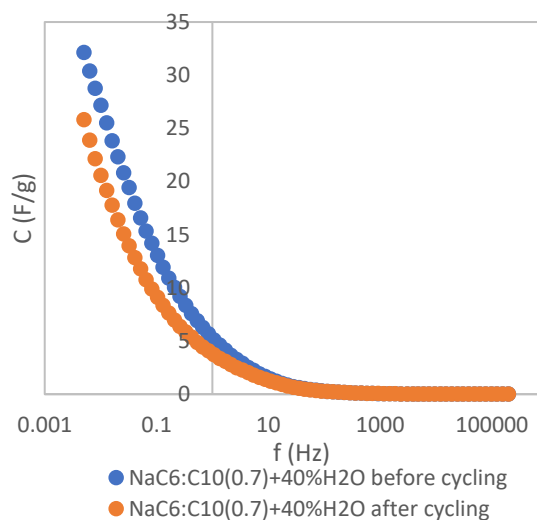


Figure 160. Specific Capacitance as function of frequency obtained from EIS for the $\text{NaC}_6\text{:C}_{10}(0.7) + 40\%\text{H}_2\text{O}$ mixture before and after cycling.

Table 57. Specific Capacitance from PEIS data before and after cycling.

mixture	Specific Capacitance (F/g) from PEIS	
	before cycling	after cycling
$\text{NaC}_6\text{:C}_6(0.6) + 50\%\text{H}_2\text{O}$	54.16	53.39
$\text{NaC}_6\text{:C}_6(0.6) + 60\%\text{H}_2\text{O}$	51.28	51.28
$\text{NaC}_6\text{:C}_6(0.7) + 30\%\text{H}_2\text{O}$	56.15	53.35
$\text{NaC}_6\text{:C}_6(0.7) + 40\%\text{H}_2\text{O}$	51.98	54.56
$\text{NaC}_6\text{:C}_6(0.7) + 50\%\text{H}_2\text{O}$	54.69	54.38
$\text{NaC}_6\text{:C}_8(0.7) + 20\%\text{H}_2\text{O}$	44.97	38.62
$\text{NaC}_6\text{:C}_8(0.7) + 30\%\text{H}_2\text{O}$	48.27	41.66
$\text{NaC}_6\text{:C}_8(0.7) + 40\%\text{H}_2\text{O}$	45.18	41.17
$\text{NaC}_6\text{:C}_8(0.7) + 50\%\text{H}_2\text{O}$	42.84	35.52
$\text{NaC}_6\text{:C}_9(0.7) + 20\%\text{H}_2\text{O}$	33.93	29.42
$\text{NaC}_6\text{:C}_9(0.7) + 30\%\text{H}_2\text{O}$	38.12	34.09
$\text{NaC}_6\text{:C}_9(0.7) + 40\%\text{H}_2\text{O}$	37.03	32.66
$\text{NaC}_6\text{:C}_{10}(0.7) + 20\%\text{H}_2\text{O}$	33.00	26.41
$\text{NaC}_6\text{:C}_{10}(0.7) + 30\%\text{H}_2\text{O}$	33.07	27.14
$\text{NaC}_6\text{:C}_{10}(0.7) + 40\%\text{H}_2\text{O}$	32.14	25.81